6 Power Take-Off Systems

In this chapter the main mechanisms that can be implemented to convert wave into mechanical and/or electrical energy are discussed. Such mechanisms are often called power take-off (PTO) or power conversion systems (the first term is adopted throughout the book). The review is directly linked with the most commonly used options and to those which are linked with the technologies described in Chapter 7. Firstly air turbines, used in Oscillating Water Columns, are focused (6.1), while in 6.2 the principles of linear generators (direct drive) are addressed. Section 6.3 is devoted to hydraulic power take-off systems and details regarding an alternative to electricity production (desalination) are given in 6.4.

6.1 Air Turbine Design for OWCs

Richard Curran and Matthew Folley

Queens University Belfast
Belfast
Northern Ireland, UK

6.1.1 Introduction

This section considers two of the most popular types of air turbine that are used in Oscillating Water Column (OWC) wave energy conversion systems: the Wells turbine and the Impulse turbine, although the Denniss-Auld turbine is also briefly introduced. Since the conception of the Wells turbine (Wells, 1976) at Queen's University Belfast (QUB) there has been considerable effort devoted worldwide to the development of the basic design. Similarly, there has been a considerable amount of development effort directed towards the self-rectifying impulse turbine that was first suggested by Kim et al. (1988). The development of the Wells turbine initially included investigations into the geometric variables, blade profile, and number of rotor planes (Raghunathan, 1995), and also the use of guide vanes (Setoguchi et al., 1988). Two further design enhancements have been the pitching of a monoplane turbine's blades and the counter-rotation of a biplane's rotors (Raghunathan and Beattie, 1996). Full-scale plant systems (Falcão et al., 1994)

have utilised more advanced turbine configurations, encouraged by the successful pioneering of prototype plants such as the 75 *kW* QUB Islay plant that used basic monoplane and biplane turbine configurations with standard symmetrical NACA profile blades (Whittaker et al., 1997a, 1997b). The development work for Impulse turbines also included investigation of the basic design parameters but much of the work then went on to focus on the design of the guide vanes and whether these would be fixed or pitching, or even self-pitching (Setoguchi et al, 2001). The Impulse turbine has been installed in several plants in Asia and there is still much interest in it as an alternative to the more widely used Wells turbine (used in plants in the UK, Portugal, India and Japan); finally the Denniss-Auld turbine has been used in the Port Kembla Australian plant (Curran et al., 2000; Finnigan and Auld, 2003; Finnigan and Alcorn, 2003).

The aim of this section is to give an overview of the key theoretical design issues concerned with the use of air turbines for wave energy conversion, including the basic performance of several types of turbine design, and then to present some operational aspects. The review also considers the integration of the turbine with the OWC type systems that typically use either a Wells or an Impulse turbine. Finally, the discussion will draw some general conclusions and highlight future developments.

6.1.2 Integrated systems: Engineering Design Requirements

An air turbine forms part of an integral system that consists of a capture device, which also includes an electrical generator. In addition, the performance of the capture device will be affected by its physical environment and may form part of an array. The turbine must be connected to the capture device by some sort of ducting arrangement, and the generator must be coupled to the turbine with minimal interference to the air flow exiting the system. One can consider the primary system integration entailing the optimal arrangement and sizing of the capture device, the turbine and the generator. The key generator design parameter to be considered in terms of the impact on the turbine's performance generator is the speed, which operationally will be determined by the required torque/speed characteristic and the generator power rating. Consequently, this section will tend to focus on the interaction between the turbine and the performance of the capture device through the Oscillating Water Column (OWC) principle. The subsequent inclusion of the generator in this design methodology is not thought to change the global design optima of the complete system as it can be sized and configured to have the necessary characteristics that have been determined by the turbine-OWC system. However, in reality there will be a small deviation off the optima due to aspects such as both fixed and varying generator losses. However, the electrical system will have a large influence if a very active control strategy is adopted where the speed is allowed to vary considerably to better match the provision of the pneumatic power at the air velocities that are preferred by the turbine.

This section addresses the optimisation of the core interdependence between the turbine and the OWC in order to maximise the potential for energy conversion. There are two matching principles that need to be addressed, namely that:

1. The turbine should provide a damping level (which effectively restricts the airflow exiting the system) that maximises the conversion of wave energy to the kinetic energy that determines the motion of the OWC and which is ultimately converted to pneumatic energy by the excitation of the air immediately above the OWC.
2. The turbine should be able to maximise the conversion of pneumatic energy to mechanical energy (and subsequently electrical energy) over the range of flow rates produced as the air exits the plenum chamber immediately above the OWC. A high value of turbine applied damping reduces flow rate and vice versa.

OWC Interface

The performance of an OWC can be modelled by the well known equation describing the damped motion of a body oscillating with a single degree of freedom due to a time varying force:

$$F(t) = m\frac{d^2y}{dt^2} + B\frac{dy}{dt} + Ky\,, \tag{6.1}$$

where F is the applied force at time t, m is the mass of the body, B is the damping, y is the displacement and K is the spring restoring constant due to the buoyancy of the OWC. The spring restoring constant K is given by: $K = A_C\rho_W g$, where A_C is the surface area of the OWC, ρ_W is the density of water and g is the gravitational acceleration. A direct analogy can be drawn with a mechanical mass-spring-damper system; however two additional terms must be included in order to account for the waves generated by the body as it oscillates. The mass of the column must include the added mass, which is frequency dependent, as well as the entrained mass. It is thus convenient to consider the mass of the column as its effective mass, M_E, which is the sum of the entrained and added masses. Secondly, the damping should be considered to consist of two components: the applied damping, B_A, which extracts energy from the system and is provided by the turbine, and the secondary damping, B_2. The secondary damping itself consists of two further components: the radiation damping due to the generation of waves by the column, and the loss damping due to energy losses which increase substantially with incident wave power.

The established solution (Mei, 1976) to the equation of motion for sinusoidal excitation is:

$$W_{OWC} = \frac{\frac{1}{2}B_A\omega_{OWC}^2\left|F\right|^2}{(K - M_E\omega_{OWC}^2)^2 + (B_A + B_2)^2\omega_{OWC}^2}\,, \tag{6.2}$$

where W_{OWC} is the average power output and ω_{OWC} is the angular frequency of oscillation. The level of turbine applied damping which maximises the power output of the OWC is then given by:

$$B_{A_{OPT}} = \sqrt{B_2^2 + \left[\frac{K - M_E\omega_{OWC}^2}{\omega_{OWC}}\right]^2} \quad . \tag{6.3}$$

Figures 6.1 and 6.2 present the results of a series of hydraulic model tests carried out in order to determine the influence of applied damping on an OWC's power output and bandwidth response respectively. Figure 6.1 shows the results for four different values of significant wave height. At low levels of applied damping it can be seen that the power output is very sensitive to changes in the applied damping. Furthermore, the power output is maximised at a certain level of applied damping which is known as the optimum applied damping. Subsequently, the power output decreases as the applied damping is further increased although the performance sensitivity is much less than for under-damping. Under-damping thus greatly reduces the efficiency of the column to an extent which over-damping does not, thus providing a further incentive to over-damp the system design.

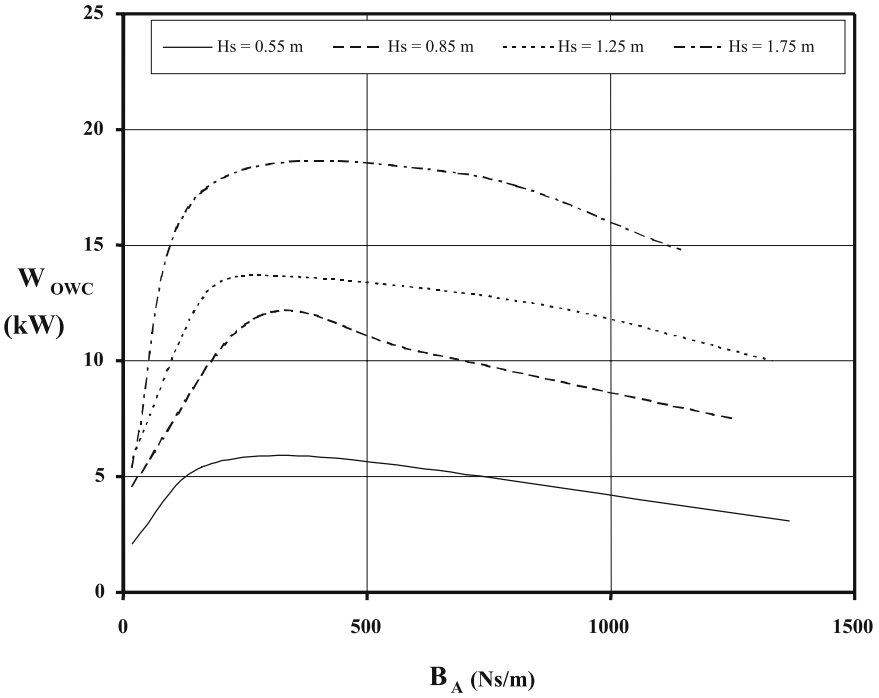

Fig. 6.1. Influence of damping and wave height on the power output of the OWC

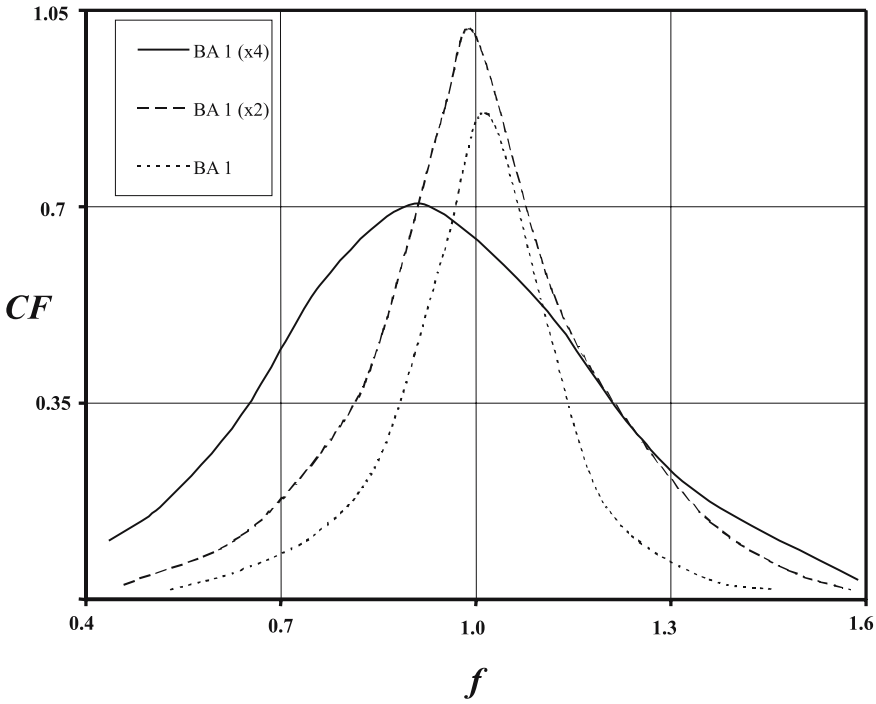

Fig. 6.2. Influence of damping and frequency ratio on the capture factor of the OWC

Figure 6.2 shows the performance bandwidth response for three different damping levels; at an initial value of B_A1 and for double (*x2*) and quadruple (*x4*) the initial level. The capture factor, *CF*, in Fig. 6.2 is defined as the ratio of the capture width of the device to the column width, is plotted against the frequency ratio: $f = \frac{\omega_{OWC}}{\omega_O}$, where ω_O is the resonant frequency. The capture factor is the amount of power 'captured' by the OWC relative to the value incident on the width of coastline spanned by the device (thus it is often called the relative capture width; see Chapter 3). It can be seen that the performance must be optimised across a range of frequencies in order to maximise the output for any particular set of wave conditions. It can be concluded that the optimal applied damping is thus a function of the wave period, incident wave power, and tide level (Stewart, 1993). Furthermore, no single level of damping will optimise the performance of the column in every individual sea although there will be a global optimum which will maximise the output over a range of mixed frequency seas, i.e. over a prolonged period.

Turbine Performance

Assuming conservation of mass flow, the damping, B_A, applied to the OWC by the turbine can be expressed as:

$$B_A = \Delta P_0 \frac{A_C}{V_C} = \Delta P_0 \frac{A_C^2}{A_A V_A}, \tag{6.4}$$

where A_c and A_A are the cross-sectional areas at the water column surface and turbine duct respectively, and V_c and V_A are the respective air velocities. Eq. (6.4) assumes that the airflow is incompressible as the turbine Mach numbers have been restricted through design to values of less than 0.5, particularly for the highest velocity vectors experienced at the blade outer tip position. The same equation can be expressed in terms of the turbine damping ratio: $B_R = \frac{P*}{\phi}$, where $P*$ and ϕ are the pressure and flow coefficients, respectively (both non-dimensional). This leads to Eq. (6.5) and with further manipulation to Eq. (6.6):

$$B_A = 4\rho_W \left(\frac{A_C^2}{A_A}\right) U_t \left(\frac{P^*}{\phi}\right); \tag{6.5}$$

$$B_A = \tfrac{1}{2}\pi\rho_W \omega D_t^3 A_R^2 (1-h^2)\left(\frac{P^*}{\phi}\right), \tag{6.6}$$

where the tip diameter is given by: $D_t = \frac{2U_t}{\omega}$, the column-to-duct area ratio is: $A_R = \frac{A_C}{A_A}$, the turbine duct area is: $A_A = \tfrac{1}{4}\pi D_t^2 (1-h^2)$, and the hub-to-tip ratio is: $h = \frac{D_h}{D_t}$, where subscripts *h* and *t* denote the hub and tip radii respectively. Figure 6.3 plots Eves empirically based characteristic of B_R against the number of rotor planes N_p and each plane's solidity *S*, shown as a dashed line (Eves, 1986); an additional solid curve is plotted following relationship:

$$\frac{P^*}{\phi} = 0.525 N_p \tan\left(\frac{\pi}{2} S\right), \tag{6.7}$$

where $S = \frac{A_B}{A_A}$, A_B is the total blade area in plan view per plane, and correlation factor = 0.525. However, the empirical results are taken from small-scale results and therefore designers would be expected to adjust the correlation coefficient upward, in order to take into account the scale effects due to the variation in Reynolds Number Re. The Reynolds Number is based on the chord length *c* and is de-

fined by: $Re = \frac{Vc}{\upsilon}$, where V is the relative airflow velocity and $\upsilon = 1.5x10^{-5}\ m^2/s$ is the kinematic viscosity of air.

The original coefficient was estimated from steady state model tests (Eves, 1986) that were carried out at a mid-span (average) Reynolds Number of $Re_{mid-span} = 1.5x10^5$ while other authors correlated their higher Reynolds Number work, as shown in Fig. 6.3. The new model results (Curran and Gato, 1997) shown were performed at $Re_{mid-span} = 5.5x10^5$ and are denoted by the clear diamonds. They also included data from the Islay prototype turbine acting in random oscillating flow denoted by the solid circles in Fig. 6.3, including two sets of conditions at $Re_{mid-span} = 1.2x10^6$ and $Re_{mid-span} = 2x10^6$, referred to as 0012 Islay and 0015 Islay respectively, in reference to the NACA 0012 and NACA 0015 blade profiles used. Consequently, the authors adjusted the correlation factor from 0.342 to 0.525, as shown by the dashed and solid curve fits in Fig. 6.3 respectively. They have assumed the mathematical form of the original Eves (1986) correlation work, as there are insufficient larger scale data to warrant change from a trend so readily evident at small scale. It is significant that Fig. 6.3 shows that the damping ratio was higher than that seen at small-scale, due to the effects of increased life realised at higher Reynolds Numbers. Consequently, air turbines that are designed with Eves correlation would over-damp the system and although the OWC is less sensitive to this, it would affect the optimal range of flow conditions for the intended wave conditions.

Eqs. (6.6) and (6.7) can be substituted to give Eq. (6.8), leading to Eq. (6.9) (noting that r_t and A_R are interrelated):

$$B_A = 0.2625\omega D_t^3 A_R^2 N_p (1-h^2) \tan\left(\frac{\pi}{2} S\right); \tag{6.8}$$

$$B_A = f(\omega, r_t, A_R, N_p, h, S). \tag{6.9}$$

Single aerofoil theory suggests that a Mach Number of 0.5 ($M = \frac{V}{a}$, where V is the relative air velocity and a is the speed of sound) is a reasonable free stream Mach number at which localised sonic conditions may be considered to be influential. Additionally, airflow cannot be assumed to be incompressible at higher values of M and so this value is a constraint at the blade tip, which consequently determines the maximum turbine diameter. Alternatively, the operational Re of the turbine must be high enough to ensure that the full potential of the blades' aerodynamic performance is realised.

Finally, given that the pneumatic power generated by the OWC is expressed by:

$$W_{pneumatic} = \Delta P_o Q = B_A V_A A_R^{-1}. \tag{6.10}$$

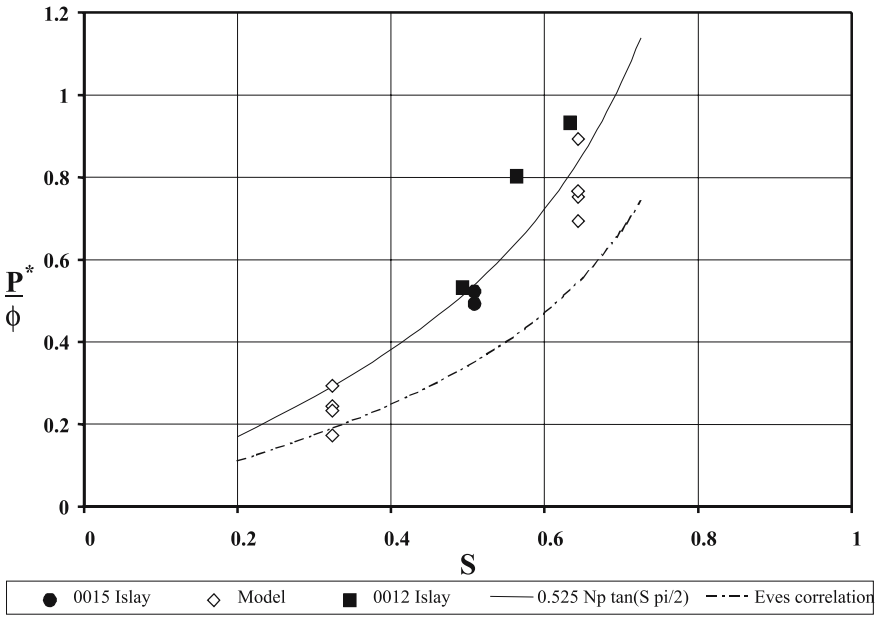

Fig. 6.3. Correlation of large scale results for prediction of the damping ratio

Eqs. (6.4), (6.8) and (6.10) can be used to show that the total power output of the turbine is:

$$W_{converted} = \eta W_{pneumatic} = \eta \left[0.265 \omega D_t^3 A_R N_p (1 - h^2) \tan\left(\frac{\pi}{2} S\right) \right] V_A , \qquad (6.11)$$

where η and V_A are instantaneous values of turbine efficiency and axial air velocity which are determined respectively, by the turbine efficiency characteristic and the flow distribution generated by the OWC.

System Optimisation

It is necessary to design a system with a level of applied damping which represents the global optimum in order to achieve the maximum accumulated value of energy converted from incident wave energy, with reference to Eq. (6.11) and Eq. (6.3). The latter tends to be the constraint that determines the lower threshold for the applied damping, as evident in Fig. 6.1. However, there is a considerable range above this value where the performance of the OWC is relatively insensitive to the level of applied damping. Figure 6.1 also shows that there is a level of damping above $B_{A_{OPT}}$ which can be beneficial in mixed seas. Therefore, a range of damping levels above the theoretical optimal value $B_{A_{OPT}}$ should be investigated in order to maximise the potential conversion determined ultimately by Eq. (6.11) for the turbine.

There are a number of additional energy losses incurred at the turbine-generator stage on a plant which need to be considered. The turbine converts pneumatic power into mechanical power that is reduced by further downstream losses prior to electrical power export, where the total instantaneous converted power is given by:

$$W_{converted} = W_{elect} + W_L + W_{inertial}, \tag{6.12}$$

where W_{elect} is the exported electrical power, W_L is the total power losses and the inertial power $W_{inertial}$ is given by $W_{inertial} = \frac{dE_{inertial}}{dt}$, where $\mathrm{E}_{\mathrm{inertial}} = \frac{1}{2} I \omega^2$ and I is the combined inertia of the turbine-generator unit. Apart from the mass of the turbine-generator unit the amount of inertial energy $\mathrm{E}_{\mathrm{inertial}}$ stored instantaneously will also depend on the resistance of the electrical generator and the degree of power smoothing required to meet the electrical supply specifications. However, with regard to Eq. (6.12), $\frac{dE_{inertial}}{dt} \to 0$ when optimising over a sufficiently lengthy period of time.

The losses W_L can be further divided into the hub windage losses $W_{Lwindage}$, and the generator losses $W_{Lgenerator}$:

$$W_L = W_{Lwindage} + W_{Lgenerator} + W_{Bearings}. \tag{6.13}$$

The mechanical bearing loss $W_{Bearings}$ is very small but can be added for completeness. The hub windage loss can be estimated by using the well known equation for the skin friction drag. For a unit width section of thin plate, the drag force produced by an air flow over the surface is given by: $F_D = \frac{1}{2}\rho V^2 l C_f$, where C_f is the friction coefficient and l is the length of section. Therefore, for a turbine hub, the drag losses can be calculated incrementally in annular rings of width δr, where the total windage loss will be equal to the integral between the hub's centre, $r = 0$, and hub's outer radius, $r = r_h$. The length is given by the circumference of each annular strip while the radial increment δr is equivalent to the plate width. Therefore, the estimate of the hub windage (where $W_{Lwindage} = T\omega$ and the torque T is $T = F_D r$) is given by integrating with respect to radius:

$$W_{Lwindage} = N_p \rho_W \omega^3 \pi C_f \int_{r=0}^{r_h} r^4 dr, \tag{6.14}$$

where $W_{Lwindage}$ is the total power loss due to hub windage (blade drag uses chord length c rather than circumference $2\pi r$ and it is multiplied by the blade number) between the shaft and the hub's outer radius, on one side of the rotor.

The generator losses $W_{Lgenerator}$ are primarily incurred due to the machine's iron loss and copper loss. The iron losses are fixed and are determined by the power rating of the particular machine being used and can be approximated to 2.5 % of the

generator's power rating. The generator's copper loss varies according to the square of the stator current, which in-turn is a function of the power output and load voltage. Typically, the copper loss increases to a maximum of approximately 1 % of the generator rating at full rated load, and consequently could be approximated to an average value of 0.5 % of the rating, corresponding to the generator operating on average at half the power rating. Cumulatively, the generator losses can be approximated to:

$$W_{L\,generator} = 0.03R\,, \tag{6.15}$$

where R is the generator rating.

The total amount of energy E_{total} which has been converted, during the time period t_1 to t_2, is given by: $E_{total} = \left[\sum_{t_1}^{t_2}\left\{E_{converted} - E_{losses}\right\}\right]$. Therefore, it can be seen that the equation which expresses the value of power being exported instantaneously W_{elect} must be optimised over the range of flow velocities at the plant in order to maximise E_{total}:

$$W_{elect} = \left[\eta B_A V_A A_R^{-1}\right] - \left[W_L\right]. \tag{6.16}$$

It can be conclude that for a turbine operating at a particular speed, the key design drivers are the instantaneous turbine efficiency, the axial flow velocity (i.e. energy levels) and the optimal applied damping. This establishes turbine applied damping B_A as one of the primary design parameters that actually maximises the potential system's power conversion. For the other two drivers, the turbine efficiency characteristic is pre-determined by the initial turbine configuration and the air velocity is governed by the incident wave power regime and the OWC's efficiency characteristic. Eq. (6.16) represents an objective function based on performance which could be used in the optimisation procedure although a minimal of cost per unit of energy output would be the ultimate objective.

System Improvement

Wave energy conversion systems would benefit greatly in terms of overall performance with control strategies and other techniques that react to the system's conditions in order to maximise the power output, according to Eq. (6.16). A simple limiting technique is to use a blow-off valve that can be opened in order to release energy from the system at a specified limiting value of pneumatic power. Effectively, this reduces the flow velocity to the range over which the turbine most efficiently converts power. Alternatively, a variable speed generator could be used so that the rotational speed can be increased during the larger sea states, and vice-versa in the smaller sea states, over an incremental range to be specified (Justino and Falcão, 1998; Sarmento et al., 1990). The principle utilised in the control strategy is that the applied damping increases with the increase in speed, according to Eq. (6.8), which leads to a reduction in the flow rate, which results in the turbine remaining at a more efficient angle of attack. However, it should be noted

that these conversion gains at the turbine-generator stage may be offset by a negative impact on the performance of the OWC, as described by Figs. 6.1 and 2.2, due to the strong performance coupling previously described.

6.1.3 Air Turbine Design Configurations

The Wells Turbine

Many of the plants built to date around the world have tended to be Oscillating Water Columns with a Wells turbine-generator power take-off. The various OWC concepts and configurations (Count, 1980; Salter, 1988; Curran, 2002) couple in a similar manner to the Wells turbine with regard to the matching strategy relative to the hydraulic performance. The Wells turbine utilises symmetrical blades located peripherally on a rotor at 90 degrees stagger to the airflow so that an alternating airflow drives the rotor predominately in a single direction of rotation (Raghunathan et al., 1985; Inoue et al 1987; Gato and Falcão, 1989). The axial air velocity at the turbine combined with the rotational velocity determines the relative velocity and angle of attack onto the turbine blades, typically of a symmetrical NACA profile (Jacobs and Sherman, 1937). Aerodynamic lift and drag forces are generated perpendicular and parallel respectively, to the relative velocity and can be resolved into resultant axial and tangential forces in the direction of flow and rotation respectively. Relevant to the aerodynamic performance of the turbine blades has been the considerable increase in the use of Computational Fluid Dynamics (CFD) tools to investigate the physics of the blade profile interaction with the air flow. This has included work into the optimisation of the blade profile (Gato and Henriques, 1994), investigation of the 3-D turbine aerodynamics (Thakker et al, 1994; Dhanasekaran and Govardhan, 2005) and detailed investigation of the design (Watterson and Raghunathan, 1997).

A Wells turbine rotor (see Fig. 6.4) consists of several symmetrical aerofoil blades set around a hub at an angle of 90 degrees with their chord lines normal to the axis of rotation. For absolute air flow velocity, V_a, which is axial at the inlet and tangential rotor velocity, U_t, at a radius, r, from the axis of rotation, the relative velocity, W, is at an angle of incidence, α, to the blade chord. This will generate a lift force, L, and a drag force, D, normal and parallel respectively to the relative velocity, W. These forces can be resolved into tangential and axial directions to the rotor given by:

$$F_T = L\sin\alpha - D\cos\alpha\,, \tag{6.17}$$

and

$$F_X = L\cos\alpha + D\sin\alpha\,. \tag{6.18}$$

For a symmetrical aerofoil in an oscillating airflow, the magnitude of F_T and F_X, will vary during a cycle but the direction of F_T will remain the same, being independent of reciprocating flow. However, at the very lowest flow rates F_T will be negative due to the aerodynamic drag on the blades and also at the very highest flow rates where lift has been lost due to boundary layer separation. For a turbine

which is well matched to the sea distribution, F_T will result in the generation of positive torque and power for the majority of the wave cycle. Furthermore, the stalling action of the aerofoils will act as a limiter during extreme wave conditions. The normal component, F_X will result in an axial thrust force which has to be borne by suitable bearings. The expressions for F_T and F_X are given in dimensionless coefficients C_T and C_X, where:

$$C_T = C_L \sin\alpha - C_D \cos\alpha , \tag{6.19}$$

and

$$C_X = C_L \cos\alpha + C_D \sin\alpha . \tag{6.20}$$

The lift and drag are subject to 3-D flow (Horlock, 1956) and it has been shown that the blade performance varies considerably from the corresponding single aerofoil data (Curran et al., 1998) due to interference effects between turbine blades (Raghunathan and Beattie, 1996). In general drag dominates over lift at the lowest angles of attack, after which lift prevails to a maximum value at the stalling incidence, at which point the boundary layer separates from the blade surfaces leading to loss of lift and a rapid increase in the dominance of drag on performance (Abbot and Von Doenhoff, 1959). The forces which determine the driving force are always resolved in the same direction of rotation, due to the blade symmetry, but the resultant axial force alternates during the wave cycle and needs to be borne by axial thrust bearings.

It is evident from Fig. 6.5 that the operational region of the Wells turbine is poor at low angles of incidence, nominally 0–18 degrees, i.e. $\approx 0\text{-}\alpha_{stall}$. The performance characteristic in this region is therefore of utmost importance in terms of turbine design. The main performance parameters are efficiency, pressure drop

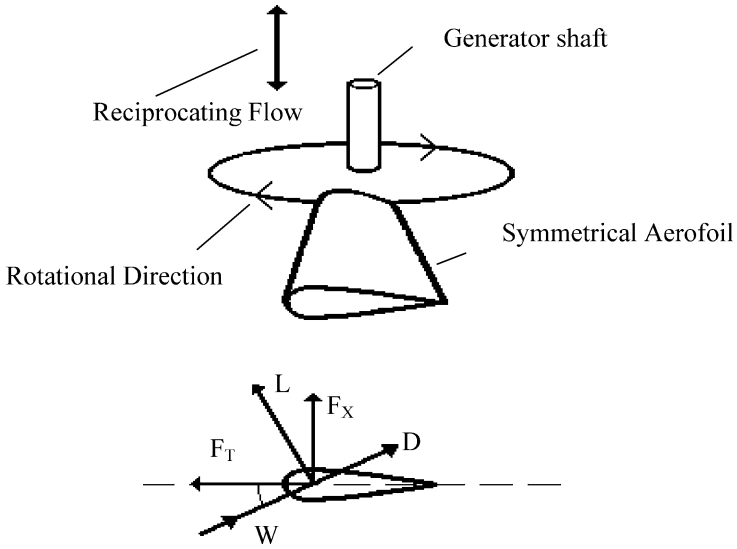

Fig. 6.4. Principle of operation of the Wells turbine

and torque. The aerodynamic characteristics of an aerofoil blade and therefore the Wells turbine are strongly dependent on the incidence of the airflow onto the blade. This can be observed from the experimental results shown in Figs. 6.5 and 6.6 for monoplane and biplane Wells turbines.

The frequency of bi-directional and random air flow in a wave energy device is very low, e.g. nominally 0.1 *Hz*, and therefore the air flow through the device is normally assumed to be quasi-steady. The values of efficiency and pressure shown are regarded as instantaneous values with respect to flow ratio or air flow incidence. The results show typical variation of η and Δp_0^* with ϕ. For a given rotor speed, p^* was proportional to the pressure drop across the rotor, Δp, and ϕ was proportional to the flow rate, Q. For a Wells turbine rotor, a linear relation-

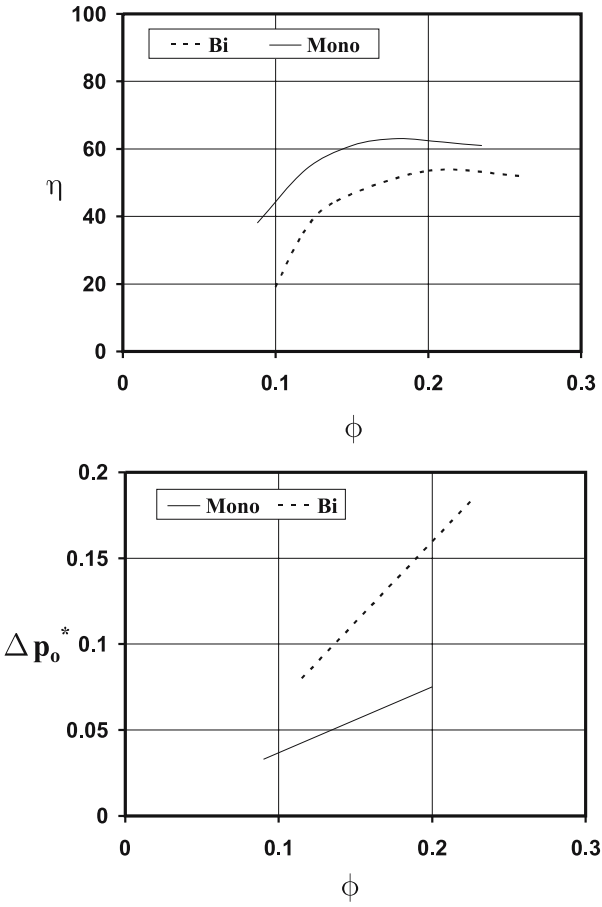

Figs. 6.5 and 6.6. Non-dimensional efficiency and pressure drop relative to the flow coefficient for the monoplane and biplane Wells turbines, respectively

ship exists between pressure drop and flow rate, except for very low flow rate values. This is true for a turbine either with low or high solidity and for both a monoplane or biplane turbine. A linear pressure drop-flow rate characteristic is well suited for matching the turbine with a wave energy device which uses the principle of the oscillating water-air column. A constant value of damping produced by the turbine can be chosen to optimally damp the OWC according to the chamber geometry and the incident wave conditions. Also, the variations in flow are minimised if one compares the ratio to that of an orifice damper which shows an exponential relation.

The aerodynamic efficiency, η, increases with ϕ up to a certain value after which it decreases. The reason for this is that at higher values of flow incidence the boundary layer on the aerofoil blades tends to separate and subsequently fully separate, there-by increasing the drag and reducing the lift. The phenomenon of flow separation, known as turbine stall, can be severe and could in extreme circumstances cause the driving torque to become negative. This is rather more gradual on thick aerofoils and so results in a more gradual drop in η with ϕ. Therefore, a Wells turbine with thick aerofoils will be able to operate over a wider range of flow rates without a significant drop in performance. At very small values of ϕ the efficiencies are negative. In oscillating airflow it can be shown that the power absorption at small incidence is a small proportion of the total power output if the turbine is well matched to the pneumatic power distribution. The time averaged cyclic efficiency has been shown to be typically 5–10 % lower than the peak efficiency of a cycle. However, there will be periods when it no longer becomes viable to operate the system as the power imported to overcome the system losses out-weighs the converted power.

The pressure-flow ratio or damping relation is related to the axial force generated, where for lower angles of attack the axial component is largely determined by the linear lift component (Curran et al., 1998). As mentioned earlier, the pneumatic energy level that any turbine accommodates varies with configuration, including solidity, size and speed, while further performance deviations will also be evident in the stall region. One turbine configuration may show an increased damping level in the post-stall region, such as for the guide-vane design, while another may show a decrease, as evident with the variable-pitch design, while that of the counter-rotating configuration remains relatively constant. It is beneficial to at least maintain the pressure-flow ratio into the stall region as this tends to restrict the flow rate to values that are closer to the turbine's efficient performance range. Some of these considerations are addressed further along this section, which compares the long-term productivity of a number of advanced Wells turbine configurations.

Advanced Wells Turbine Configurations

The following sections introduce a number of variations to the basic Wells turbine configuration that can be termed advanced configurations. The productivity of these configurations needs to be predicted in order to facilitate practical comparison. Such comparison has hitherto been difficult to undertake as nothing short of a

full productivity analysis fails to fully address the productivity expectations of the turbine types. Classically, wave energy turbines have been compared in terms of their efficiency over a flow range (Curran and Gato, 1997). However, the pressure drop and resultant pneumatic energy range over which the turbines operate may vary greatly for like flow ranges. Furthermore, the efficient conversion of power determines economic feasibility and consequently is a more practical basis for comparison. It was assumed that the turbines operate in the same typical pneumatic power distribution but that in each case, the turbine's sizing can be optimised to maximise that configuration's output. A comparison of the results for torque, pressure drop and efficiency is shown in Figs. 6.7, 6.8 and 6.9 respectively.

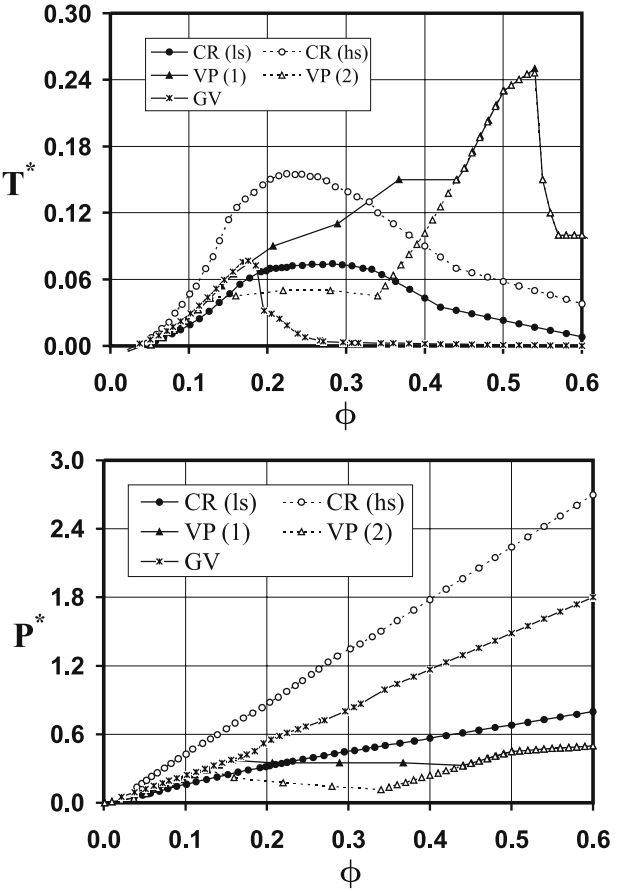

Fig. 6.7 and 6.8. Non-dimensional torque and pressure drop relative to the flow coefficient for the low (ls) and high solidity (hs) Counter-rotating turbine (CR), variable pitch turbine (VP) with two control strategies, and guide vane Wells turbine (GV)

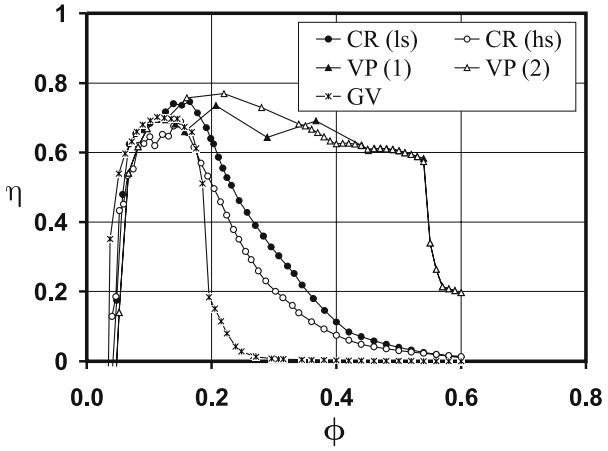

Fig. 6.9. Efficiency relative to flow coefficient for the low (ls) and high solidity (hs) Counter-rotating turbine (CR), variable pitch turbine (VP) with two control strategies, and guide vane Wells turbine (GV)

Variable-Pitch Monoplane

In principle, a variable-pitch turbine limits the angle of attack by rotating the blade about its radial axis so that the turbine can maintain an efficient angle of attack, requiring a control strategy for pitch-control that can also be implemented at the lowest flow rates (Gato and Falcão, 1989). However, the pitching process also reduces the effective solidity of the turbine and consequently the concept is disadvantaged by the need to pitch ever further to meet the increased flow induced by the pitching action, a direct consequence of the reduced damping ratio (Curran and Gato, 1997). Due to the variation in the damping ratio, it is not clear to what degree the turbine's instantaneous efficiency or torque output should be the driving variable that determines the required pitch angle. The turbine blades can be pitched when the torque produced by the turbine begins to fall substantially at stall and thereafter the pitching rate can be made to match that of the angle of attack, i.e. equivalent-angle control. Alternatively, the blades can be pitched in order to always maximise efficiency rather than just maintain torque at stall.

The equivalent angle method is denoted by *VP1* in Figs. 6.7 through 6.9, while the maximal efficiency method is denoted by *VP2*. It was found that the maximal efficiency method pitched at a substantially lower flow rate of $\phi = 0.13$ than that of the equivalent-angle method where $\phi = 0.165$. Furthermore, the pitch rate was greater where the rate of *VP1* was equal to the increase in the angle of incidence over that of stall. It should be noted however, that the intention of the study was not to find the exact optimal control mechanism but to determine which control

method was more likely to maximise productivity. Additionally, the performance at the more extreme stall flow rates had to be estimated as the experimental data did not extend over the full range necessary for analysis. A comparison of the results shown in Figs. 6.7 and 6.8 shows that the equivalent angle method did maintain the torque and pressure levels respectively, while Fig. 6.9 shows that the efficiency was actually lower than for the maximum efficiency method. It is clear from the results that the variable-pitch turbine operates with high efficiency over a significantly greater flow range in contrast with the other configurations being investigated (introduced in the following sections), although the pressure drop remains low after the pitch control is initiated.

Fixed Guide-Vane Monoplane

The main aim of a fixed guide vane configuration is to maximise the turbine's conversion efficiency over a limited but optimal flow range, while forfeiting conversion at more extreme flow rates. Consequently, this configuration has a smaller operational flow range outside of which the performance is poor due to flow separation off the guide vanes at those angles of attack not accommodated in the aerodynamic design of the vanes. The guide vanes are used to optimally direct the airflow to and off the blades for a given profile, thereby also ensuring axial airflow from the turbine and minimal air-swirl losses for the exit stage. Moveable guide vanes are not considered but offer the possibility of optimising the upstream and downstream vane angles, whereas fixed vanes must be deployed in a symmetrical and compromised orientation. The rotor of any air turbine imparts a swirl component to the airflow due to the viscous interaction of the blade surface on the air particles. Consequently, in a similar level of complexity to the variable-pitch turbine, the vanes could be controlled by a pitching mechanism although this additional capability is generally deemed to be not worth the extra complexity and cost, in both non-recurring and maintenance terms. The sharp decrease in torque output at stall due to the limiting vane angle is very evident in Fig. 6.7 but it can also be seen from Fig. 6.8 that there is a slight increase in the damping ratio.

Counter-Rotating Biplane

The main turbine performance issue being addressed in the counter-rotating configuration is the recovery of air swirl exiting the turbine. It was noted above that the rotor of a Wells turbine imparts a swirl component to the airflow relative to the work done. However, an alternative to utilising guide vanes is to rectify the swirling airflow with the opposing action of a counter-rotating downstream rotor. This alternate concept also has an added attraction in benefiting from the favourable interaction evident between the rotors during turbine stall, resulting in a more gradual loss of efficiency. Another major feature of multi-plane machines is the wide range of damping ratios and pneumatic power levels that can be accommodated. Both high and low solidity counter-rotating configurations were tested and are included in Figs. 6.7 through 6.9. It is readily evident that a change in solidity re-

sults in a significant variation in the performance and that the efficiency decreases as solidity is increased. Notwithstanding, the performance characteristics are regular with a reasonable range in efficiency relative to flow rate.

Impact on Productivity

The predicted annual distribution of pneumatic power is presented in Fig. 6.10 in terms of occurrence and actual contribution to power (converted power, W). The latter is given in terms of contribution to pneumatic power rating where the sum is the annual rating while multiplying across by time yields the contribution to energy. It is evident that the most frequent power band to occur, $400\,kW$, is actually lower than the average figure of $500\,kW$ and that the highest power band is almost four times the average. Figure 6.11 presents an example of the relation of pneumatic power to converted power for the low solidity counter-rotating turbine while Fig. 6.12 presents the conversion results for all configurations.

Figure 6.11 shows that the lower distribution of converted power mirrors the shape of the pneumatic power distribution as the turbine is well designed to operate efficiently over the range of pneumatic power levels. The distribution of converted power would become more skewed if the diameter was inappropriate and provided unsuitable flow rates at the pneumatic power bands that contribute most energy, i.e. through mismatching. Figure 6.12 is surprising as there is little to distinguish one turbine from another, especially considering the variation that was so prominent in Fig. 6.9.

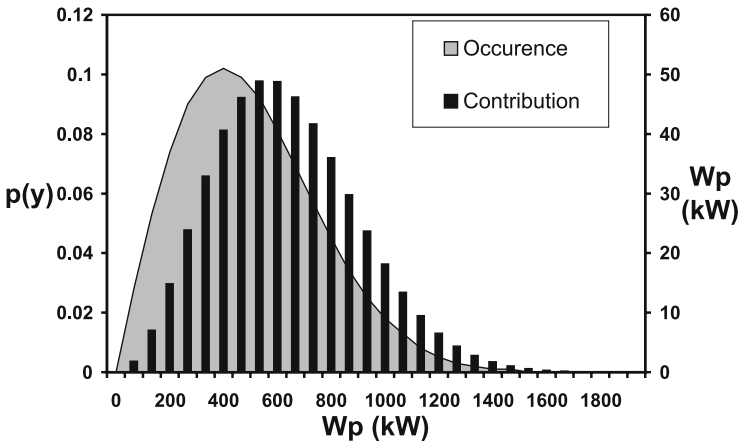

Fig. 6.10. Comparison of pneumatic power occurrence and actual contribution

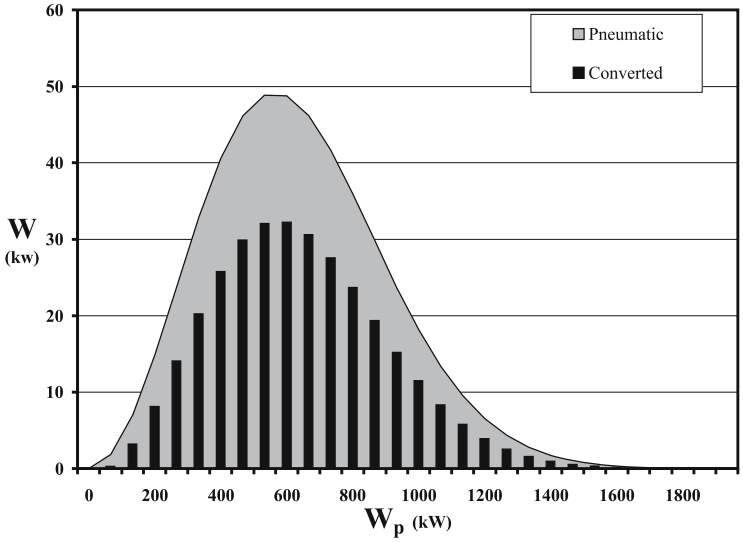

Fig. 6.11. Comparison of pneumatic and converted power for the low solidity counter rotating turbine

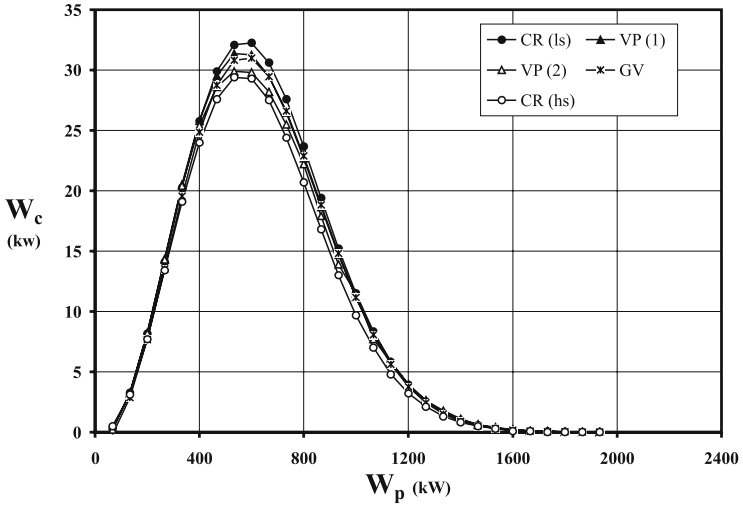

Fig. 6.12. Comparison of converted power for several configurations

It can be seen that the high solidity counter-rotating turbine was least efficient over the majority of the power bands and that the other turbines only really differed in mid-range. The low solidity counter-rotating turbine achieved the highest efficiency of 64 % while the equivalent-angle pitching turbine was next with 62 %. However, one must consider the pneumatic power range within which the turbines operate in order to understand why the variable pitch turbines were not superior, given the considerably wider range of efficient flow rates suggested by Fig. 6.9. Therefore, the torque and efficiency of the turbines can be considered relative to a coefficient that incorporates pneumatic power, as suggested through Eq. (6.21):

$$\Pi_p = \frac{W_p}{\pi \rho_A \omega^3 R_t^5 \left(1 - h^2\right)}. \tag{6.21}$$

The torque and efficiency from Figs. 6.7 and 6.9 was re-plotted and is presented in Figs. 6.13 and 6.14 respectively, where the first is divided to facilitate more detailed inspection of the efficiency at the more congested power points. Comparing Figs. 6.10 and 6.13 highlights the direct relation between torque output and pneumatic power input, and that all turbines generate similar levels when operating at lower power coefficients, although the variable pitch turbines have considerably superior range. Also, it is interesting to note that the higher efficiencies of *VP (2)* now cover a much smaller operational range when pitching due to the reduced pressure drop evident from Fig. 6.8, resulting in the pneumatic power remaining relatively constant.

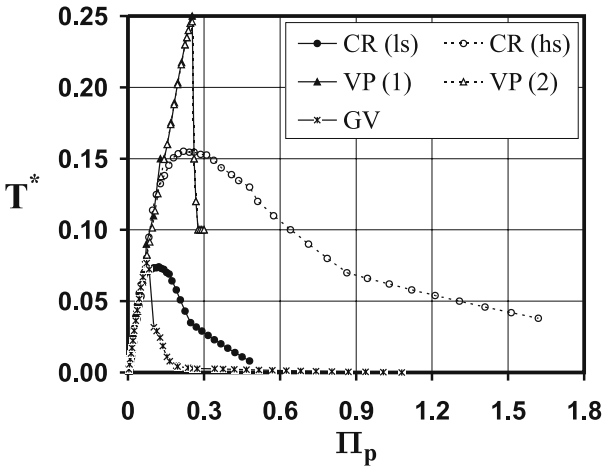

Fig. 6.13. Comparison of torque and pneumatic power conversion

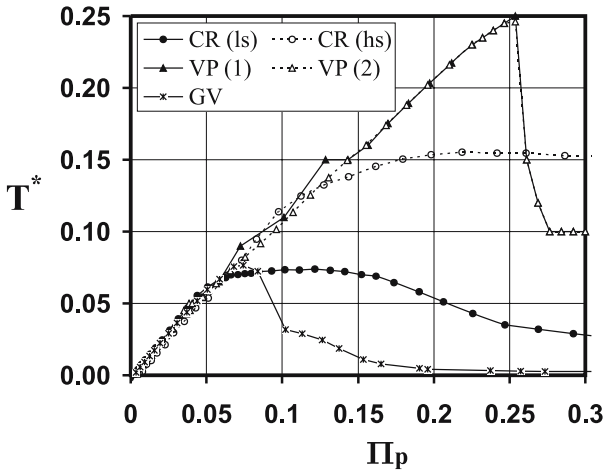

Fig. 6.13. a Comparison of torque and pneumatic power conversion (zoom on the horizontal axis)

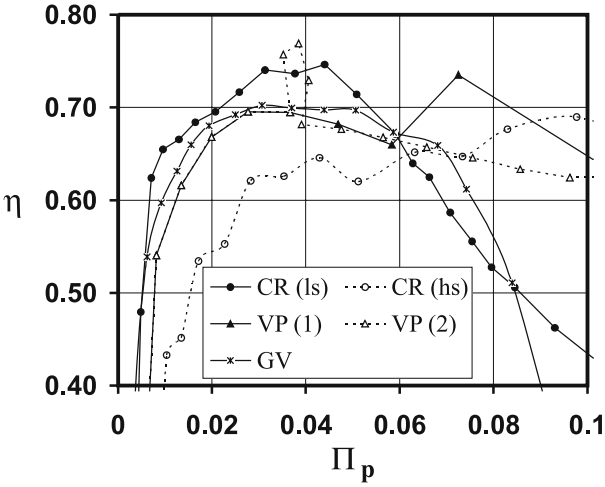

Fig. 6.14. Comparison of efficiency and pneumatic power conversion

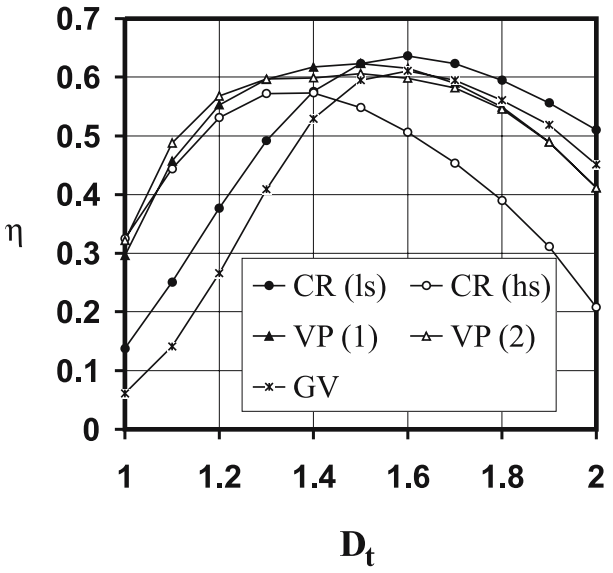

Fig. 6.15. Effect of diameter change on overall efficiency

Figure 6.15 presents the variation in efficiency with tip diameter in order to show the degree of sensitivity in the determination of the optimal diameter that maximises productivity. However, the figure is also representative of the sensitivity to power fluctuations to a change in either diameter or input pneumatic power, which will have the same ultimate effect in causing the air velocity and angle of attack to change, as evident in Eq. (6.13). It can be seen that as expected the variable pitch turbines is the least sensitivity while in all other cases slightly higher tip diameters would present a more robust design, as the characteristics are more steeply sloped towards the lower values.

Impulse Turbines

The use of a self-rectifying impulse turbine for wave energy conversion was first suggested in 1988 (Kim et al., 1988). The axis of rotation of the self-rectifying impulse turbine is aligned with the principle direction of air flow within a duct, with guide vanes used to deflect the flow onto the rotor as shown in Fig. 6.16. To maximise the power capture the setting angle of the upstream and down stream guide-vanes needs to be different, which due to the oscillatory nature of the flow means that the guide vanes would ideally move to provide the optimum setting angle depending on the instantaneous direction of flow. This has been achieved by using pivoting guide vanes that use the aerodynamic moment induced by the movement of the air to change the setting angle both upstream and downstream of the rotor, denominated “self-pitch-controlled” guide vanes. Potential problems

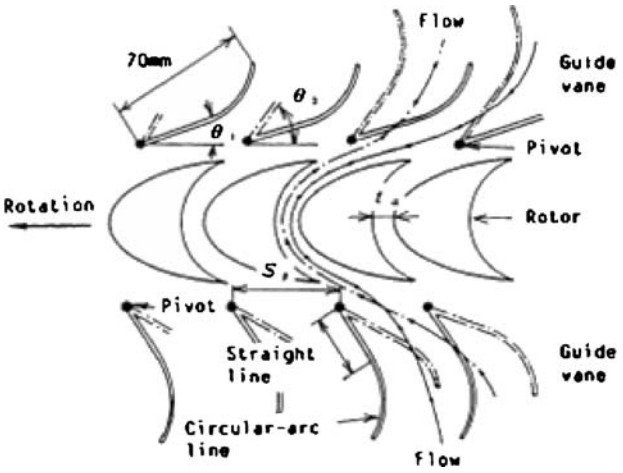

Fig. 6.16. Self-rectifying impulse turbine (Setoguchi et al., 2001)

with maintenance of such a complex mechanism led to the mechanically simpler, though fundamentally less efficient solution, where the guide vanes do not move, leading to the denomination of "fixed" guide vanes (Maeda, 1999).

In addition to the classification of "self-pitch-controlled" and "fixed" guide vane configurations, it is possible to sub-divide the "self-pitch-controlled" guide vanes into "mono-vane" and "splitter" types. In "mono-vane" type guide vanes the whole vane moves around the pivot, whilst for "splitter" type guide vanes only the section of guide vane closest to the rotor moves, engaging with stationary curved stators; for "fixed" guide vanes plate and aerofoil type guide vanes have been investigated (Setoguchi et al., 2001). A further modification to the design of the guide vanes has also been made by linking the two sets of guide vanes so that they move together. This was done because it was found that at times the downstream guide vanes did not move appropriately in response to the aerodynamic couple experienced (Setoguchi et al., 1996). In addition to these differences in the design of the guide vanes, it is also possible to vary the number, setting angles and dimensions of the guide vanes to provide an infinite number of possible guide vane arrangements. Although these different guide vane configurations have some influence on performance as discussed in Setoguchi et al. (2001), it has been found that the critical parameters are the upstream and downstream setting angles and the guide vane length to pitch ratio. For "self-pitch-controlled" guide vanes the optimum upstream setting angle is 15 to 17.5 degrees, the optimum downstream setting angle is 55 to 72.5 degrees and the guide vane pitch to length ratio should be less than 0.65. For "fixed" guide vanes the optimum setting angle is 30 degrees.

Prior to discussing the specific performance of self-rectifying impulse turbines, it is useful to outline their general characteristics relative to the Wells turbine, against which they are typically compared. Unfortunately this simple comparison has been complicated by the use of different turbine configurations by different re-

search teams so that comparisons using readily available data cannot easily be made. In particular there are large differences between different research teams on the cyclic efficiency of the Wells turbine. However, the following differing characteristics are generally accepted:

- The optimum flow coefficient of the impulse turbine is significantly larger than that for the Wells turbine;
- The impulse turbine is self-starting, whilst the Wells turbine has poor starting characteristics;
- The impulse turbine has no stall condition thereby maintaining relatively high efficiency at high flow coefficients, unlike the Wells turbine that has a clear stall point;
- The pressure – flow relationship of the impulse turbine is non-linear, unlike the Wells turbine that has an almost linear relationship.

The larger optimum flow coefficient of the impulse turbine means that for the same power the turbine is smaller and spins at a slower angular velocity than a similarly rated Wells turbine. Coupled to the absence of stall, this means that typically the impulse turbine is quieter than the equivalent Wells turbine. In addition, the slower rotational velocity means that windage losses of the impulse turbine are likely to be smaller, whilst the potential for energy storage using a directly coupled flywheel is reduced. While these factors are unlikely to have a large effect on the power output the turbine, they may have a large influence on design, which means that certain circumstances may dictate the choice of the turbine largely irrespective of their differences in performance. For example, the lower noise generation of an impulse turbine may make it more suitable for locations with a mixed use, such as breakwaters, where the noise generated could be a nuisance to people working nearby. Conversely, if steadier power generation is required then the Wells turbine may be preferred due to its larger potential for energy storage, which could be used to smooth the power output.

The pressure – flow relationship of a turbine influences the damping applied to the motion of the water column and thereby influences the amount of energy extracted by the oscillating water column plant. At any instant there is an optimum amount of damping that should be applied to the water column to maximise the power capture. In small amplitude monochromatic waves the optimum damping condition equates to a linear relationship between the water column velocity and damping force. This is achieved with a linear pressure – flow relationship, implying that the Wells turbine has more suitable characteristics for wave energy conversion. However, the optimum relationship differs for the oscillating water column when it is subjected to more realistic wave conditions, although determining what constitutes the optimum relationship cannot easily be defined, varying with the particular wave characteristics and oscillating water column design. It remains unclear if in realistic conditions whether the pressure – flow characteristics of the Wells turbine remains superior, or whether the impulse turbine characteristics are typically more suitable.

Figure 6.17 illustrates the typical characteristics for an impulse turbine. For this particular configuration it can be seen that the peak efficiency of the turbine is approximately 60 %, with a broad bandwidth of high efficiency due to the absence of stall in an impulse turbine. In oscillating and realistic flow conditions, this broad bandwidth translates into a relatively high efficiency of 48 % for an impulse turbine with self pitch controlled guide vanes and 35 % for an impulse turbine with fixed guide vanes (Setoguchi et al., 2001).

In addition to the experimental work that has been described above, computational fluid dynamic studies have also been performed to investigate the performance of impulse turbines (Thakker and Hourigan, 2005). CFD studies have enabled the design of impulse turbines to be focused on two important effects: the tip clearance losses (Thakker and Dhanasekaran, 2003) and the guide vane losses (Thakker and Dhanasekaran, 2005). As would be expected the efficiency of the turbine decreases as the tip clearance increases due to increased leakage around the rotor. However, the CFD models indicate that if the tip clearance is less than 1 % of the rotor diameter then the losses are negligible, whilst for tip clearances greater than 4 % the effect on efficiency is negligible, though by this point the peak efficiency has reduced by approximately 25 %. CFD studies on the effect of guide vanes have so far concentrated on the fixed guide vane configuration. These studies have shown that whilst the upstream guide vane accounts for a minimal amount of pressure drop, the downstream guide vane can account for a large proportion of the pressure drop leading to a reduction in efficiency.

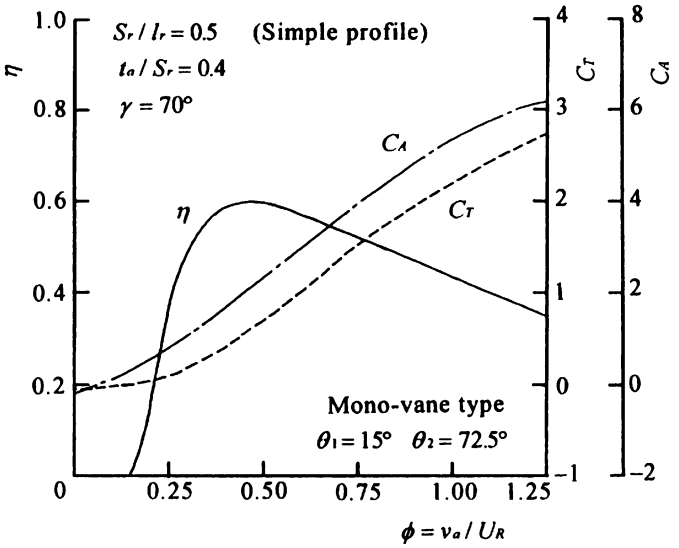

Fig. 6.17. Typical impulse turbine characteristics in steady flow (Setoguchi et al., 2001)

The Denniss-Auld Turbine

The Denniss-Auld turbine was developed at the University of Sydney, Australia in collaboration with the Australian company Energetech who used the turbine in the design of their first plant at Port Kembla (Curran et al., 2000; Finnigan and Auld, 2003; Finnigan and Alcorn, 2003). This turbine is aerodynamic in principle with aerofoil blades that pitch in order to provide an optimal angle of attack, in a similar manner to the variable pitch Wells turbine. However, the blades are located on the periphery of the rotor hub in a neutral position that is parallel to the axial direction of the flow rather than tangential to the direction of rotation as for the Wells and Impulse turbines. Also, the blade profile is symmetrical about the maximum thickness line at half chord as well as being symmetrical about the chord line itself. Consequently, the blade is rotated about its centre of gravity and pitches into the direction of rotation to optimise the angle of attack. The aerofoil shape was determined as that which gave maximum lift at zero incidence and was achieved by merging the two forward sections with NACA 65-418 profiles. This is a laminar flow profile with a maximum camber of 6 % chord and a maximum thickness of 18 % chord.

The performance of the turbine is presented in Fig. 6.18 in terms of the efficiency and pressure drop relative to the flow coefficient (Curran et al., 2000). It can be seen from the efficiency characteristic that the turbine performs at higher flow rates than the Wells and Impulse turbines but otherwise there is a lot of similarity in terms of running losses at the lowest flow rates, a peak efficiency (that is more similar to that of a Wells turbine), and then decreasing efficiency levels at the highest flow rates when losses tend to dominate.

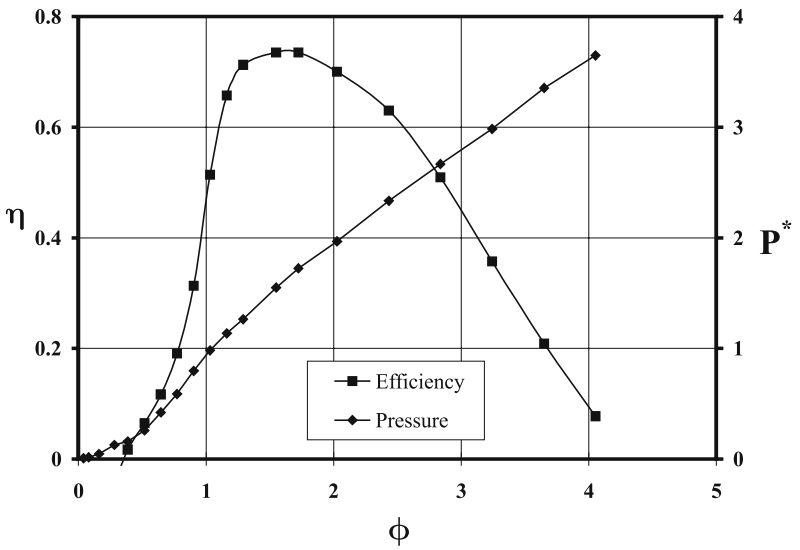

Fig. 6.18. Efficiency and pressure drop against flow coefficient for the Denniss-Auld turbine

6.1.4 Operational Findings for the Wells Turbine

Conclusions and designs derived from numerical and laboratory-based modelling of air turbines can only be partially valid. When a turbine is mounted in an oscillating water column, the real circumstances of its installation will influence its performance in potentially unexpected ways. Invariably, unlike laboratory based turbine testing facilities, the design of the turbine and duct are constrained and modified by constructional and cost factors that are not present with model turbines. From their nature these operational issues are difficult to predict; however an example of the effect of these operational issues is provided by the analysis of the performance of the contra-rotating Wells turbine installed in the LIMPET oscillating water column (Boake et al., 2002).

The turbine duct for LIMPET was fully instrumented so that the pressure drop across any of the valves or turbine rotors could be measured; however, more importantly the duct allowed the insertion of a hot-wire anemometer both upstream and downstream of the contra-rotating turbine, which enabled the flow profile across the duct to be measured and analysed (Folley et al., 2002). The analysis of the flow profiles, together with the information on the pressure drop across the turbine identified two operational issues that were not identified during the laboratory-scale testing. These two operational issues were: the effect of an uneven flow profile during the intake stroke and the reduction in instantaneous turbine torque due to unsteady flow conditions (Folley et al., 2006).

During laboratory testing much care is taken to ensure that there is minimal variation in the flow across the turbine duct. A mesh is typically used to minimise flow turbulence and the wind-tunnel duct taper angles chosen to avoid flow separation in a rapidly diverging duct. Unfortunately, these ´perfect´ conditions are more difficult to achieve on a real plant, with the consequence that the flow conditions for installed turbines are often far from ´perfect´, though results from the $75\,kW$ oscillating water column prototype installed on Islay indicated that Wells turbines were relatively robust when the flow is turbulent due to the presence of control valves within the duct (Whittaker et al. 1997a; 1997b) with a minimal reduction in performance identified. However, high levels of noise from the LIMPET turbine meant that the acoustic attenuation chamber (silencer) the end of the turbine duct had to be re-designed, which whilst generating a minimal additional pressure drop created a large mal-distribution of the intake flow. This is illustrated in Fig. 6.19 (the circumferential positions were approximately evenly spaced with positions 4/5 being at the top of the duct), with the flow at the bottom of the duct being over twice the flow at the top of the duct, indicating a dramatic mal-distribution. The poor flow profile means that the amount of circulation around any particular blade of the turbine is increasing and decreasing every full rotation of the turbine. This high frequency fluctuation in circulation tends to inhibit the generation of circulation, thus reducing the pressure drop across the turbine when compared to a turbine with an ideal flow distribution.

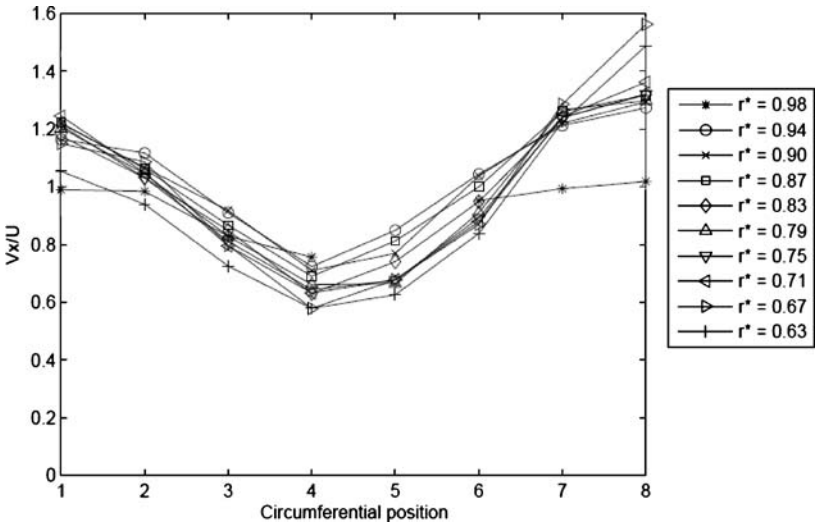

Fig. 6.19. Circumferential flow distribution during the intake stroke (from Folley et al., 2006)

However, this effect is only small as illustrated by only an 8 % reduction in the damping coefficient during the intake stroke of the LIMPET turbine. The turbine torque characteristic is also affected by the reduction in circulation, with a 25 % reduction in the torque coefficient at stall when compared to the exhaust stroke, which does not have an azimuthal variation in flow profile. Figure 6.20 shows the difference between the intake stroke (negative flow coefficients) and the exhaust stroke (positive flow coefficients) on the turbine torque coefficient. It is also interesting to note that during the intake stroke the downstream rotor has a higher peak torque, possibly indicating that the upstream rotor has helped to redistribute the flow and thereby reduce the fluctuations in flow experienced by the downstream rotor blades.

Figure 6.20, in addition to illustrating the difference between the intake and exhaust strokes, also illustrates that the torque coefficient of the LIMPET turbine is lower than that derived from the constant flow model testing. This is further illustrated in Fig. 6.21, which shows the variations in turbine efficiency with flow coefficient. It is clear that something other than the mal-distribution of flow has a dramatic effect on the turbine efficiency.

A number of studies into unsteady flow conditions (Setoguchi et al., 1988; Alcorn et al., 1998; Muman et al. 2004) have identified a hysteresis in the pressure-flow characteristic of Wells turbines due to differences in the wake behind accelerating and decelerating flow processes. However, the contra-rotating Wells turbine demonstrates a more significant difference in performance between constant and unsteady flow conditions.

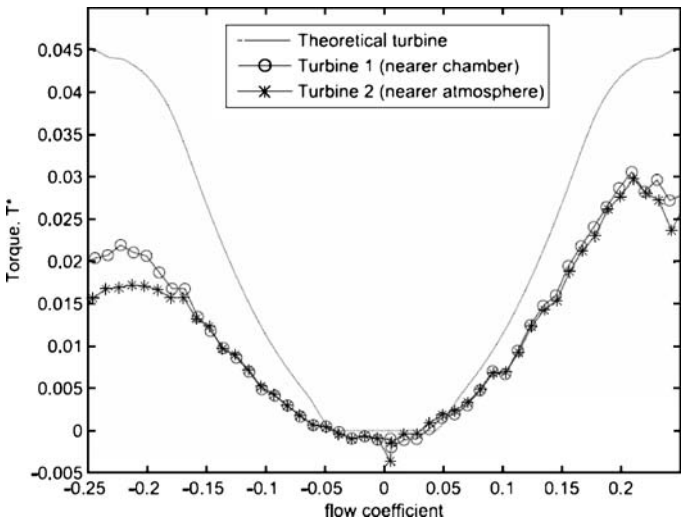

Fig. 6.20. Torque coefficients for both LIMPET rotors during intake and exhaust (from Folley et al., 2006)

It is convenient to define three aspects of unsteady flow: the accelerating and decelerating flow processes already identified in previous studies, the reversal of the flow through the turbine and the characteristic time constant of the turbine for stable flow conditions to be achieved. In comparing the LIMPET contra-rotating Wells turbine with other Wells turbines, the only significant difference that has been noted in model testing is the extended time it takes for the contra-rotating turbine to stabilise following changes in flow. In mono and bi-plane Wells turbines the turbines would adapt to the new flow conditions without any apparent delay; however the contra-rotating turbine could take 20–30 seconds to stabilise. It is suggested that this is the primary reason for the reduced efficiency of the LIMPET turbine in comparison to predictions based on constant flow testing.

Although the instability of the turbine during constant flow testing could have been used as an indicator that a more complex scenario existed, the lack of test facilities that can provide carefully controlled oscillating flow conditions limits the opportunity for investigation in this area. As new refinements to turbines are developed, doubts must exist on their actual benefit if only constant velocity unidirectional testing is used. In addition, these results must call into question the extensive use of quasi-steady state numerical modelling of turbines, since such models would not identify these essentially transient and possibly chaotic characteristics (although to date quasi-steady state modelling for other forms of Wells turbines has produced adequate predictions). It would thus seem critical that appropriate test facilities are available and that turbines should, as far as practicable, be tested in realistic conditions, which includes the configuration and layout of the turbine duct.

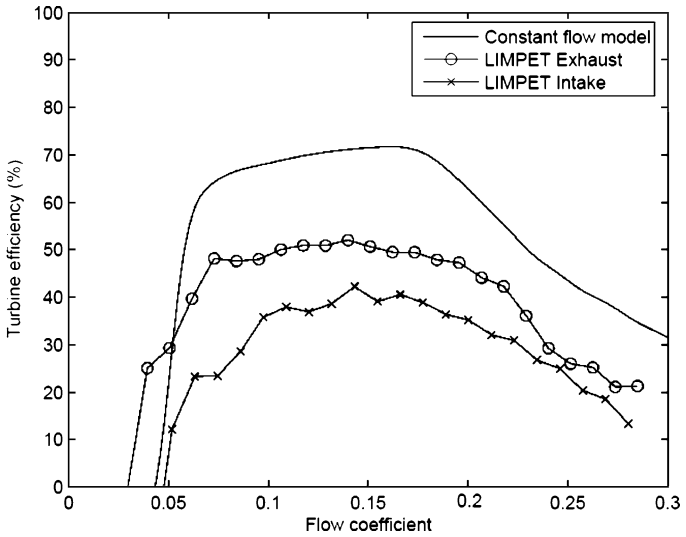

Fig. 6.21. Comparison of LIMPET and constant flow model turbine efficiencies (from Folley et al., 2006)

6.1.5 Discussion and Conclusions

It is evident that there are a number of alternative air turbines that can be successfully utilised in wave energy conversion systems. The two most common types are the Wells turbine and the Impulse turbine. Relative to the Impulse turbine, the Wells turbine operates over a smaller and slower range of air flow rates but typically operates at higher rotational velocities and higher peak efficiencies. The Denniss-Auld turbine was briefly considered and it was shown that it operated over the widest flow range while achieving relatively high efficiency, albeit still at a development stage with a pitching mechanism.

It was highlighted that any of the turbines needs to be properly integrated into the energy conversion chain, with particular reference to the OWC. The turbine needs to provide a suitable level of damping to the OWC in order to maximise its hydrodynamic performance. However, the level of damping provided by the turbine also determines the range of flow rates that will be generated from the pneumatic power provided by the OWC. Therefore, the diameter, speed and solidity of the turbines in particular need to be carefully selected in order to provide the majority of the pneumatic power at flow rates that correspond to a high efficiency. It was also highlighted that these parameters would be set at significantly different levels for either a Wells or Impulse turbine, for the same OWC rating, due to the different performance characteristics mentioned previously. In this respect it is advantageous that the Impulse turbine would have a smaller diameter and lower rotational speed, although the standard monoplane or biplane Wells turbines are mechanically simple and do not require guide vanes, whether fixed or moving.

A number of more advanced Wells turbines were considered in some detail, including the variable pitch monoplane, fixed guide vane monoplane, and counter-rotating biplane. It was concluded that of these three design types, the low-solidity counter-rotating turbine provided the best performance in terms of efficiency and range. However, while still being less complex than a standard configuration Wells turbine or a Impulse turbine with guide vanes, there is a requirement for a second generator which may have significant impact on the overall economic viability, relative to the cost of the converted electrical energy.

There has been a considerable amount of development work carried out for both the Wells and Impulse turbine. This has included experimental studies, numerical modelling and Computational Fluid Dynamic (CFD) modelling. The CFD modelling has not been addressed in detail as there has been little validation possible for rotating blades, in terms of flow velocities and detailed pressure measurements for example. However, the CFD work has contributed to the understanding of the aerodynamic performance and has been used in the optimisation of blade profile in particular, and in investigating the flow through the turbine from the OWC chamber. This CFD work may contribute to new developments in the future.

Another aspect touched on briefly is the economic analysis of the design for the various alternative turbine types. As more plants are now being commissioned, the manufacture and operational issues are becoming more prevalent in terms of the financial effectiveness of the designs. This may lead to new developments that are driven by different requirements, potentially exploiting new materials and focusing on the life cycle analysis and optimisation of the various turbine types and technologies being exploited. It is likely that researchers will continue to come up with new developments, such as boundary layer control (Raghunathan, 1995), and these innovations will have to be assessed in terms of the overall relevance of to the impact on overall power conversion and cost effectiveness. Completely new designs may also be considered, such as the Darius-type design.

There has also been a considerable amount of work over the years in the use of speed control, to control the operational range of the turbine relative to the OWC performance. This may well offer the greatest potential increase in the overall performance of the turbines when assessed on a longer term annual basis. Naturally, this focus may lead to new innovations in the turbine design that help in the improved exploitation of speed control.

It can be concluded that air turbines are still an important component of a significant number of wave energy devices being developed globally. Although many new concepts for wave energy conversion are being proposed, it is highly likely that commercial exploitation will strongly feature the use of air turbines. Consequently, researchers need to also focus on operational performance as well as developing new fundamental work. This may lead to new improved future innovations that are driven by the need to analyse the role of the turbine in the context of the OWC scenario (and economics), rather than from a purely aerodynamic basis.

6.2 Direct Drive – Linear Generators

Oskar Danielsson, Karin Thorburn, Mats Leijon

Uppsala University
Uppsala
Sweden

It may prove advantageous to utilise linear machines for applications that involve linear or reciprocal motion as the mechanical interface often can be reduced compared with systems based on rotating machines. Such configuration enables a direct drive approach and the schematic for a linear generator system with direct drive conversion is shown in Fig. 6.22. The idea of direct drive is appealing since it enables simple systems with few intermediate conversion steps and reduced mechanical complexity, but the demands on the generator increase.

One of the first concepts where linear generators were suggested as power take-off, filed as a US patent in 1980 (Neuenschwander, 1985), was later changed to a system with rotating generators. Direct drive linear generators where at that time ruled out as heavy and inefficient. Progress, mainly in permanent magnet materials but also in power electronics, has dramatically changed the conditions for linear generators and they have lately appeared as one of the most commonly used power take-off in point absorber wave energy converters (Mueller, 2002).

Using a directly coupled linear generator as power take-off in the wave energy plant reduces the structure and mechanic components to a minimum, but poses new requirements on the generator. Those requirements are to a great extent determined by the nature of ocean waves. The generator also needs to be connected to the grid, which must be taken into account in the design specification. It is important to consider the whole chain of conversion when designing linear generators for wave energy applications. The demands on directly coupled linear generators in wave energy applications are extraordinary regarding torque, overload capability, and compatibility with converter systems.

This sections explains the fundamental principles of linear generators in direct drive wave energy conversion systems and gives an overview of the basic types of linear machines suitable for wave energy conversion. The section ends with a case study of an offshore trial of a full-scale linear generator concept.

6.2.1 Principles of Direct Drive Wave Energy Conversion With Linear Generators

Direct drive in wave energy conversion is similar in principal to direct drive in wind energy, where the moving part of the generator is directly coupled to the energy absorbing part - the wind turbine. The basic principles of a linear generator are illustrated in Fig. 6.23. It consists of a moving part, the translator, on which

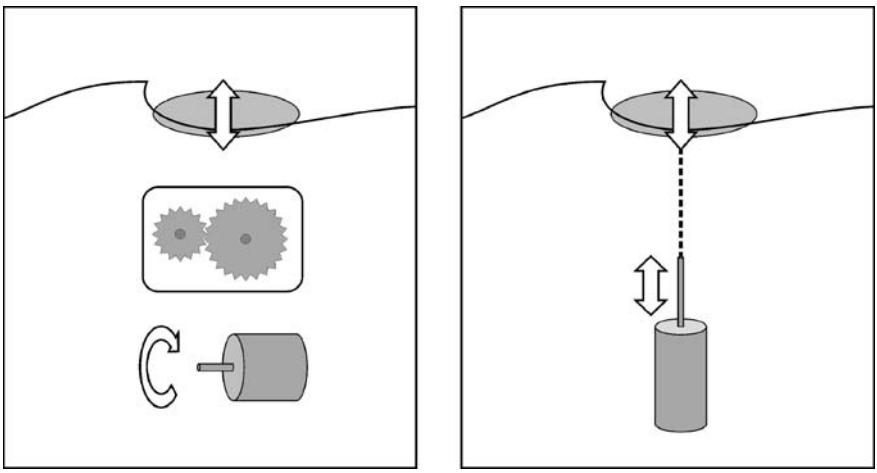

Fig. 6.22. Basic idea of direct drive wave energy conversion with linear generator. To convert the slow reciprocal motion of the ocean wave into a fast rotating motion, required by conventional high speed rotating generators, some kind of intermediate conversion step is necessary. A slow speed linear generator can be coupled directly to a point absorber and no intermediate system is needed

magnets are mounted with alternating polarity. The translator moves linearly next to a stationary stator that contains windings of conductors, the armature windings. Between the translator and the stator is a physical gap, the air gap. A voltage is induced in the windings as the magnetic field changes due to the translator motion, all in accordance with Faraday's law.

A number of direct drive WEC concepts that uses linear generators have been suggested over the years. Almost all of these concepts involve a point absorber and a reference system, where the relative linear motion between the two to drives the generator. Figure 6.24 illustrates four main concepts. The first three concepts all comprise floating point absorbers but have different reference frames, namely, the sea floor (a), a floating structure (b), and a damper plate (c). The last concept (d) uses a submerged gas filled vessel to absorb the power of the wave, here illustrated with the sea floor as reference. Other concepts have also been suggested, e.g. with the use of a mass as reference; these are however not illustrated here for simplicity.

Two different WEC systems will be used as examples. Both systems have been tested offshore and use linear generators as power take-off, but differ widely in several aspects. The first system is of type (a) in Fig. 6.24, and is representative for a small and slimmed system where control and auxiliary systems is reduced to a minimum (Leijon et al., 2006). The system has been tested offshore on the Swedish west coast in a low energy wave climate (Waters et al., 2007). It consists of a point absorber buoy with a diameter of $3\,m$, and a design significant wave height of $1.6\,m$ and a nominal power rating of $10\,kW$. This concept will be further

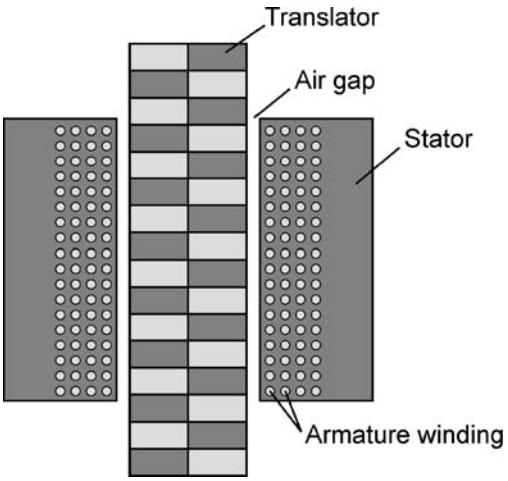

Fig. 6.23. Basic principles of a linear generator

described in the case study at the end of this section. The other concept is based on principle (d) in Fig. 6.24. It is known as the Archimedes Wave Swing (AWS) and has been tested offshore outside the coast of Portugal (Prado et al., 2006). This represents a larger WEC with higher complexity in terms of more auxiliary systems. The absorber has a diameter of 9.5 m and a rated power of 1 MW (see also Chapter 7).

Damping

The point absorber and the reference system form an oscillating system where the waves are the driving force and the generator acts as a damper. The absorption level of the device strongly depends on the damping of the generator. Optimal damping is determined by a number of factors where, above all, are the size and weight of the absorber; the speed is also essential (Falnes and Budal, 1987). Different approaches are used to increase the absorption of energy by the WEC and these can differ between a system that uses active control or tuning of resonance frequency to optimise the energy absorption and a passive system far from resonance. Generally, the optimal damping is lower for a resonating system than for a system which is not in resonance. There can also be a need for additional damping in harsh climates to reduce the translator speed and stroke length as well as loads on end stops. In the AWS this problem is addressed by adding hydrodynamic dampers, which can provide the extra damping needed (Polinder et al., 2004). In Table 6.1 typical damping, given as force per speed, is given for the two example systems.

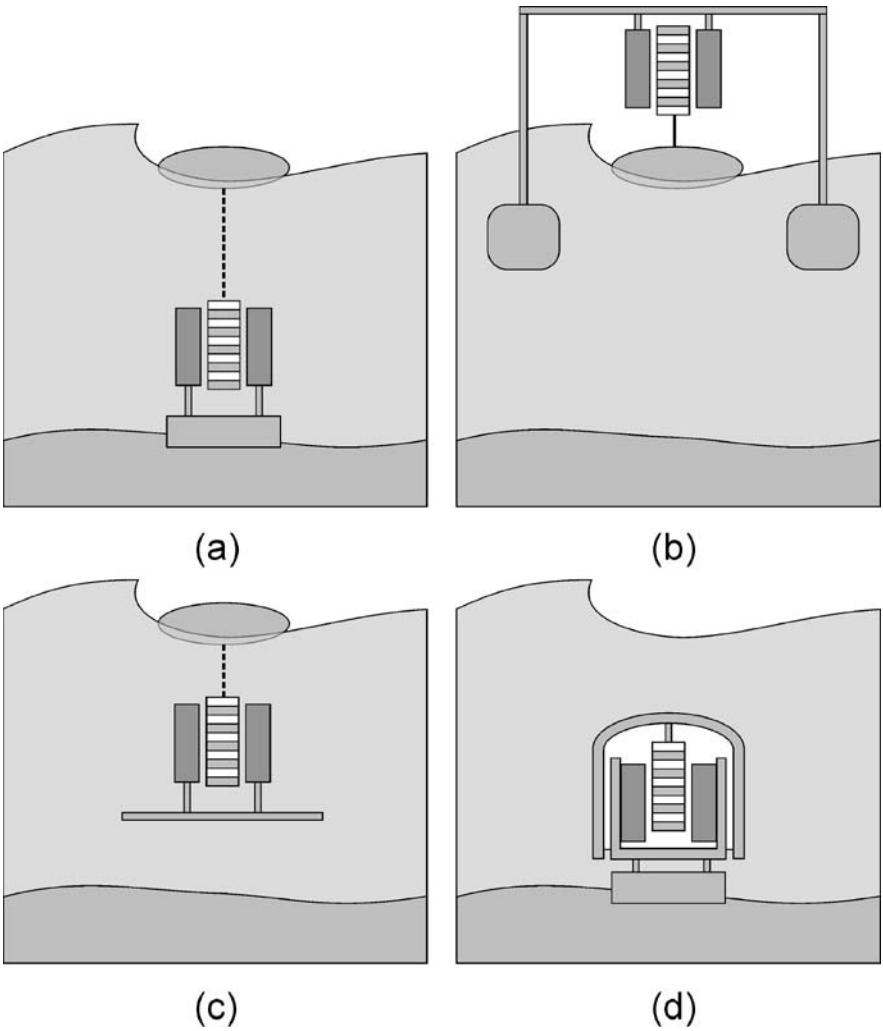

Fig. 6.24. Different concepts of direct drive WECs using linear generators. (*a*) Floating point absorber with the sea floor as reference system, (*b*) floating point absorber with floating structure as reference, (*c*) floating point absorber with submerged damper plate as reference, and (*d*) submerged gas filled vessel with sea floor as reference

Reaction force

One of the most obvious differences to conventional generators is the slow speed. The slow speed is a direct consequence of the direct drive concept. The speed of the moving part of the generator, the translator, will to a first approximation, be determined by the vertical speed of the sea surface, which is in the order of 1–2 *m/s*. This is 15–50 times slower than conventional synchronous rotational generators

and the reaction force, consequently, needs to be 15–50 times larger to give the same output power. To achieve the required damping force, a direct drive generator will need to be significantly larger than a high speed generator. The air gap areas for the two examples WECs are given in Table 6.1.

Overloads

The output power from a direct drive WEC will be determined by the instantaneous speed of the translator since there is no intermediate power storage. The translator will more or less follow the waves which results in a continuously varying speed, and consequently, a continuously varying power. As a result the generated power will vary both on a short timescale, due to the varying translator speed, and on a longer time scale, due to the changing wave conditions.

It is difficult to estimate the maximum short term overload resulting from steep wave fronts impinging on the device. Experimental results show that sudden peaks reaching eight times the average power may be encountered (Leijon et al., 2006). Short-term overloads pose demands on voltage stability and on rectifier and converters. The thermal load from a short term overload has limited effect on the machine, whereas the long term overload can cause heating problems. The long term overload will be determined by the most extreme wave condition at the site and the absorption factor of the plant. Even though the absorption factor is reduced as the wave power increases, the maximum long term overload power could be expected to be several times higher than the annual average power of the generator.

In the AWS the hydrodynamic dampers limit the overloads, both short and long term, which reduces the need for overload capacity. Typical short term and long term overloads are given for the two examples in Table 6.1.

Stroke length

The stroke length of the generator should be matched to the wave heights and is in the range of meters. Compared with other linear machine applications this is a relatively long pitch length. The induction in the machine will be reduced if the stator and translator have equal length. In order to maintain a constant induction air gap area for a longer part of the stroke length, either the stator or the translator must be longer than the other. The Ohmic losses will increase as the conductor length increases if the stator is made longer, whereas a longer translator only cost more initially. It is therefore more common to have a translator longer than the stator. The total stroke lengths for the two WEC systems are given in Table 6.1.

Grid connection

The translator motion of a linear generator is in most cases reciprocal and the speed varies continuously as the translator accelerates and decelerates near the turning points. This will give a varying frequency of the induced voltage and, furthermore, the order of the phases in a multiphase machine will be interchanged

Table 6.1. Basic prerequisites for linear generators in Uppsala University project and Archimedes Wave Swing wave energy converters

Parameter	Uppsala University project, 3 *m* point absorber	Archimedes Wave Swing
Nominal speed	0.7 *m/s*	2.2 *m/s*
Nominal power	10 *kW*	1 *MW*
Nominal reaction force	14.3 *kN*	454 *kN*
Long term overload	2–5 times nominal load	2 times nominal load
Short term overload	~ 10 times nominal load	2 times nominal load
Stroke length	1.5 *m*	7 *m*
Air gap area	2.1 m^2	20 m^2
Load	Passive rectifier	Current source inverter (passive)

when the translator changes direction. A direct coupling of a linear generator to a utility grid is thus practically impossible. This problem is addressed in Danielsson (2006) for wave energy applications where a number of connection solutions are presented. In practice, the current from a linear generator needs to be rectified before it can be converted into a 50 or 60 *Hz* AC with power semiconductor components.

6.2.2 Linear Generators

The internal structure of a linear machine has, in most cases, its origin from a rotating machine. The geometry of a linear generator can be produced from a rotating generator by an imaginary cutting and unrolling of the rotating machine. This is illustrated in Fig. 6.25, which shows the cross-section of a rotating generator, an arc shaped generator, and finally a linear generator. The linear geometry also opens up for tubular machines, which have a circular cross-section along the axis of motion. A tubular machine can be produced by rotating the cross-section geometry of a flat linear machine along an axis parallel to the direction of motion. This is illustrated in Fig. 6.26. Tubular machines forms a new type of geometry not encountered in the rotating machine fauna.

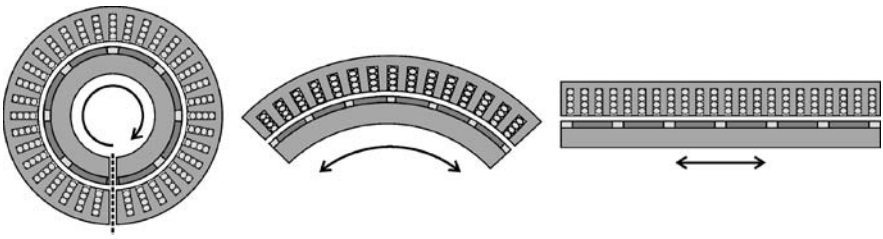

Fig. 6.25. Rotary becomes linear

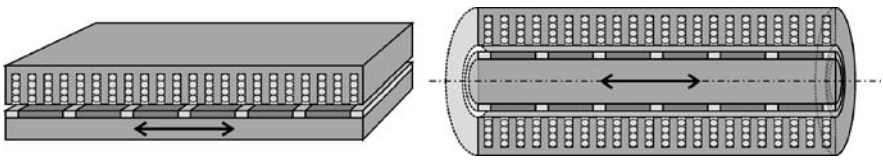

Fig. 6.26. Flat and tubular linear generator

There are however some marked differences in both the functioning and design of linear generators:

- Direct connection to grid is not possible and a rectification step is necessary.
- The supporting structure of a linear generator differs from that of a rotating machine. In contrary to a rotating machine, a linear machine cannot use one axis to fix the translator but will need several points of fixation to maintain the geometry of the air gap.
- The magnetic circuit of a linear machine differs in one significant aspect from a rotating machine - the linear machine will have open magnetic circuits in both ends, whereas the magnetic circuit of a rotating machine forms a closed circle. Unlike a rotating machine, the active area of the air gap can vary as the translator moves in and out of the stator. Furthermore, these ends have influence on the magnetic flux and the magnetic flux pattern of linear machine is thus different from a rotating machine (Danielsson, 2006).

Basic generator theory

When the permanent magnet on the translator moves in relation to the stator an electromotive force (*emf*) is induced in the armature windings. This *emf* will, if the armature winding is coupled to a load, drive a current in the armature winding. This current, in turn, creates a magnetic flux that interacts with the flux of the permanent magnet and results in a force on the translator. The mechanical energy, mediated by the translator, can in this way be converted to electrical energy, which is consumed in the load. This is the basic principle of a permanent magnet generator.

A generator can be described electrically by a simple lumped circuit diagram. Here a simplified theory will be presented given the scope of this review. The lumped circuit diagram of one phase of a synchronous generator is illustrated in Fig. 6.27. One phase of the generator is modelled by an electromotive force *emf*, a resistance, a reactance, and a load. The *emf*, E, is the voltage induced by the permanent magnet flux wave. This voltage is also called the *no-load voltage* since it is the voltage that will be measured over the phase terminals if no load is connected. Inside the generator there is a resistive voltage drop, due to the winding resistance, R_g, and an inductive voltage drop modelled by the synchronous reactance, X_s. The load, Z_l, could be either purely resistive or have a reactive component.

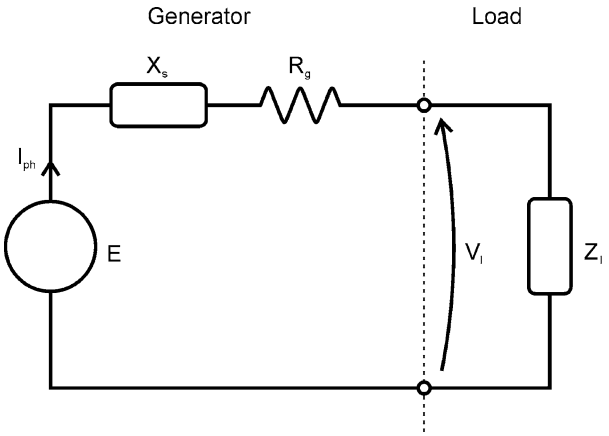

Fig. 6.27. Lumped electric circuit diagram of one phase of a synchronous generator

Induced emf

The permanent magnets on the translator are mounted with alternating polarity, which will create a magnetic flux wave with alternating direction. This flux is the *permanent magnet induced flux* of the machine and the flux wave will follow the translator as it moves. Figure 6.28 shows a schematic illustration of the permanent magnet induced flux and the armature windings of one phase. The flux encircled by one coil, shaded in the figure, will be a function of the translator position and will change as the translator moves. From the Faraday's law of induction, $E = -\frac{d\psi}{dt}N$, we can calculate the induced *emf*:

$$E = \omega \psi_{pm} N \,, \tag{6.22}$$

where ω is the angular frequency, ψ_{pm} is the permanent magnet induced flux per pole, and N is the total number of coil turns. The angular frequency is given by the translator speed v and the distance between the poles, the *pole pitch* w_p, as follows:

$$\omega = 2\pi \frac{v}{w_p} \,. \tag{6.23}$$

A small pole pitch and high speed thus gives a high angular frequency. The magnet induced flux per pole is determined by the magnetomotive force provided by the permanent magnets and the magnetic reluctance of the magnetic circuit. In practice all direct drive machines utilise high energy permanent magnets of Neodymium-Iron-Boron type, which can produce high magnetomotive force for relatively small magnet heights. The magnetic circuit consists to a large extent of ferromagnetic steel, which reduces the magnetic reluctance of the circuit. The magnetic reluctance depends on the geometry of the magnetic circuit, and especially the cross section of narrowest parts in the flux paths, the bottle necks, and

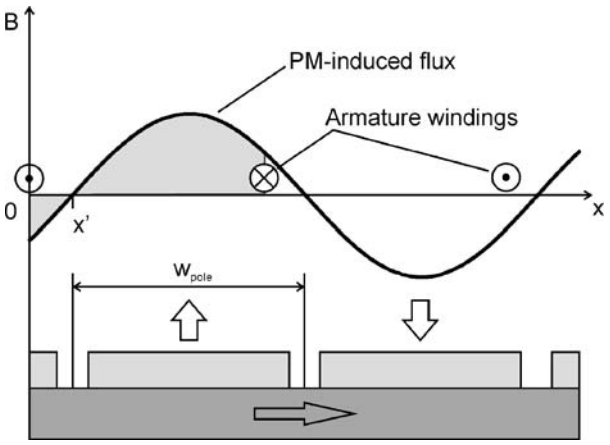

Fig. 6.28. Permanent magnet flux wave in air gap; the integration of the flux over one coil width is shaded

the magnetic properties of the steel. This will be discussed further for the different generator topologies. The total number of coil turns in a generator is equal to the number of poles, N_{pole} multiplied with the number of turns in each pole, N_{turn}: $N = N_{pole}N_{turn}$.

Synchronous reactance

The armature winding consists of a set nestled coils, which will have associated inductances. The *synchronous inductance,* L_s, is a combination of the self inductance of one phase together with the mutual, phase shifted inductances of the other phases. The *synchronous reactance,* X_s, models the voltage drop caused by the self-induced armature flux and is given by multiplying synchronous inductance with the electric frequency:

$$X_s = \omega L_s \,. \tag{6.24}$$

The electric frequency varies with the translator speed and the synchronous reactance will thus be a varying parameter.

The synchronous inductance can be divided into two parts, one which is associated with the flux that is coupled with the translator, the *main inductance* L_m, and one which is associated with the leakage fluxes, the *leakage inductance* L_l,; the result is $L_s = L_m + L_l$. The main inductance plays an import role in the generator since it represents the magnetic coupling between the armature winding and the permanent magnets of the translator. The inductance of one coil is proportional to the square of the number of coil turns. The main inductance of the generator can thus be expressed as:

$$L_m \infty N_{coils} N_{turns}^2 \,. \tag{6.25}$$

The load

The current from a directly driven linear generator is by necessity rectified before it is converted and delivered to a grid. The rectification can be passive or active. A simple diode rectifying bridge represents a passive rectifier and is characterised by having a power factor equal to one, *i.e.* the load voltage and current will be in phase. A passive rectification can, in the lumped circuit, be represented by a purely resistive load[1] and $Z_l = R_l$. In machines with high synchronous reactance the available active power can be considerably increased if the load has a power factor different from one (Xiang et al., 2002). This can be provided by using an active rectifier. In an active rectifier the power factor can be controlled and the load voltage can be made to lag or lead the current. There are also possibilities to do phase compensation by using capacitor banks (Chen et al., 1998). Both active rectification and phase compensation with capacitor banks increase complexity and add components to the system. The load will then be described by the general expression: $Z_l = R_l + jX_l$.

Output power

Knowing the components of the lumped circuit the active power in the load can be calculated:

$$P_l = E^2 \left(\frac{R_l}{\left(R_l + R_g\right)^2 + \left(X_s + X_l\right)^2} \right). \tag{6.26}$$

The active output power of a generator depends on the induced *emf*, the synchronous reactance, the armature winding resistance and the load. The induced *emf* varies with the translator speed and the output power will thus vary as the translator changes speed during a wave period. By changing the load the output power for a given translator speed can also change. By varying the load, the damping of the generator the generator can be varied. This can be used as control strategy to control the power absorbed by the WEC. Especially in harsh climates it can be necessary to over-damp the WEC, e.g. to reduce forces and stroke length.

Flux ratio

As mentioned above, generators with relatively high synchronous reactance need to be phase compensated in order to increase the power from the generator. The need for phase compensation is traditionally described in terms of *power factor*. However, in these applications, where the generator often is connected to a load via a passive rectifier, the power factor is constant and equal to 1. The need for

[1] A rectification bridge is a non-linear component, which cannot be modeled accurately with li near theory. A resistive load, however, resembles a passive rectification bridge by having a power factor equal to one, i.e. the voltage and the current is in phase.

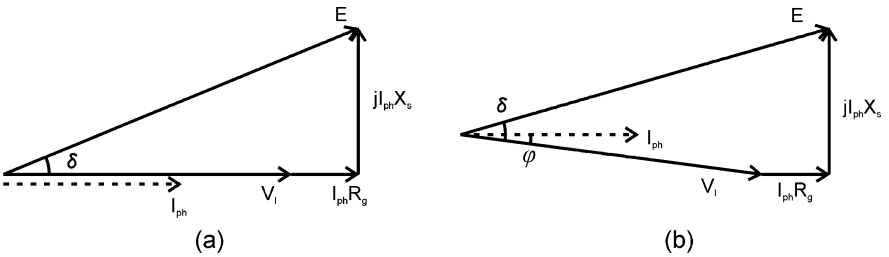

Fig. 6.29. Phasor diagram of synchronous generator, (*a*) purely resistive load and (*b*) phase compensated load

phase compensation can also be described by the *flux ratio* between the permanent magnet induced flux and the armature current induced flux. The concept was introduced by Harris et al. (1997) and was used to describe the problem of low power factor in TFPM (transverse flux permanent magnets) motors. The flux ratio can be produced from a phasor diagram of the voltage components in the generator. Two phasor diagrams are illustrated in Fig. 6.29, where (a) represents a purely resistive load and (b) a phase compensated load. The voltage components, $I_{ph}X_s$ and E, are proportional to the armature winding induced flux, ψ_{arm}, and the permanent magnet induced flux, ψ_{pm}, respectively. The quota between the two,

$$\frac{I_{ph}X_s}{E} \infty \frac{\psi_{arm}}{\psi_{pm}}, \tag{6.27}$$

can be given as a figure of merit for the need of phase compensation. A low quota means low need for phase compensation and a high quota indicates a large need for phase compensation. Another, often used term, is the *load angle*. The load angle is the angle between the *emf*, E, and the load voltage, V_l , and is indicated with δ in the figure. The load angle is often used as a measure of how hard a machine is loaded.

6.2.3 Linear Machines Topologies

There exist today a large number of different linear machines types most of them derived from rotating machines (Boldea and Nasar, 1999; McLean, 1988). Not all linear machines are suitable for wave energy conversion and only a handful fulfils the basic prerequisite stated in Table 6.1. Induction machines and field wound synchronous machines can at an early stage be ruled out since they cannot compete with the permanent magnetised machines at the slow speed at hand (Polinder et al., 2005). Today there are mainly three main classes of machines that have been investigated for wave energy applications, longitudinal flux permanent magnet generators also known as synchronous permanent magnet generators, variable reluctance permanent magnet generators with transverse flux permanent magnet generators as a special case, and air-cored tubular permanent magnet generators.

Longitudinal flux permanent magnet generator (LFPM)

The name refers to the flux path in the yoke which is in the longitudinal direction. This machine is also known as a *synchronous* permanent magnet generator, which reflects that the armature winding flux and the permanent magnet flux are moving synchronously in the air gap. This is however the case for all generators described here and the name can be somewhat misleading. LFPM generators have been investigated with finite element methods (Danielsson et al., 2006) and analytical methods (Polinder et al., 2004) for wave energy applications and tested offshore in both the AWS project and the Uppsala University project.

A cross-section of the magnetic circuit of a longitudinal flux permanent magnet generator is illustrated in Fig. 6.30. The main magnetic flux is illustrated with dashed lines and the direction of the flux is indicated with arrows. The magnetic flux from one magnet crosses the air gap and is conducted by the stator teeth through the stator coils. In the stator yoke the flux is divided into two paths, which return through the stator teeth, via the air gap and through the adjacent magnets. The steel plate in the translator connects the magnetic flux at the back of the magnets. The LFPM has an inherently small synchronous reactance and the stator construction is simple and robust. The geometry of LFPM, however, limits the stator teeth width and cross-section area of the conductors for a given pole pitch. Increasing the tooth width to increase the magnetic flux in the stator or increasing the conductor cross-section demands a larger pole pitch and the angular frequency of the flux is thus reduced. This sets a limit for the induced *emf* per pole and consequently the power per air gap area. The basic features of a LFPM are summarised in Table 6.2.

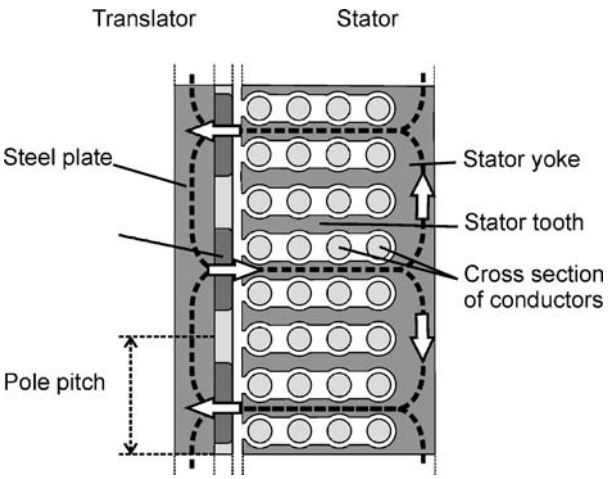

Fig. 6.30. Cross-section of a LFPM generator, magnetic flux path is illustrated with a dashed line and the direction of the flux with arrows

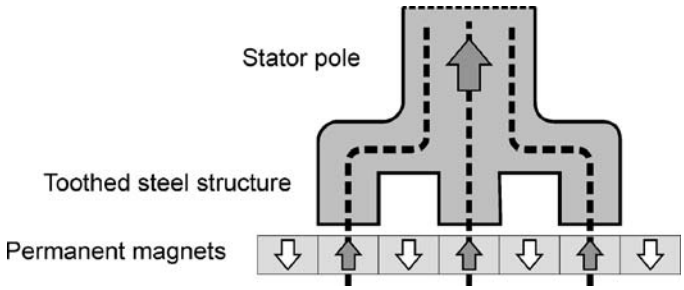

Fig. 6.31. Basic principles of a variable reluctance machine

Variable reluctance permanent magnet generator (VRPM)

Variable reluctance machines form a whole set of different generator geometries. The limiting coupling between the cross section area of the magnetic circuit and the pole pitch, found in synchronous machines, is avoided here by using alternate return path through a toothed steel structure. The basic principles are illustrated in Fig. 6.31. This enables large magnetic fluxes combined with a very short pole pitch but the synchronous reactance of these machines tends to be very high. Different types of VRPM have been suggested for use in direct drive WECs (Baker, 2003).

Transverse flux permanent magnet generators (TFPM)

The TFPM was introduced by Weh et al. (1988) and has been investigated for wave energy applications by Mueller (2002), and more generally, by Harris et al. (1997). The geometry of TFPM machine is illustrated in Fig. 6.32, which shows a double sided TFPM with the translator with permanent magnets in the middle and a set of C-cores on the top and bottom providing closed magnetic flux paths around the two coils. As the translator moves the permanent magnets will couple their flux alternately with the coil above and with the coil below. The illustration to the right (*b*) show the flux paths of two parallel magnets, with the flux path of the adjacent magnets illustrated in shaded nuance. This special arrangement avoids the conflict between high cross-section areas of both yoke and armature conductor combined with small pole pitch. Accordingly, both PM-induced flux and armature current flux can be high while pole pitch remains small and these kinds of machines can produce a very high force per pole. The drawback is the relatively high synchronous inductance and that they are intended to work at relatively high armature current level. Phase compensation or some kind of power converter with high power rating is needed to fully appreciate the generator performance. Another drawback is the relatively complex stator composition, which is made of several independent C-cores of laminated steel. The main characteristics of a TFPM are summarised in Table 6.2.

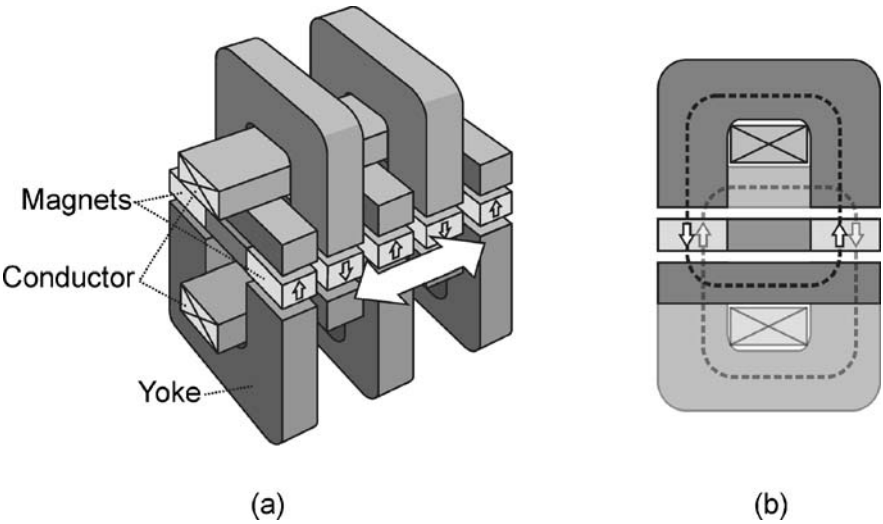

Fig. 6.32. Transverse flux permanent magnet machine. (*a*) 3D-view of double sided TFPM with the translator with permanent magnet in the middle and two sets of C-cores, one on above and one below the magnets (*b*) 2D-wiev along the axis of motion, flux path of two parallel magnets are illustrated together with the flux path o the adjacent magnet pair (shaded)

Tubular air cored permanent magnet generator (TAPM)

Lately, an air cored tubular permanent magnet generator has been suggested for wave energy applications (Baker and Mueller, 2004). The principles are illustrated in Fig. 6.33, which shows a 3D-view (*a*) and a cross-section (*b*) of a TAPM. Here the magnets are magnetised in the axial direction and placed with altering direction of the flux. Flux concentrators are placed between the magnets and a varying flux wave is created outside the translator. Other configurations are also possible, *i.e.* surface mounted permanent magnets. By removing the steel in the stator the normal forces are virtually eliminated. This is a large constructional advantage

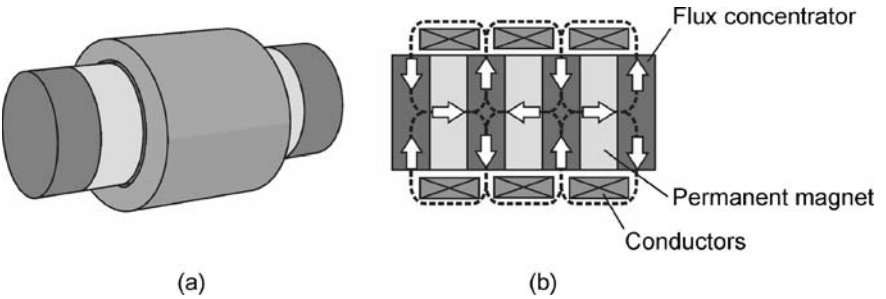

Fig. 6.33. Tubular air cored generator. (*a*) 3D-view of TAPM (*b*) cross-section showing the flux paths

Table 6.2. Basic features of different linear generators

	Power per air gap area* (kW/m^2)	Flux ratio *IX/E*	Pros	Cons
LFPM	~25	0.1–0.5	Low synchronous reactance. Simple and robust stator.	Low power rating per air gap area.
TFPL	~50	1.6–2.6	High power per air gap area.	High synchronous reactance. Complex stator.
TAPM	>12.8‡	<0.3	No normal forces in the air gap.	Very low power per air gap area.

*The power is given for a speed of 1 *m/s*
†Synchronous reactance per unit is the synchronous reactance divided by the load resistance
‡Experimental values from Baker (2000)

since normal forces in other permanent magnet linear generators are in the order of 200 kN/m^2 (Nilsson et al., 2006). Significant support structures are needed to overcome these forces and maintain a constant air gap width. The drawback is that the magnetic reluctance in the magnetic circuit is increased considerably, since the distance the flux travels in air now is in the range of the pole pitch and not, as in steel stator machines, just over the air gap. The flux of an air cored machine is thus much smaller and the power per air gap area is thus considerably lower. The main characteristics of a TAPM are summarised in Table 6.2.

6.2.4 Case Study: 3 m Point Absorber

Uppsala University in Sweden has developed and tested a WEC on the Swedish west coast in the spring of 2006. The basic principles of the concept are illustrated in Fig. 6.34. The WEC consists of a floating buoy, coupled via a rope directly to the translator of the linear generator. The generator is placed the seabed and the tension in the rope is maintained by springs connected underneath the translator. A end stop at the top of the generator limits the stroke length of the translator. The concept is unique in several aspects and protected by a number of patents.

The basic idea behind this concept is simplicity. Auxiliary systems, such as dampers and active rectifiers are avoided. As stated in the introduction, a reduction in complexity often increases the requirements posed on the generator. The short time overload on the generator is, as can be seen in Table 6.1, expected to be up to 10 times larger than the nominal load. Excess capacity in damping will also be needed since no additional damping is provided.

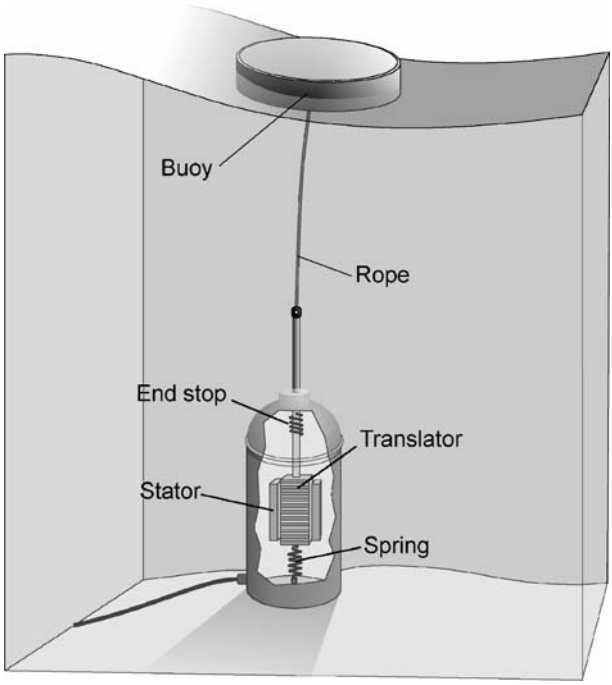

Fig. 6.34. Basic principles of the Uppsala University WEC concept

Generator design

The generator is of the LFPM type with surface mounted Neodymium-Iron-Boron permanent magnets. Standard cables with circular cross-section are used as armature windings. In contrast to other generators, where the design to a larger extent is determined by the thermal loading, the heat generation is a minor problem for this generator since the generated power per volume is so small. Furthermore, the WEC will be surrounded by sea water with a temperature in the range of 4–8º*C*. The main issues in this generator are the *size*, the *efficiency*, and the *load angle*. The goal of the design study is to construct a small generator with high efficiency and low load angle at nominal load (Danielsson et al., 2006). In contrast to other wave energy converters where the generator only is a minor component, this generator will actually carry a large part of the total construction cost of the wave energy converter. A reduction in generator size will be directly reflected in the cost of the plant. Furthermore, the efficiency has a direct influence on the energy delivered to the grid and will thus affect the annual revenue of the plant. A nominal wave with wave height 1.6 *m* and a period of 4.6 *s* was chosen, based on the moderate wave climate on the Swedish west coast. The nominal load of the generator was set to 10 *kW* at a speed of 0.7 *m/s*.

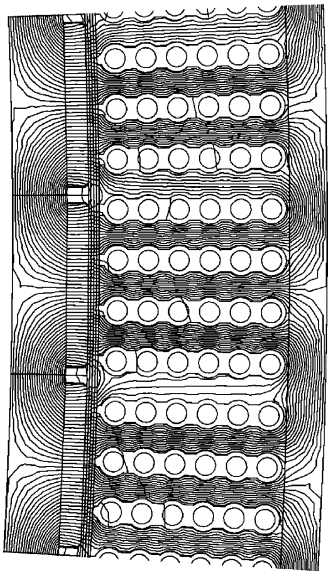

Fig. 6.35. Cross-section of a segment of the linear generator showing the magnetic flux lines at load

A combined field and circuit equation model is utilised to model the electromagnetic behaviour of the generator. The finite element equations and the circuit equations are solved simultaneously. Such models permit transient simulations, where the translator speed is continuously varying. This tool is used in a design study over five hundred simulations from the basis of a first laboratory prototype generator (Leijon et al., 2005). The simulated magnetic flux during load is illustrated in Fig. 6.35. The main features of the generator are summarised in Table 6.3.

Table 6.3. Main features of generator at nominal load

Nominal power	10 kW
Main voltage	200 V (r.m.s)
Armature current r.m.s.	28.9 A
Fundamental frequency	7.0 Hz
Synchronous reactance	0.44 Ω
Load angle	6.6º
Pole width	50 mm
Air gap width	3 mm
Total air gap area	2.08 m^2
Efficiency	86 %
Hysteresis losses	0.53 kW
Eddy current losses	0.04 kW
Resistive losses	1.0 kW

Experiment

Based on the design study, a first prototype generator was constructed. An illustration of the prototype generator is shown in Fig. 6.36. The prototype generator was half the length of the designed generator and the air gap area was $1.04\,m^2$. The generator has four sides with the square shaped translator in the middle and four separate stator packages on the outside facing the translator sides. The translator and stator are attracted to each other by magnetic forces. By using a multiple side translator, these forces can be reduced, since the forces of the opposing sides of the translator act in different directions. However, the forces increase rapidly with decreasing air gap widths and a small horizontal displacement of the translator will give a resulting force on the translator, acting in the direction of the smallest air gap. A support structure is necessary to maintain a constant air gap width and to counteract the significant attractive forces that are developed between the translator sides and the stator packages. The normal forces proved to be a large challenge and the smallest realizable air gap width was $5\,mm$, which is $2\,mm$ larger than the original design.

A hoist system with a $75\,kW$ induction motor was connected to the test generator. The translator was pulled at a constant speed of $0.86\,m/s$ and the phases where connected to a purely resistive load. The resulting voltages are presented in Fig. 6.37 together with the simulated voltage. The amplitude of the voltage is changing although the speed is constant. This is a result of the changing active air gap area as the translator moves in and out of the stator.

Full-scale offshore testing

Full-scale on-site testing of the wave energy converter adds a number of new challenges, but provided information and experiences impossible to be obtained in a laboratory (Waters et al., 2007). For the first time the full dynamics of the wave energy converter concept could be studied. The plant is illustrated in Fig. 6.38. The generator is placed inside a watertight steel structure, which is mounted on a concrete foundation. The linear motion is translated by a piston through a water tight piston sealing. The rope is guided at the top of the structure by four rolls, which ensure that the piston force only has a vertical component. The buoy is cylindrical and has a diameter of $3\,m$ and a height of $0.8\,m$ and is connected to the piston with a Vectran rope. The plant is placed at a depth of $25\,m$ and the structure is pressurized continuously during the submersion to a final pressure of $2.5\,bar$. A sub-sea cable connects the test site with a land station. The on-shore measurement station is equipped with heat sink variable resistive loads.

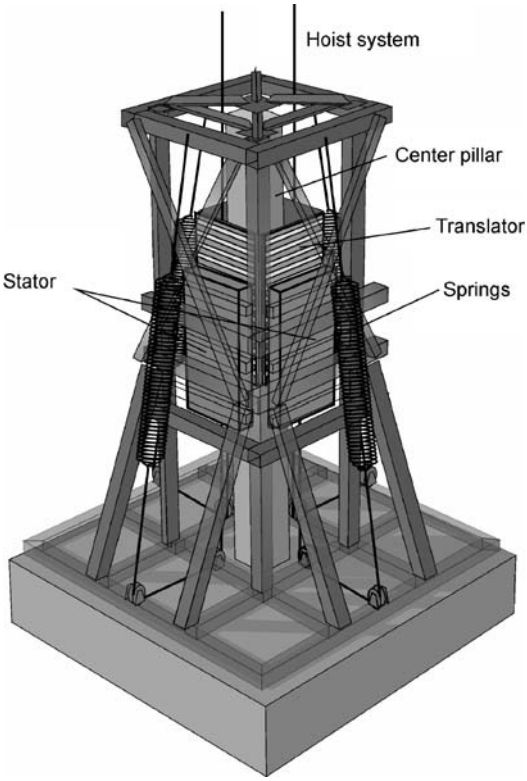

Fig. 6.36. Illustration of experimental generator with support structure is made transparent over the active parts of the generator

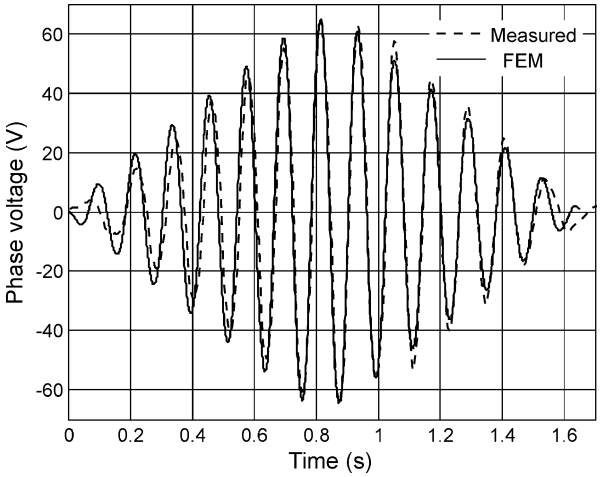

Fig. 6.37. Measured and simulated phase voltage from laboratory prototype

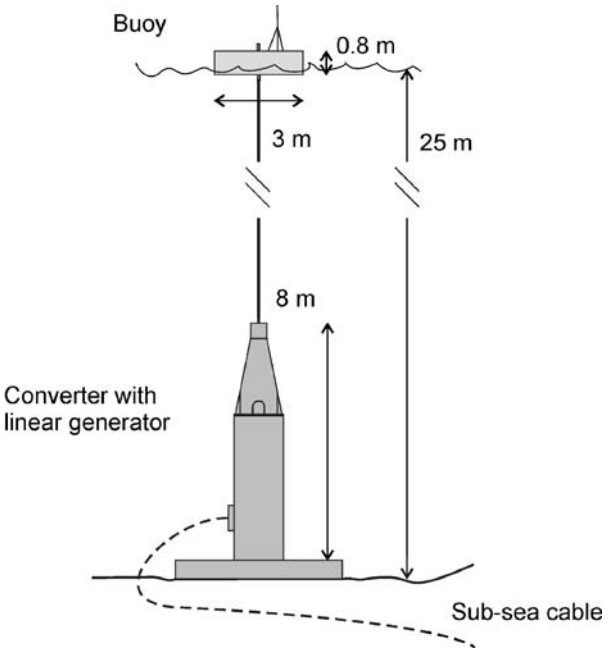

Fig. 6.38. Illustration of full-scale offshore wave energy converter

The magnetic circuit of the generator has the same design as the laboratory generator except for some small modifications. The length of the stator was increased and the air gap area was $2.04\,m^2$ and the stroke length is $1.8\,m$. The support structure was modified into a significantly stiffer structure and the designed air gap width of $3\,mm$ was achieved without problems. An illustration of the generator is shown in Fig. 6.39.

The complete WEC was launched in March 2006 outside Lysekil on the Swedish west coast. The voltages over the load were continuously measured and all important electrical entities in the system, such as power, resistive losses in generator and cable, no-load voltage, load angle, etc. can be estimated by using the lumped circuit model. Moreover, both the position and speed of the translator can be determined from the phase voltages, knowing that two successive zero-crossings of one phase correspond to a movement of the translator by one pole pitch. A sample of the main voltages is illustrated in Fig. 6.40. A typical pattern is achieved where the voltages varies both in frequency and in amplitude as the translator follows the motion of the waves.

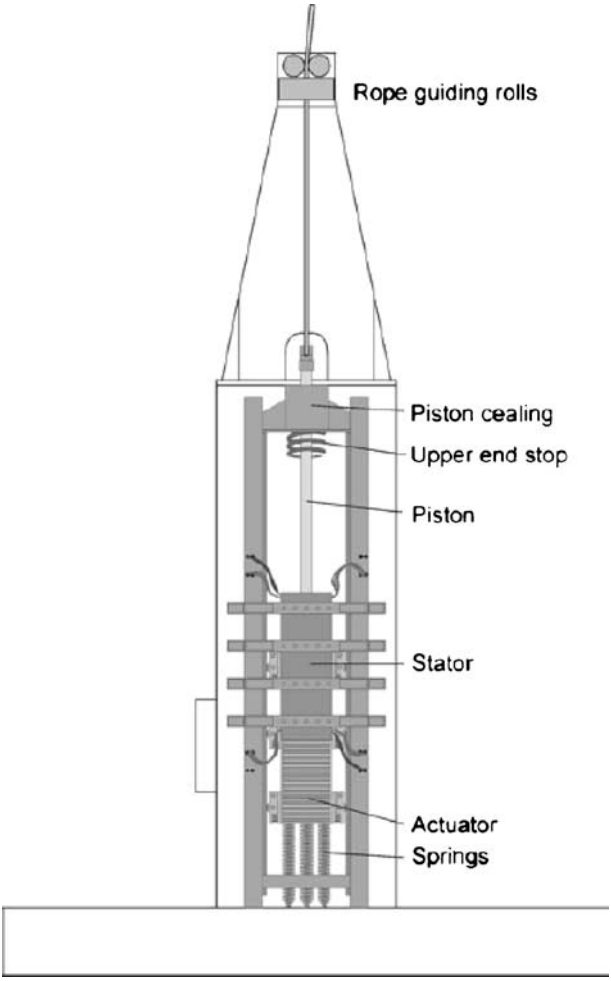

Fig. 6.39. Illustration of linear generator employed in the offshore WEC

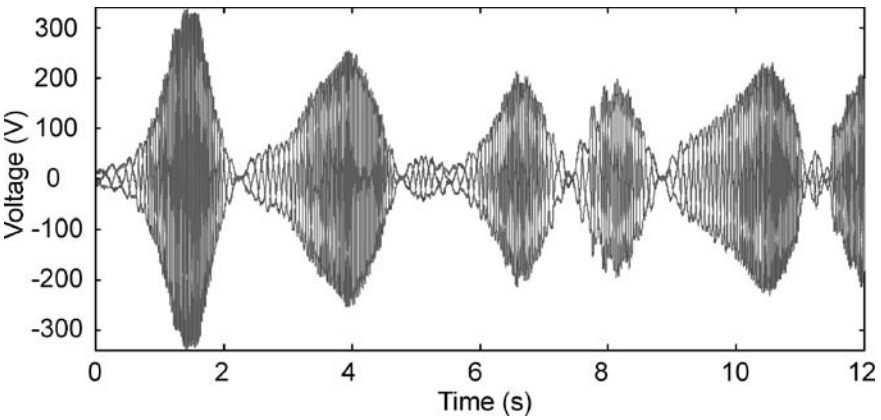

Fig. 6.40. Three phase voltages measured over the load resistances from the offshore WEC

6.3 Hydraulics

Jamie Taylor

University of Edinburgh & Artemis Intelligent Power Ltd
Edinburgh
Scotland, UK

> "It is easy to make a device that will respond vigorously to the action of sea waves. Indeed it is quite hard to make one that will not. However the conversion of the slow, random, reversing energy flows with very high extreme values into phase-locked synchronous electricity with power quality acceptable to a utility network is very much harder." (Salter et al. 2002)

6.3.1 Introduction

If it was possible to make a perfect wave energy converter, it might be compared with a graceful and clever dancer who only ever gets to work with a mad orchestra. As the band swings without warning from jig to waltz, to punk, to minuet, to raga, to jig, to bebop, to reel – sometimes all of these at once – the dancer instantly finds each new tempo without losing a single step. Fascinated by the equivalent wave energy conversion problem, engineers have suggested many ways to improve the amount of energy that their devices might capture from changing seas. Salter et al. (2002) consider the range of such *control strategies* that have been proposed, ranging from fixed amplitude and variable force, through pre-emptive over-damping, to full complex-conjugate control (Nebel, 1992) and stiffness

modulation. Each control strategy defines a relationship between the motions induced on the system by wave action and the corresponding reaction forces that should be provided by the power take-off system. The simplest and best known idea is to make force proportional to the instantaneous velocity. The ratio of these is then referred to as the *damping coefficient* and damping can be compared to the occasional domestic sensation of stirring a jar of syrup.

Whatever the strategy, a wave energy converter must have power take-off machinery that can be ordered to do things according to the changing values of digital and analogue commands – switch on, switch off, increase, decrease, connect, disconnect. A simple power take-off may have very few things that can be changed, but for the best performance and to deliver the cheapest energy it will be better if it can provide many such control-variable 'hooks' for the commanding computer to attach to. High-pressure oil-hydraulic systems are often particularly well suited to this sort of task. However, machines of sufficient size for larger wave energy devices are generally not available commercially. Spurred on by this need, a great deal of effort has gone into designing pumps and motors that are particularly suitable for wave energy devices.

Most of the topics discussed in this section are treated in greater depth in Salter et al. (2002). A deeper understanding of the behaviour of fluids can be gained from a comprehensive textbook on fluid mechanics such as Douglas et al. (2005). Three handbooks that may be useful in the design of high-pressure oil-hydraulic systems are Hunt and Vaughan (1996), Majumdar (2001) and Chapple (2002). The latter is published in conjunction with the British Fluid Power Association. A specialist book that explores the detailed design of high-pressure oil-hydraulic machines has recently become available in English, Ivantysyn and Ivantysynova (2000). For readers in the UK, the monthly trade magazine Hydraulics & Pneumatics is available on free subscription and is a valuable source of information regarding commercially available equipment and practices.

6.3.2 Spline Pumps

As a first example, Fig. 6.41 shows Stephen Salter's (1974) initial hydraulic solution to the conversion problem referred to at the start of this section. Each of the forty or so wave absorbing vanes of this classic wave energy converter rotates about the centre of the common supporting cylindrical member. The paraxial ridges on the cylindrical member and the inward facing ridges on the vane comprise double-acting spline-pumps. With non-return valves rectifying the flow, deoxygenated and decarbonated water is forced through the one metre diameter manifold pipes at a pressure of 400 pounds per square inch (*psi*) to a water-turbine and generator which are shared by all of the vanes. The water returns to the spline-pumps through the low-pressure manifold which is provided by the hollow centre of the cylindrical member. The system is a closed-circuit, high-pressure water, hydraulic transmission that incorporates an integral custom designed pump.

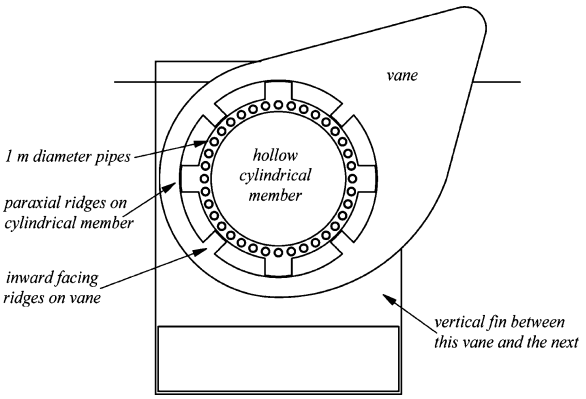

Fig. 6.41. Vertical section through early 'vane' showing spline pump (Salter, 1974)

6.3.3 Increasing Complexity

Five years later, the power take-off of the duck, as it was now called, had changed beyond recognition. Figure 6.42 shows how prolonged exposure to the energy conversion problem had led to a startling new arrangement. The treated water of the 1974 design had been replaced by mineral oil and its pressure had been increased by a factor of more than ten. The entire power take-off system was now enclosed within a closed and evacuated steel canister. This was located within the nose of the duck which could now go through much bigger angles because there weren't any spline-pump ridges to crash into one another. As it was rocked by waves of ever-changing periods and amplitudes, constant-frequency grid-quality electric current would be transmitted down the cable from the power take-off tube to the network. This grand design, which exploited the precession of gyros as a means to synthesise large inertial reaction, seemed to provide all of the good things that wave engineers dreamt of: complete environmental protection of the power conversion machinery from the sea; a generous amount of energy storage (in the spinning gyros); super-clean hydraulic oil (centrifuged by the gyros); high-class synchronous generation (thanks to a decoupled transmission); relative ease of control by computers (a new kind of valve); and high energy conversion efficiency (extensive use of hydrostatic bearings).

The elaborate arrangements of the gyro duck (Salter, 1980; 1982) reflect both the difficulty of designing robust and efficient wave energy converters and the historic fact that the target market for early UK wave energy designers was perceived as being for 2 *GW* installations. Accordingly, every part could be designed for the job. After 1979 the power take-off for the duck continued to evolve. The upper inset image in Fig. 6.42 shows a string of ducks at sea. The hollow cylindrical member of the spline-pump duck was now replaced by an articulated spine and it had

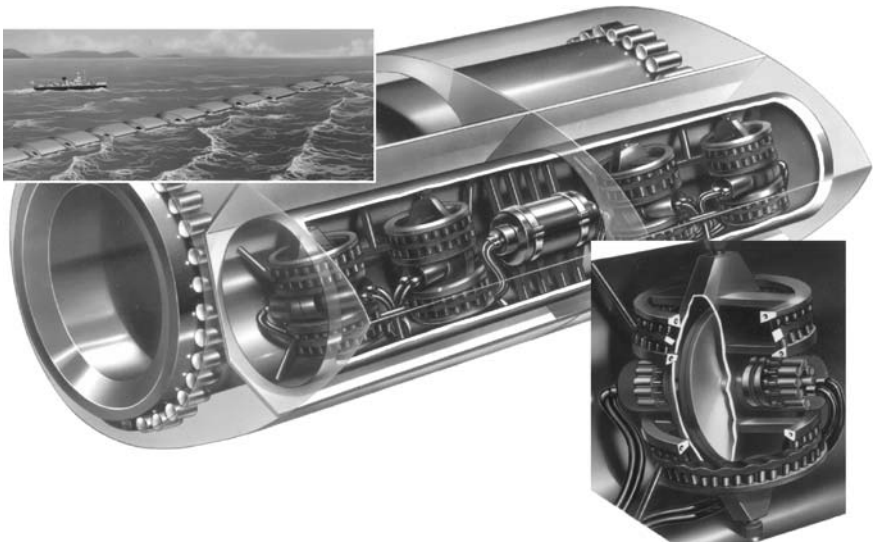

Fig. 6.42. A 1979 artist's impression (by L. Jones) showing duck with complete gyro power-take-off system contained within a sealed canister. The close-up view shows two axial-piston motors driving a gyro flywheel and two ring-cam pumps capturingenergy from the precession of the gyro-frame. Note that the bearing arrangement shown here between duck and spine is purely symbolic

been experimentally discovered that the power generated by the duck could be increased if the compliance of the spine joints could be actively controlled by high-pressure hydraulic rams, Fig. 6.43. The same rams could also provide damping forces that could contribute to the net generated power of the whole system (Salter, 1993).

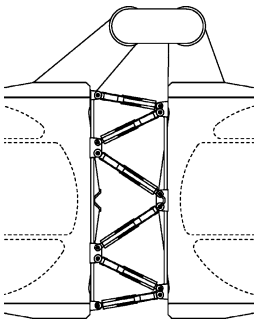

Fig. 6.43. Side-view of the joint between two spines, coupled together by a 'coronet' of 12 high-pressure hydraulic cylinders to give six degrees of controlled freedom (Salter, 1993)

What is still of particular interest is that the 1979 duck contained two new high-pressure oil-hydraulic machines. They can be seen in the cut-away view on the right of Fig. 6.42. One of these machines was a large diameter low-speed ring-cam pump that captured wave energy from the duck via the precession of the gyro frames and the other was an axial-piston variable swash-plate motor. Two of the latter are seen driving each gyro flywheel and another was assigned to drive the generator. Still more of the variable axial-piston machines would subsequently be assigned to control the spine joint rams.

The reason for going to so much trouble in the design of the power take-off was that the designers believed that, if they were going to have to pay very large sums of money for the front-end of the wave energy converter, its construction yards, moorings, underwater cables, sub-stations and maintenance fleet and then somehow persuade mariners to stay out of its way once at sea, they were obliged to do their best to get as much energy as possible from it. The generator of any wave power plant will spend most of its time operating at a fraction of its name-plate rating. To get the best possible energy return, the power take-off machines must therefore have the highest possible part-load efficiencies. They should also be easy to control with computers. The hydraulic components that were commercially available in 1979 were generally not designed with these requirements as priorities.

Of course nobody has got round to building a $2\,GW$ wave energy converter system, and so the approach of most current wave energy designers is necessarily different to that of the team who designed the gyro duck (the University of Edinburgh, John Laing Ltd & the Scottish Offshore Partnership). Most systems that have been built have been prototypes. In place of the public money that it was hoped would finance the designs of the 1970s, much of the money has come from private investors who have to reduce their risks by reducing the amount of technical innovation. Hence, the hydraulics used in the wave energy systems that have gone to sea are generally based on commercially available components and machinery.

The effort that went into designing the gyro duck later led to a new kind of hydraulic machine. Artemis Intelligent Power Ltd, a University of Edinburgh spin-out company that was set up by Win Rampen and Stephen Salter in 1994 to continue the work that had been started for wave energy and to progressively bring it to market, came up with the phrase Digital Displacement™ to describe this development. The features of their machines will be described later. In the meantime it should be emphasised that it takes a long time before new designs of large hydraulic pumps and motors can be launched on the market with the necessary warranties for tens or hundreds of thousands of hours of operation. This is why it has always been important, but not necessarily easy, to continue the development of the kinds of specialised power conversion equipment that is appropriate to wave energy in parallel with the development of the hydrodynamic and naval architectural aspects.

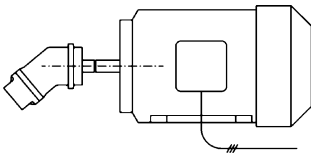

Fig. 6.44. Relative sizes of a typical fixed-displacement hydraulic pump (on left) and an electric motor (based on a 1,500 *rpm*, 110 *kW* system)

6.3.4 Advantages of Oil-Hydraulics

Hydraulic engineers often seem to have a hard time compared with their electrical friends who don't have to spend hours filling their wires with electrons or removing air bubbles from every corner of their circuits. Electricians don't worry about slipping on dirty electrons that have leaked onto the floor. Hydraulic hoses break too often, hydraulic connectors leak too easily, hydraulic oil ruins clothes and needs constant attention. It must be filtered, de-watered, de-aired, and either cooled or heated depending on its mood. The super-sensitivity of its viscosity to temperature frustrates machine design. Electricity is in a class of its own when it comes to transmitting energy over almost any distance but hydraulic circuits of more than a few metres in length can seem maddeningly lossy.

However, remarkably small and light-weight hydraulic machines can handle enormous forces and hydraulics has no rival when trying to capture power from large objects that are being pushed around relatively slowly by enormous wave forces. The net forces created by a typical hydraulic pressure of 350*bar* (5,000*psi*) are around fifty times greater than those from the magnetic circuits of the best electrical machines. This is why an electrical machine is best employed when it can use high velocity to compensate for its relatively low torque. It's also why a hydraulic pump that is driven by an electric motor of equivalent power usually looks very small in comparison (Fig. 6.44). Where necessary, hydraulics can also provide static forces for indefinite lengths of time with little expenditure of energy.

6.3.5 Hydraulic Circuits

In the late 1990s, Richard Yemm and his company Pelamis Wave Power Ltd started to develop their Pelamis device (Yemm et al., 2000). The prototype which was launched in 2004 is undoubtedly the most advanced floating wave energy converter that has gone to sea. Although he took some ideas from the duck's actively-controlled spine, Yemm decided to use only commercially available components in the power take-off system in order to boost investor confidence. Hydrostatic transmissions that are built for applications such as heavy winches and excavators generally use variable displacement pumps to deliver continuously variable pressure and flow. Their overall efficiencies can be well below 60 % when operating away from their full-load ratings. The Pelamis designers tried to find a way to use conventional components without incurring such inefficiencies.

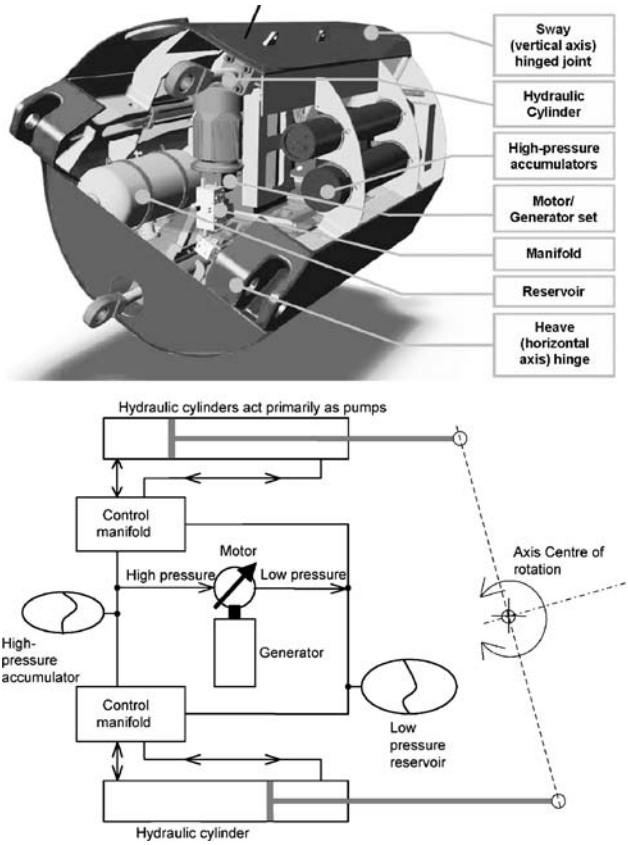

Fig. 6.45. A power module from the Pelamis wave energy converter. Top: cut-away view from solid-model. Bottom: Simplified hydraulic circuit of one active joint (Henderson, 2006)

Ross Henderson (2006), who has been closely involved since the start of its development, describes the Pelamis power take-off, as consisting of "sets of hydraulic cylinders that pump fluid, via control manifolds, into high-pressure accumulators for short-term energy storage. Hydraulic motors use the smooth supply of high-pressure fluid from the accumulators to drive grid-connected electric generators." Figure 6.45, from his paper, shows a cut-away view and a simplified hydraulic circuit of one of the Pelamis power modules.

The accumulators that provide the crucial decoupling between the hydraulic cylinders and the hydraulic motors are devices that store hydraulic energy through the compression of a gas within a pressure vessel. The gas, usually nitrogen, is separated from the fluid within a bladder or by a free-piston. Rising fluid pressure compresses the gas and admits more fluid to the vessel. Falling pressure expands the gas and expels fluid back into the circuit. At the risk of great thermodynamic

simplification, the accumulator behaves like a spring. If it is of adequate volume, and with a suitable gas pre-charge pressure, it can provide enough energy storage to decouple the *primary* wave side of the power take-off from the *secondary* generator side.

Largely to avoid the danger of *cavitation* (the creation and collapse of damaging vapour bubbles due to low pressure transients), it is normal practice to operate hydraulic machines with a small *boost* pressure, up to 5 *bar*, at the intake port. The low-pressure accumulator shown in the hydraulic circuit schematic of Fig. 6.45 helps to maintain this boost pressure.

In the Pelamis power take-off, different combinations of chambers within the hydraulic cylinders, are used to pump oil directly to the accumulator. The chambers are switched in and out by electronically controlled valves during each wave cycle (within the "control manifolds" of Fig. 6.45). The reaction torque about each Pelamis heave or sway hinge can thus be varied through a range of values depending on the accumulator pressure and the number of cylinder chambers that are connected, (see Fig. 6.46). The pressure in the accumulator depends on the difference between the rate at which energy is supplied to it from the primary circuit and the rate at which it is taken from it by the secondary generator-driving circuit. With three heave joints, three sway joints, and six generators in the prototype machine, this allows the Pelamis control engineers to try out a number of different control strategies.

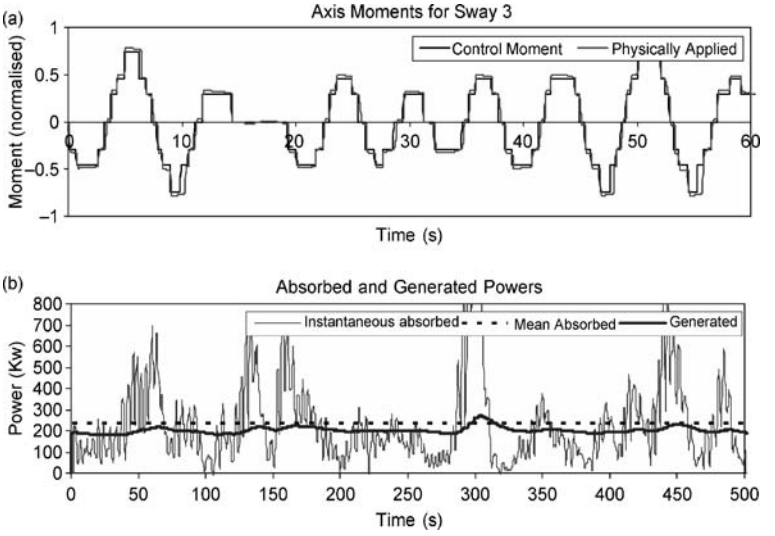

Fig. 6.46. Traces from a computer simulation of a Pelamis sway joint (Henderson, 2006). The steps in the reaction moment provided by the separately switched ram compartments are clearly seen in the upper image. The lower image compares the rapidly changing instantaneous power absorbed in the primary circuit with the slowly varying power of the secondary generation circuit

With reference to the emerging generation of Digital Displacement™ machines, Henderson notes the development of "a novel digital hydraulic pump/motor, originally intended for a wave energy application, capable of offering a continuously variable transmission of hydraulic power at much higher efficiencies than conventional hydrostatic transmissions". He wisely concludes that "while the technology is nearing commercial application, it is still at the prototype stage and unsuitable for immediate deployment in a WEC". He considers the losses in the Pelamis primary transmission, from oil compressibility, bearings and seal friction in the cylinders and flow losses in pipes and valves and estimates that with good design these can be kept below 20 % over a wide range of operating conditions. He also points out that the primary transmission can absorb instantaneous power levels that are ten times higher than the average power that the secondary transmission is designed for (see Fig. 6.46).

6.3.6 Linear Pumps

Because of their familiarity in impressively powerful everyday machines such as diggers and cranes, linear hydraulic cylinders or rams as used in the Pelamis power take-off are an obvious choice for use in wave-driven pumps. Salter et al. (2002) report the availability of rams up 24 *m* in length with diameters up to 1 *m*. The Pelamis rams are protected from the sea by flexible rubber bellows. The Ceramax plasma-sprayed coating process used by the Dutch company Rexroth Hydraudyne for the rods of some hydraulic cylinders may allow them to be used directly in sea-water without further protection. The maximum velocities that rams can deal with are governed by the material of the hydraulic seal and the temperature rise across it due to shear loss and friction. With adequate cooling, velocities up to 30 *m/s* seem to be possible.

6.3.7 Rotary Pumps

For some wave energy devices such as the duck, rotary hydraulic pumps may be more appropriate in the primary stage of the power take-off. However, it may not be possible to find a pump that can develop sufficient torque at the very low angular velocities produced by waves. The Swedish company Hägglunds claim that their Marathon, which has a long record of service in exposed marine conditions, is by far the largest hydraulic motor in the world. It is of interest here because hydraulic motors can usually be used in reverse as pumps with little modification (the reverse is generally not true). Table 6.4 includes the maximum ratings of the biggest machine in the Marathon range.

Machines such as the Marathon have fixed displacements. They are designed to be used in systems where the flow or the pressure can be varied by external means.

Table 6.4. Some details of the Hägglunds MB4000 (from Hägglunds, 2006)

Displacement	251.3	*litres/rev*
Specific torque	4,000	*N/bar*[1]
Rated speed	8	*rpm*
Maximum speed	12	*rpm*
Maximum pressure	350	*bar*
Max. intermittent output power	1.58	*MW*
Case diameter	1,460	*mm*
Length excluding shaft	2,095	*mm*
Shaft diameter	460	*mm*
Weight	10.75	*Ton*

[1] 1 $bar = 10^5$ Pa ($Pa = N/m^2$)

6.3.8 Ring-cam Pumps

A rotary-machine topology that is often used for slow, high power machines such as the Marathon is sketched in Fig. 6.47. A central cylindrical block is driven by the shaft and incorporates within it a number of cylinders within which pistons slide freely. Rollers are pressed by the cylindrically shaped pad at the foot of each piston against an undulating multi-lobed cam that forms the outer part of the pump case. As in the design of all hydraulic machines, a detailed understanding of hydrostatic and hydrodynamic processes is required to ensure that all moving surfaces that are in close proximity are always separated by a film of oil so as to avoid metal to metal contact.

Figure 6.47 does not show the valves and galleries that connect the cylinders alternatively to the low-pressure and the high-pressure ports of the machine. Neither does it show compression springs that might be fitted between pistons and cylinders to help hold the rollers always in contact with the ring-cam. Some form of radial guides would usually be fitted to support the circumferential forces on the rollers to ensure that only axial forces are transmitted between pistons and cylinders. The machine of Fig. 6.47 has a twelve lobed cam and thirteen pumping-

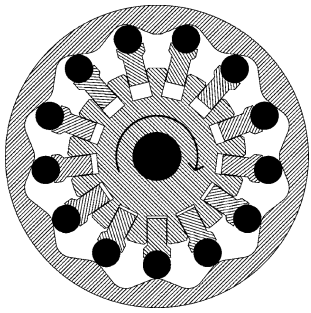

Fig. 6.47. Diagram of a ring-cam pump. In this case, with 12 cam lobes and 13 cylinders, there would be 156 piston strokes per revolution

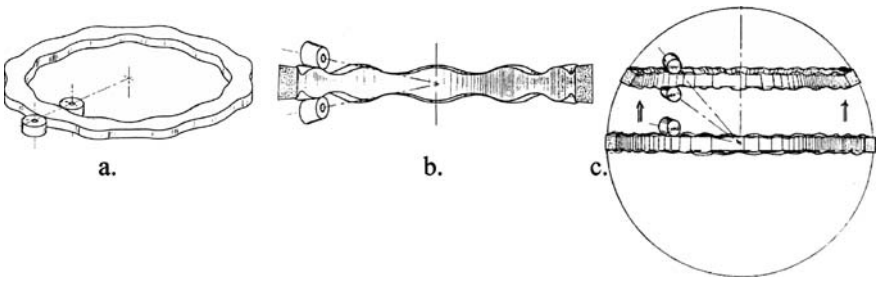

Fig. 6.48. Transformation of ring-cam topology for gyro duck (Salter, 1980) a) duplex, lobes on outside as well as inside of cam; b) twisted cam with conical rollers; c) cam moved from the equator to the tropics

groups. Every pumping-group is worked by every lobe, and so during a single revolution there are a total of 156 pumping operations. In a low angular-velocity drive, the multiple lobes of the ring-cam provide a means of stepping up the frequency and combined volume of pumping operations, to produce a machine that has a high power-density. Salter et al. (2002) suggest that the value-for-money of a ring cam machine becomes steadily better as it becomes larger and more powerful because, whilst the cost depends on the sum of the costs of the pumping modules and the lobes, the value depends on their product.

Figure 6.48 shows the progressive transformation of a simplex ring-cam into the open duplex arrangement of Fig. 6.42 that was designed to capture power from the precession of large gyro-frames. The first stage of transformation, shown in the left-hand image, is to add a second external series of cam lobes so that pairs of opposing pumping-modules can be placed around the ring. Most of the mechanical stresses are then transmitted locally through the thickness of the cam and directly between module pairs rather than around the circumference of the whole ring. In the central image of Fig. 6.48, the cam surfaces are twisted through ninety-degrees and the rollers become conical to allow a more compact placement of pumping-modules. Finally, to free up room for the gyro flywheel drive motors, the ring-cam migrates, as shown in the right-hand image, from the equator position of the gyro frame to the tropic position.

6.3.9 Hydraulic Motors

Whatever the type of pump that is used in the primary circuit, the secondary circuit will almost certainly require a hydraulic motor that can drive a synchronous or an induction generator at speeds around 1500 or 3000 *rpm*. Of the commercially available machines, axial-piston bent-axis types, made by companies such as Parker or Bosch Rexroth, are the most obvious choice for generator drive.

Axial machines can be converted to variable displacement by the introduction of a swash-plate. Salter et al. (1988) reported the design by Robert Clerk (1908-1993) and the construction by Matthew Rea of a refined version of such a machine. Clerk's original specification was for flywheel storage applications, and he was

particularly concerned to obtain the lowest possible losses when idling, along with a capacity for high torque and high speed. These attributes were also appropriate for the high-speed motors inside the power canister of the gyro duck.

Referring to the simplified sectional view of Fig. 6.49, the motor operates as follows. The cylinder block 'A' rotates past the ports in the port-head 'B'. The shaft 'C' is coupled to the cylinder block by drive lugs 'D'. Ball-ended rods 'E' connect the pistons 'F' to the drive-plate 'G' which is forced axially against an angled swash-carrier 'H'. The angle of the swash-carrier can be changed by a piston which is not shown, and the friction between it and the drive-plate is reduced by the use of hydrostatic support pads. The reaction between the swash-carrier and the drive-plate induces output-torque which is passed to the shaft through Clerk's tri-link mechanism which is shown half-way along the shaft. The machine's displacement per revolution clearly depends upon the angle of tilt of the swash-carrier because this directly controls the length of the pistons strokes.

The use of spherical bearings in the tri-link, push-rods and main-shaft greatly reduced the accuracy of alignment that was required in the construction and assembly of the motor and made it tolerant of dimensional changes under high stress. Clerk also used hydrostatic bearings throughout the machine to reduce loss and extend life. Hydrostatic bearings require great attention to oil cleanliness, but if this can achieved the complete separation that they provide between running surfaces, makes it possible to consider the use of working fluids such as water-emulsions, that have no natural lubricity.

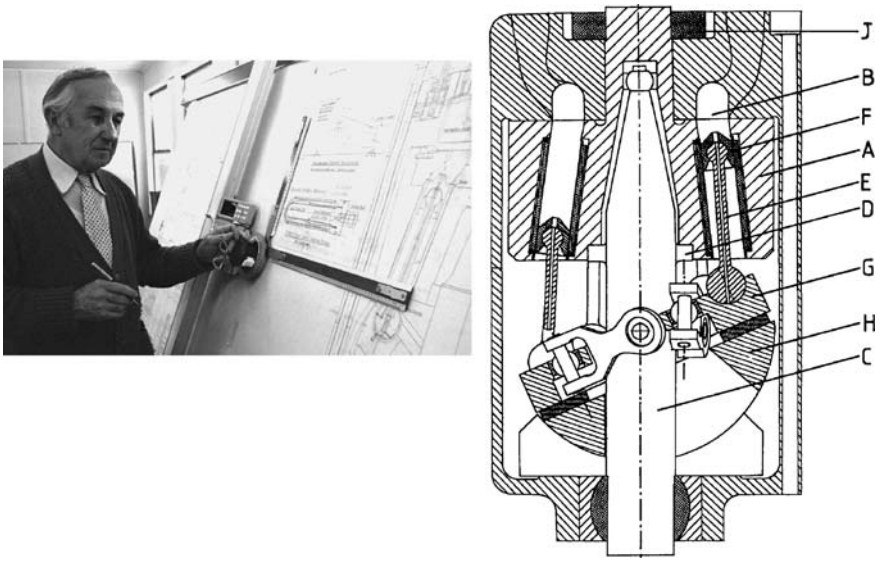

Fig. 6.49. Robert Clerk, shown in 1985 working on his high-speed axial-piston variable displacement machine of which a simplified section is shown on the right. (Photo: University of Edinburgh. Drawing: Salter et al., 1988)

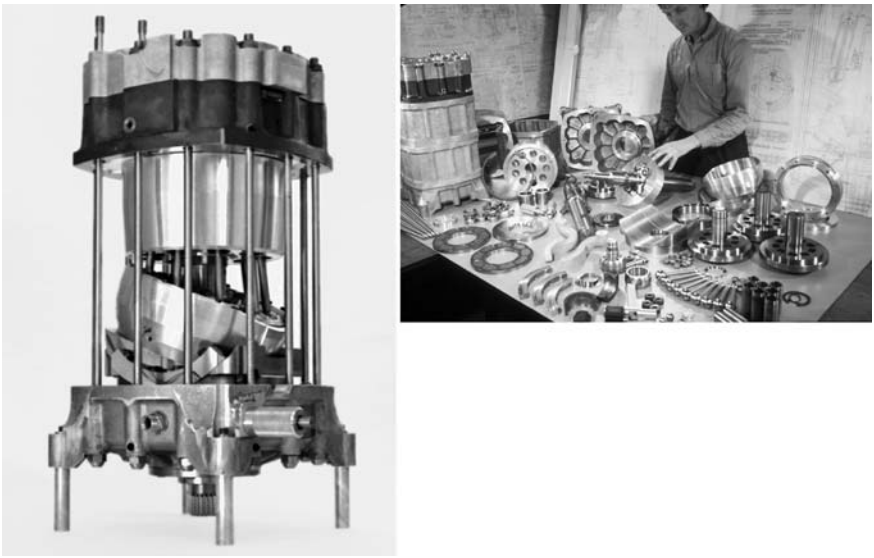

Fig. 6.50. Matthew Rea, in 1985, with parts that he and Carn Gibson made for a 600 *kW* Clerk high-speed motor. On the left, the motor is shown assembled without its case. The angled swash-plate is clearly visible (Photos: University of Edinburgh)

Figure 6.50 shows a prototype of Clerk's high-speed motor that was built and tested at the University of Edinburgh.

6.3.10 Flow Commutation

Cylinders within rotary machines must be connected alternatively with the low-pressure and high-pressure ports that join them to the external system. The mechanisms that are used for this are comparable in function to the commutator of a *DC* brush motor. The port-plate arrangement used in the Clerk motor and typical of bent-axis and swash-plate machines in general, is shown in Fig. 6.51. Two kidney ports on a stationary block are connected respectively to the low-pressure and the high-pressure ports of the machine. A barrel with multiple ports rotates with the cylinders and this alternatively connects them to the low- and high-pressure ports. The design of such a flow-commutator requires great subtlety and experience and is possibly the hardest aspect of a rotary hydraulic machine to treat successfully.

6.3.11 Losses

The main processes of energy loss within rotating hydraulic machines are through churning, leakage, shear, compressibility and breathing.

The cases of most high-pressure oil-hydraulic machines remain fully flooded during operation. In high-speed machines the energy absorbed by the resultant

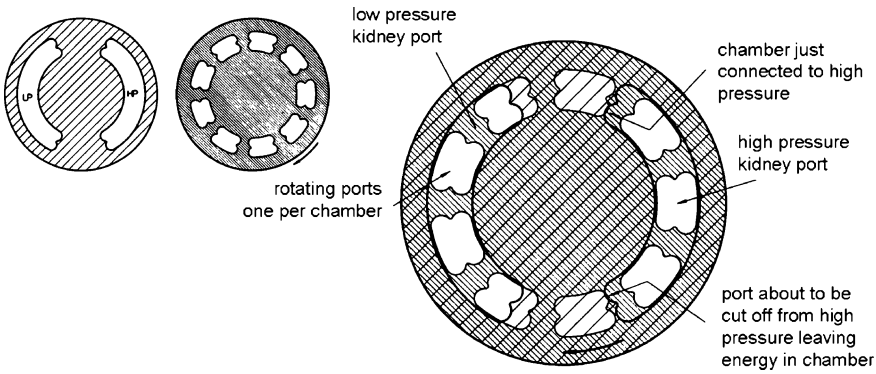

Fig. 6.51. Port-plates as used to provide flow-commutation in axial-piston machines. The stationary plate shown at top left is connected through to the low- and high-pressure ports. The rotating barrel at top centre has one port per cylinder. The two parts are shown on the right at a particular point in their relative rotation (modified from Salter et al., 2002)

churning can be several percent of the full power rating. The Clerk tri-link machine was designed to run 'dry' so as to eliminate these losses. Hydraulic fluid escapes through any gap that has a pressure difference across it. However some of these leakages may be intentional if they are designed as part of a hydrostatic-bearing to provide controlled separation between moving parts. Shear losses occur through the viscous forces generated between moving surfaces that are separated by a layer of oil. Leakage power-loss depends on the square of pressure and can be reduced by making the clearances finer, using higher viscosity fluid or by increasing the lengths of leakage paths. However these changes have the effect of increasing shear losses which depend on the square of speed. The machine designer has therefore to carefully balance the conflicting aims of reducing leakage and shear losses.

Compressibility losses arise because the working fluid has a bulk modulus that is not infinite, typical values for a hydraulic oil being around $1.6\times10^9\ N/m^2$. Potential energy is absorbed by the compression of the oil as well as by elastic deformations of machine parts. If the compressed oil in a cylinder is suddenly depressurised, for instance as a result of poor timing of the commutation mechanism, the stored energy may be suddenly and wastefully dissipated with consequent noise, wear and energy loss. With mechanical flow-commutation and variable operating conditions, it is virtually impossible to avoid compressibility losses at some parts of the operating regime.

Breathing losses result from pressure drops caused by the rapid movement of fluid around bends and through changes of section in the generally complicated passages between cylinders and ports. These pressure drops are particularly critical on the low-pressure side because of the need to avoid cavitation and are compensated by boosting pressure by at least a few bar above ambient. This fixes the problem, but reduces the working pressure differential across the cylinders of the machine. Good breathing requires the sort of attention to detail shown in Fig. 6.52. It also needs space so that flow velocities can be kept as low as possible.

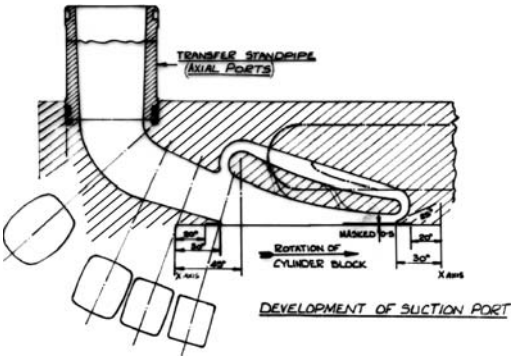

Fig. 6.52. Suction port detail for high-speed swash-plate motor, drawn by Robert Clerk

6.3.12 Active Valves

However well a conventional machine is designed there is a limit to how far its losses can be reduced, particularly when it is operating well below its rated capacity. One reason is that all of the cylinders experience the full pressure cycle at all times and so are always subject to leakage losses. Furthermore, flow-commutation by mechanisms such as port-plates or pintle-valves offers little timing flexibility, poor control of compressibility losses, and may compromise the space available for good valve breathing. An alternative approach where cylinders are only pressurised when they are required to contribute flow (in a pump) or provide torque (in a motor) is made possible by the kind of active low-pressure poppet-valve that was conceived of for the gyro duck low-speed ring-cam pump. An early drawing of this valve is shown in Fig. 6.53. Its further development is currently leading to a new generation of higher efficiency hydraulic machines that naturally interface to control computers.

To best capture energy from waves of varying heights and periods, some means had to be found in the gyro duck design of Fig. 6.42 to vary the reaction torque that the ring-cam pumps provided against gyro precession. It was also important to reduce losses at times of low incident power. The new active low-pressure intake valves provided the means to satisfy both requirements.

As the piston in each of the many pumping modules reached bottom-dead-centre it would have filled with oil from the low-pressure manifold and would be ready to start a power-stroke. At this moment in a conventional machine, the inlet-valve would close, the piston would start a compression stroke, the oil pressure within the cylinder would rise, the outlet-valve would open and a unit of high-pressure oil would be delivered to the high-pressure system. However, in the new design, when the piston was at bottom-dead-centre, a computer would decide whether or not another unit of high-pressure was required. If the answer was yes, then the operation would be as for the conventional machine. If the answer was no, a pulse of current would be sent to a coil in the new inlet-valve and the magnetic-bistable latch would hold the valve open so that the piston would merely return the un-pressurised oil to the low-pressure manifold.

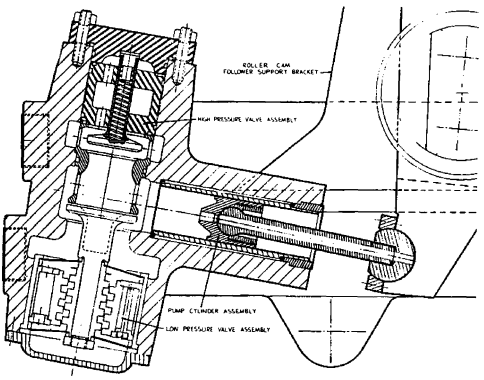

Fig. 6.53. Detail of pump module from the gyro duck ring-cam pump. The upper high-pressure outlet-valve is of conventional passive design. However, the low pressure intake-valve assembly at the bottom features a magnetic bistable latch and marks the beginning of Digital Displacement™ hydraulics. From an unpublished Edinburgh-SCOPA-Laing report to the UK Department of Energy, 1979

By choosing an appropriate enabling-pattern for the intake-valves of the pumping modules, the displacement of the entire pump could be varied in discrete steps.

By only pressurising cylinders that are required to do work, the pressure-related losses of the pump would be greatly reduced and the part load efficiency would be increased. The physical layout made possible by the new active valve gave a new freedom to provide good breathing arrangements and impressive power density. The proposed 5 *m* diameter units would have a power rating of up to 30 *MW*.

6.3.13 Active Valve Machines

The design and construction of Robert Clerk's low-loss high-speed motor (Figures 6.49 and 6.50) was an impressive achievement. However its operation was subject to the limits imposed by mechanical commutation and so there was room for further improvement in its losses and its controllability. Active commutation can be applied to high-speed motors if the high-pressure valve as well as the low-pressure valve is of the active type. Such a machine is described by Salter and Rampen (1993) and various views of it have already been shown in an earlier section of this book (Fig. 2.15). The new machine used a radial rather than an axial configuration with the pistons working against a single-lobed crankshaft eccentric as shown in Fig. 6.54. The kinematics of this arrangement are near perfect.

In this version, the surface of the shaft eccentric forms part of a sphere. The piston big-end pads are designed to support themselves on this surface with a combination of hydrostatic and hydrodynamic lift. Springs provide additional

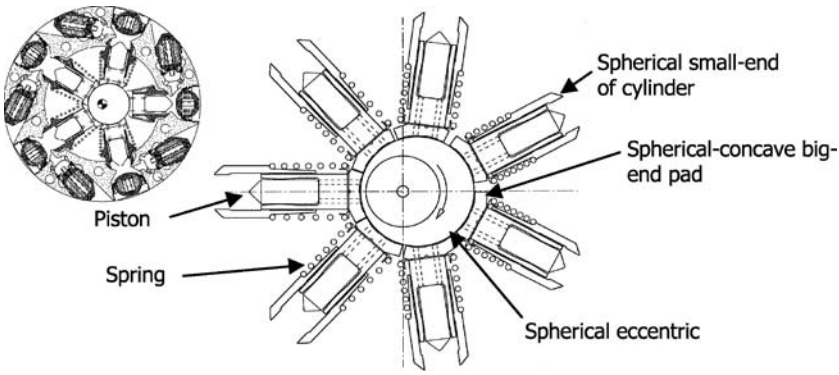

Fig. 6.54. Radial-piston geometry used for high-speed active-valve machines (adapted from Salter and Rampen, 1993)

acceleration force to hold the pads to the eccentric at high rotational speeds. The outer small-ends of the cylinders also fit to the body of the machine via spherical surfaces (see the inset in Fig. 6.54). This arrangement protects the pistons and cylinders from side loads and gives them the freedom to take up any dimensional changes in the machine under high load.

The radial arrangement of pumping-modules around the eccentric shaft places the piston pads at the centre of the machine where the linear velocity of the eccentric is at a minimum. This helps to reduce the shear losses. The valves are placed around the periphery of the machine where there is plenty of space to optimise the breathing arrangements. Figure 6.55 shows how several radial machines can be arranged along a common shaft to produce a more powerful machine, or one that can provide multiple services.

An application of a multiple-service machine to a wave energy power take-off is sketched in Fig. 6.56. In this case, the active-valve radial-machine provides a total of six services that are grouped in three pairs. The wave-excited part of the device is represented by the large piston at centre-left which moves relative to the bodies of the two single-acting hydraulic rams. The varying reaction forces provided by the rams are controlled by the active high- and low-pressure poppet-valves of the multi-eccentric machine. High force peaks and instantaneous overloads are passed directly to the gas accumulator which is managed via dedicated circuits on the multi-eccentric machine. The shaft of the machine drives a synchronous generator at 1500 *rpm* and can be compared with the summing junction of an operational amplifier. In this case, energy rather than currents are balanced along the length of the shaft. Depending on the control algorithm, power can flow in any direction in any of the services including the electrical machine. Any instantaneous energy deficits within the power take-off could then be supplied by the generator acting as a motor for part of the cycle. Ehsan et al. (1995) describe the time-domain simulation of such a system.

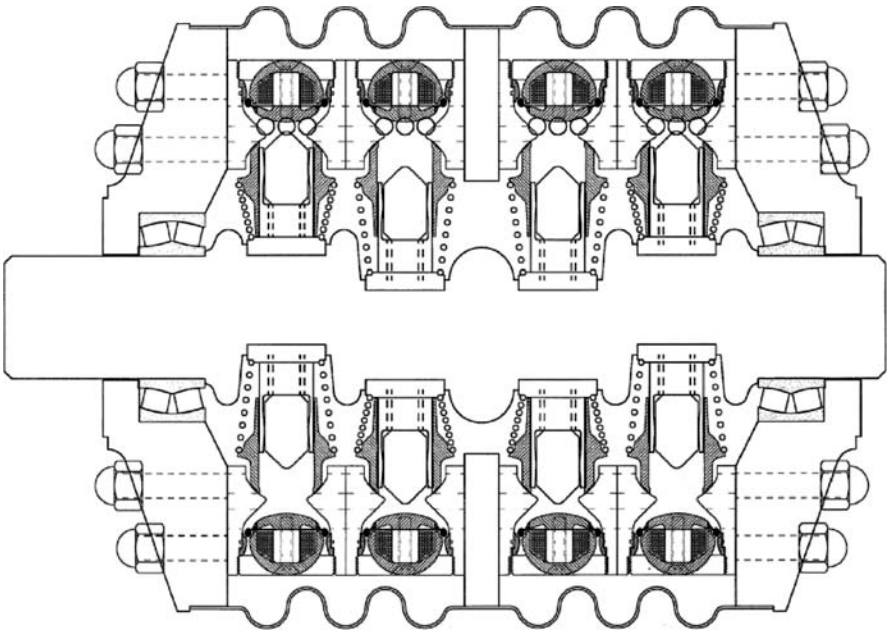

Fig. 6.55. A four-layer active-valve radial-piston machine. From Salter et al (2002)

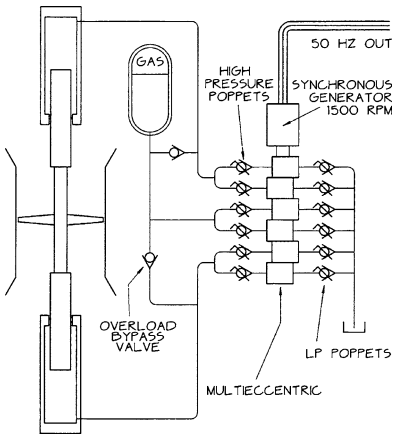

Fig. 6.56. Simplified schematic of a multiple-service, active-valve machine controlling two rams and an accumulator for use in wave energy devices such as the IPS Buoy or PS Frog (Salter et al., 2002)

6.3.14 Digital Displacement™

The phrase Digital Displacement™ was coined by Artemis Intelligent Power Ltd, a spin-off company from the University of Edinburgh, for the active-valve hydraulic machines that they are currently developing with industrial partners. Figure 6.57 shows components for the first such machine which was built by Artemis in the late 1990s.

This real 12 *cc* per revolution pump is small compared with the original vision of an active valve machine within the power canister of the gyro duck. Even so, it has a nominal power rating of around 20 *kW* at 3000 *rpm* and 350 *bar*. The demanding specification for hydraulic machines that would be suitable for power conversion in large wave energy devices provided the impetus for this new technology which has started to find application in automotive transmissions and mobile hydraulics. In the meantime the cylinder sizes and power capacities of such machines are being gradually increased to the stage where they can at last start to find application in wave energy devices (Payne et al., 2005).

Figure 6.58 shows the sequences of ones and zeros that are used to command the enabling or disabling of cylinders within Digital Displacement™ machines. The time-averaged result is a close linear fit between the flow demand signal and the flow into or out of the machine. This feature illustrates the suitability of such machines for certain open-loop applications including metering.

The final plots, in Fig. 6.59, compare the measured efficiency characteristics of a 250 *cc* bent-axis machine and predicted efficiency of a 192 *cc* Digital Displacement™ machine. The upper plots correspond to full displacement and the lower plots to 20 % displacement. The contours for the 192 *cc* Digital Displacement™ machine are based on a numerical model that was calibrated against data from tests of smaller prototype machines. The broad plateau of high efficiency operation across a wide range of speeds and pressures is typical of the improved per-

Fig. 6.57. The first Digital Displacement™ radial-piston pump built by Artemis Intelligent Power. Parts for the active low-pressure valve are in the left foreground. In the centre is a passive high-pressure check-valve. A 2 *cc* pumping module is at front right. The microcontroller is at back right. Photo: Artemis Intelligent Power Ltd

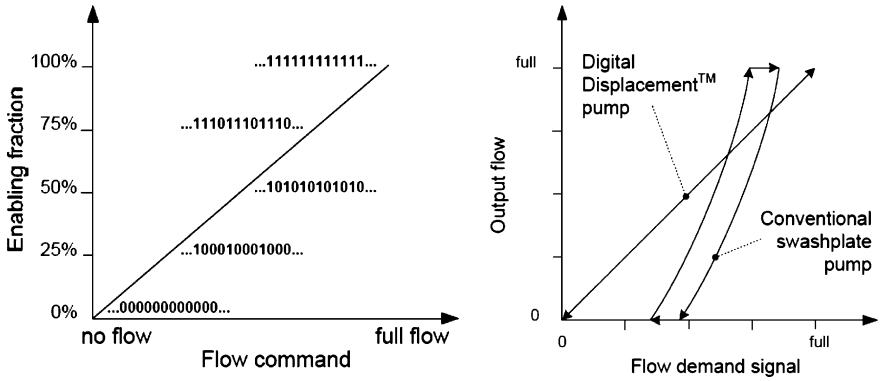

Fig. 6.58. Digital Displacement™ pump control. On the left: binary valve control sequences are used to vary the enabling fraction between 0 % and 100 %. On the right: the resulting linear relationship of output flow to the demand signal. (Payne et al., 2005)

formance that has already been demonstrated by small Digital Displacement™ machines. The systematic development of megawatt class Digital Displacement™ machines is currently underway and these are likely to be of great benefit to wave energy power take-off systems.

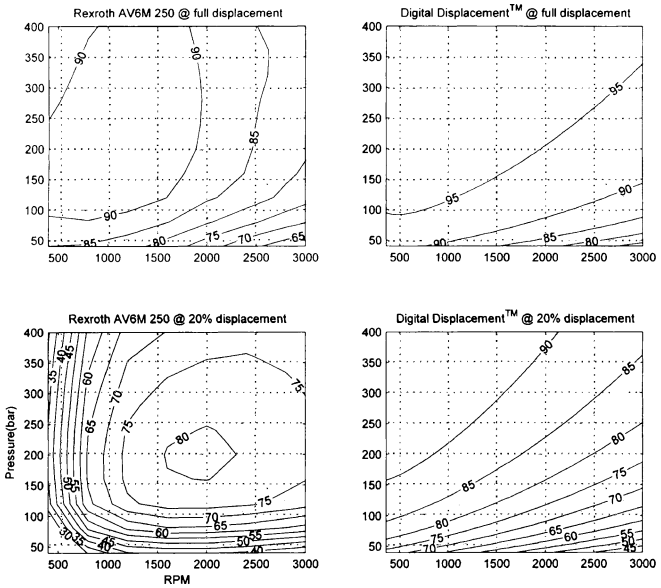

Fig. 6.59. Predicted efficiency contour plots of a Digital Displacement™ pump (on the right) at full and 20 % displacement compared with an equivalent-sized commercially available machine (Payne et al., 2005)

6.4 Alternative Applications: Desalination

Matthew Folley,

Queens University Belfast, Northern Ireland, UK

João Cruz,

Garrad Hassan and Partners Ltd, England, UK

It would seem that anybody who has worked in wave energy has at sometime considered the potential for wave-powered desalination. However, few have progressed to investigate the challenges and prospects of wave-powered desalination in depth, so that within this subject there appears to be a lot of talk with very little substance. This section attempts to clarify the topic of wave-powered desalination, putting it in context with desalination technology in general and detailing the historical development of wave-powered desalination. Thus the section starts with an introduction into the context of desalination and a description of the different types of desalination technologies currently used. This is followed by a review describing the history of wave-powered desalination and details of the already approached technologies. The challenges that are faced by the use of wave power for desalination are also presented and the section is concluded with a discussion on the prospects for wave-powered desalination.

6.4.1 Introduction

The lack of available fresh water is considered by many to be one of the greatest challenges facing the world. Whilst water shortages affect countries from both the developed and developing worlds, it is in countries in the developing world where its effects are most pronounced. A lack of fresh water is directly associated with 80 % of all diseases in these countries and 30 % of all deaths worldwide. Desalination technologies, which convert salt water into fresh water, are used extensively to produce fresh water where there is a scarcity. The current worldwide desalination capacity is approximately 16,000,000 m^3/day, providing fresh water for irrigation and human consumption in many arid parts of the world. It is estimated that this capacity is growing by approximately 1 % per annum; however this is lower than the estimated increase in demand for fresh water, which is growing at twice the rate of population growth; that is a rate of 3 % per annum. It is thus predicted that unless circumstances change the number of avoidable deaths due to a lack of fresh water will increase, with some authors predicting that future wars will be fought over this scarce commodity (Engelman et al., 2000; Barlow and Clark, 2002).

The obvious solution to the scarcity of fresh water is to increase the desalination capacity in the effected regions. However, desalination technologies are energy intensive, which places them in direct conflict with the other great challenge facing the world: the energy crisis. It is relatively easy to show that the minimum energy requirement for desalination is approximately 2.5 kJ/kg (0.7 kWh/m^3) of fresh water produced (physically it corresponds to the free energy change associ-

ated with the process of salt dissolution). But the majority of current desalination plants are based on distillation processes with a specific energy consumption of around 35 *kJ/kg* (10 kWh/m^3). Putting this is in context: standard agricultural practices require 0.1 m^3 of fresh water, equivalent to 3.5 *kJ* (1.0 *kWh*), to produce 1 *kg* of tomatoes. Although more modern technologies utilising reverse osmosis together with energy recovery from the reject brine flow have reduced this energy consumption to approximately 10.0 *kJ/kg* (3.0 kWh/m^3), the energy consumption for desalination remains significant.

In many regions the scarcity of both traditional, non-renewable, sources of energy and fresh water has understandably led to proposals of desalination plants powered by renewable energy, including wave power. Indeed, wave-powered desalination would seem to offer particularly good prospects because the two main requirements, salt water and energy, are both available in abundance. Whilst a few prototype wave-powered desalination plants have been developed, the development of desalination plants powered by wind and solar energy has been much more significant (Subiela et al., 2004; Bouguecha et al., 2005; García-Rodríguez, 2003; Raluy et al., 2004; Koklas, 2006). These have demonstrated that renewable energy powered desalination plants can be cost-effective and it is reasonable to expect that wave-powered desalination can be similarly successful.

Desalination plants powered by renewable energy have an additional advantage where the electrical distribution network is weak because they can help to increase the proportion of renewable energy utilised. In these locations the electricity is typically supplied by diesel generators using imported fuel making the cost of electricity from traditional power plants high, often 3–4 times higher than the cost where coal, gas or nuclear power stations supply power to a large distribution network. Ironically the exploitation of renewable energy to generate electricity is limited in these locations due to the weakness of the grid, exactly where it would be most profitable to locate renewable energy plants. For example, in Gran Canaria the peak power demand is 230 *MW*, however to maintain grid stability the maximum installed capacity of wind turbines is limited to 80 *MW*, although there is much more wind power (and wave power) available. By using renewable energy to power desalination plants directly, the problems with the weak grid can be circumvented and the total amount of renewable energy exploited increased. It is possible to think of the desalinated water as an alternative and cheap form of energy storage, with a capacity of 7–35 *kJ/kg* (2–10 kWh/m^3).

Finally, offshore wave-powered desalination plants have a number of environmental benefits when compared to traditional desalination plants. Firstly, the concentrated brine, which is a by-product of desalination, can be disposed of away from the coastline, reducing the environmental impact. Secondly, noise generated by the desalination plant would occur out of earshot from the local population and thirdly, a minimal amount of the valuable land close to the shoreline is required.

6.4.2 Desalination Technologies

Two basic processes can be used to separate salt from water: thermal processes and physical processes. Thermal process utilise a change in phase, exclusively liq-

uid to gas in current technologies, to separate the salt from the water. Physical processes involve a physical barrier, a membrane, which allows the water across, but not the salts. In addition chemical processes can be used and involve changing the chemical composition to separate the salt by means such as precipitation. However, chemical processes are typically expensive and require a supply of chemicals and thus will not be discussed further.

Thermal Processes

Thermal distillation processes have been used for large-scale desalination for over 50 years and make-up the majority of commercial desalination plants. Earlier plants used a multi-stage flash (MSF) process which involves bulk heating of water that is subsequently passed through a number of stages. In each stage the pressure is reduced resulting in some of the water evaporating and condensing on heat exchangers that preheat the feed water. This technology is often coupled with a conventional thermal power station utilising its "waste heat". Multi-effect evaporation (MEE) is related to MSF, but rather than using the latent heat in the water vapour to pre-heat the feed water, it is used to provide additional heat for evaporation to the subsequent stage. MEE plants typically have a better thermal efficiency than MSF plants, however problems with scaling has limited their application. Finally vapour-compression processes involve reducing the pressure to cause the water to evaporate. The heat required to make the water evaporate comes either from a mechanical pump, and the process is then called mechanical vapour-compression (MVC), or from the expansion of steam and the process is called thermal vapour-compression (TVC). In both cases a heat exchanger is used to recover the energy from the product water and recycle it back into the process.

To determine the efficiency of thermal processes there are essentially two means of energy loss: the heat lost to the atmosphere through the walls of the plant and the temperature difference between the intake and brine/product waters. Thermal insulation is typically used to reduce the first loss, whilst heat exchangers are used to reduce the latter. Clearly, the more thermal insulation used and the larger the heat exchangers used the more efficient the process becomes. Each particular configuration lends itself to reduce these losses and it is typically found that MSF has the highest specific energy consumption of 100–300 kJ/kg (28–83 kWh/m^3), MEE the second highest with 100–200 kJ/kg (28–56 kWh/m^3) and VC the lowest with 15–60 kJ/kg (4–17 kWh/m^3). The variations are due to different plant arrangements, plant size, operating temperatures and recovery-ratios (the ratio of product water to feed water).

Thermal processes are relatively maintenance-free due to the absence of moving parts. One problem that can occur is scaling. Scaling becomes progressively more problematic as the operating temperature and recovery-ratio increase and so can be avoided by limiting the operating temperature and recovery-ratio; however this typically increases the specific energy consumption of the process. Most commonly pre-treatment chemicals are added to the feed water to inhibit the precipitation of the salts. A potential alternative, which has not been commercially proven,

is to use an anti-scaling coating, which stops the adhesion of the salts onto the plant surfaces, so that they continue to operate effectively.

A potential advantage of thermal distillation processes is that they produce a high quality output with a salt concentration typically less than 10 *ppm*. However, for human consumption a salt concentration of less than 500 *ppm* is considered palatable, whilst the World Health Organisation limit for human consumption is 1000 *ppm*. The maximum salt concentration acceptable for irrigation depends on the plant being grown, but is typically around 2000 *ppm*.

Physical Processes

The only physical process used for seawater desalination is reverse osmosis (RO). Electrodialysis (ED), the other main physical process has thus far been found to be uneconomic for use with seawater. Reverse osmosis involves pressurising water so that it is forced through a membrane that allows the passage of the water but not the salts. The pressure required to force the water through the membrane increases with its salinity and so initially the use of RO membranes was limited to brackish waters with a salinity of less than 10,000 *ppm*. For seawater the osmotic pressure is typically 25–28 *bar*. Once the osmotic pressure has been overcome, the flow of water through the RO membrane is approximately proportional to the amount of excess pressure applied.

Together with the water a small amount of the dissolved salts leak through the RO membranes so that the product water typically has a salinity of around 100–500 *ppm*. Because the leakage rate of salts depends primarily of the salinity gradient across the membrane and is independent of the feed pressure, higher product salinities occur with lower feed pressures and lower product salinities with higher feed pressures. For current membranes a feed pressure of 50 *bar* will produce a product with a salinity of approximately 150 *ppm*.

Appropriate pre-treatment of the feed water is required to ensure that the RO process remains efficient and to ensure a reasonable longevity of the membranes; RO membranes typically need replacing every 2–5 years. The first stage in the pre-treatment is filtering the feed water to reduce the maximum particulate size to less than 0.1 μm. This is normally achieved in two stages, a sand filter removing particles larger than 20 μm, and then a cartridge filter, which removes the remaining particles larger than 0.1 μm. However, if the geology at the location is appropriate then the feed water can be drawn from a "beach-well", utilising the natural porosity of the rock/sand/silt as a filter. The next stage is to sterilise the feed water, killing any organisms that may grow on the surfaces of the membranes. This may be achieved by using UV light, the addition of chlorine or other chemical treatment. Again, the use of a "beach-well" can eliminate the need for this stage, where organisms cannot survive in the rock sufficiently long to reach the feed water intake. The final pre-treatment involves treating the feed water to eliminate the problem of scaling, which increases with the recovery-ratio. This can be achieved by adding acid to the water to increase its *pH*, or chemical additives to stop the scale from forming. Depending on the chemicals added then some post-treatment may be required to remove the carbon dioxide produced.

The optimal pre-treatment processes required depend on the characteristics of the feed water and desalination plant. In some circumstances extensive pre-treatment is required, whilst in others it has been found that no pre-treatment has been required. However, if the correct pre-treatment has been applied then the reliability of a RO plant is similar to other desalination technologies, with a minimum level of maintenance.

Whilst membrane technology has continued to improve, the major advancement that has made RO suitable for desalination of sea-water is in energy recovery technology. Energy recovery involves recovering and recycling the energy contained in the discharge stream of un-desalinated water. Because the specific energy consumption of a RO plant increases with salinity the recovery-ratio has typically been limited to approximately 40 %, so that a large amount of energy was lost in the 60 % of pressurised sea-water that was not desalinated.

Early energy recovery technologies were simply reverse-running pumps or Pelton wheel turbines connected to the main high pressure pump of the plant to reduce the load on the drive motor. These were capable of recovering around 75 % of the brine stream energy. More recently energy recovery technologies have been designed that transfer the pressure directly from the brine to the feed water, thereby eliminating the conversion of energy into shaft power, with resultant energy recoveries of over 95 % (Andrews and Laker, 2001; Harris, 1999; Geisler et al., 1999; Stover, 2004). Consequently, the specific energy consumption for RO plants has recently plummeted with a number of plants claiming a specific energy consumption of less than 7.0 kJ/kg (2.0 kWh/m^3), though a more typical figure may be 10.0 kJ/kg (3.0 kWh/m^3).

An additional beneficial effect of the increased efficiency of energy recovery is that RO plants can operate economically at lower recovery-ratios, thereby avoiding problems associated with scaling and the need for this pre-treatment. By using UV light to sterilise the feed water the need for chemicals in the pre-treatment can be avoided and so the plant can more easily be operated in remote locations where the supply of chemicals could be problematic. This strategy has been used by ENERCON in an autonomous wind-powered desalination plant for remote locations (Paulsen and Hensel, 2005).

Costs of Desalination Technologies

Investigating the specific cost of desalinated water from the different technologies shows a vast range of costs for each technology, making it difficult to compare technologies effectively. Part of the reason for this is the lack of a standard methodology by which the costs can be calculated, but this is exasperated because a large proportion of the cost of a desalination plant is in its construction, therefore once it is built it is likely to be operated because the marginal cost of the desalinated water is acceptable, even though the specific cost based on the plant's full life-cycle cost may be high. Alternatively, it is possible to look at what is being built to indicate what the most profitable technology is currently, indicating that reverse osmosis is currently the preferred technology. However, it must be recognised that this is for standard plants powered by non-renewable energy sources.

The specific cost for each proposed plant will be minimised based on the plant construction and maintenance costs and the relative cost of energy in the specific circumstances; the assumptions used may no longer be valid for of wave-powered desalination plants.

The cost of desalination can be split into three basic cost centres: plant construction costs, operation & maintenance costs and energy costs. The contribution from each cost centre will differ for the different technologies and for different scenarios making it difficult to generalise. However, it is useful to understand the basic mechanics of the cost calculations so that the design optimisation of desalination plants can be understood. As an example, consider the case of a reverse osmosis plant. The capital cost of a medium-sized, 5,000 m^3/day, RO plant is about £1000 per m^3/day, operation and maintenance costs are about £100 per m^3/day per year and energy costs are about 0.09 $£/m^3$ (based on a specific energy consumption of 3 kWh/m^3 and electricity cost of 0.03 $£/kWh$). If the plant life is 25 years and an 8 % rate of return is applied then the cost of water is 0.62 $£/m^3$, with 41 % capital costs, 44 % operation & maintenance costs and 15 % energy costs; the plant has a capital cost of £ 5,000,000 and consumes 625 kW of power. Alternatively, where diesel generators are used the real cost of electricity is closer to 0.13 $£/kWh$, so that if the same plant were used the cost of water would be 0.92 $£/m^3$, with energy accounting for 42 % of the cost. However, in this scenario more RO membranes would be used to reduce the specific energy consumption, which increases the capital cost, but would reduce the specific cost of the water produced.

If only the energetic cost of the processes are considered, then comparison of the specific energy consumptions of the different desalination technologies indicates that vapour-compression and reverse osmosis technologies have a significantly lower specific energy consumption than the rest, with the energy recovery technologies developed in the last 5–10 years giving reverse osmosis a slight edge. However, it must again be emphasised that these energetic costs have been optimised for standard desalination plants; the relative costs for wave-powered desalinations plants may be different.

6.4.3 Current Status of Wave-Powered Desalination

Renewable energy schemes experienced a major boost during the 1970's oil crisis. Wave energy was no exception, and it began to be seriously studied around this time, although the first ideas from Girard and sons date back to the 18th century (McCormick, 1981). The main alternative to the traditional output (electricity) is typically assumed to be desalinated water. Wave energy devices are usually associated with direct conversion from wave to electrical energy. The global resource is of the same order of magnitude of the world's consumption of electrical energy (Isaacs and Seymour, 1973), which makes it one the most promising and attractive forms of renewable energy. Generic introductions to wave power technologies can be found in Salter (1989) and Clément et al. (2002). Several devices and schemes are nowadays on a pre-commercial stage, in a clear sign that wave

energy is being seriously considered not only by the scientific community but also by the industrial world.

By adding the need of fresh water, the first attractive feature about wave powered desalination is to have both the energy resource and the raw material (seawater) in the same site. Davies (2006) presents both a review on wave-powered desalination schemes and an application exercise to some notably dry countries. African countries are assessed in detail, with the fresh water potential from wave powered desalination being quantified through a mathematical model. It is clearly pointed out that many other arid regions can be typical examples, like regions of the USA, Western Australia and Chile, and islands like the Canaries and the Maldives. The reduced number of such coupled schemes is addressed and the review is concluded with the notion that, due to the predicted increase of the problems surrounding fresh water supplies, the interest in such systems is likely to grow, either with further development of the current alternatives or with the emergence of completely new ones.

In this section, several concepts that reached the prototype stage are addressed. The technologies differ both in the desalination process used and in the way that it converts wave into mechanical energy.

The Delbuoy

The first device that used wave energy directly for the production of fresh water from seawater was the Delbuoy, a system studied and developed at the University of Delaware, USA. The concept introduced by Pleass (1974) is described in detail in Hicks et al. (1989), where the system's design, operating principle and sea trials results are presented. The main motivation was the same as today's main goal: such systems are useful to remote areas, with unreliable or even insufficient power sources or with expensive and polluting ones. Typically the optimal candidates to such technology are islands or arid costal regions exposed to large oceans.

The Delbuoy concept involves a buoy, which is subjected to the waves that pass by it, a linear pump and an anchoring system that interacts with single-pass reverse osmosis membranes to produce fresh water (Fig. 6.60). The basic operating principle relies on heave for the pumping motion, which produces the pressure required by the reserve osmosis module, as showed in Fig. 6.60.

Following nine years of research and development activities at the University of Delaware the system underwent sea trials, conducted by the Department of Marine Science of the University of Puerto Rico, in 1982. A total of seven full-scale prototypes (1 *m* radius buoy) were installed. The final configuration included six devices and the first commercial installations took place in 1989, in the Caribbean (Puerto Rico and Belize). This location could guarantee a device output from 1100 to 1900 litres of fresh water per day (Hicks, 2004).

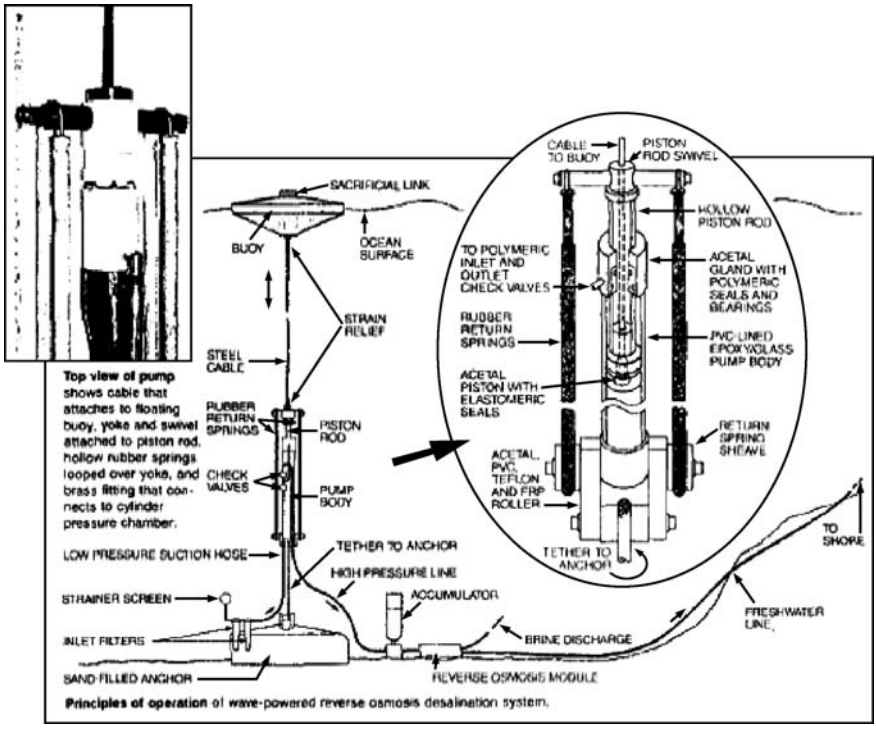

Fig. 6.60. The Delbuoy system (Hicks et al., 1989)

It is relevant to point out that the designers had in mind the fundamental issue of survivability. From Figs. 6.60 and 6.61 it is clear that most of the equipment was kept submerged, ensuring that under extreme conditions the system would not be compromised. A sacrificial linkage was therefore on the engineering list, and enabled the loss of the floater if the survivability of the remaining (expensive) components at the sea bed was at risk. It is possible to say that the solution was successful, as the system withstood two tropical storms at the test site.

An economic study of the system was also conducted, comparing the cost of the water produced with that from a conventional reverse osmosis scheme. It is legitimate to wonder why this system did not achieve a full commercial status. Dr. Hicks tries to answer some questions, include this one, in a communication to the Horizon International website (Hicks, 2004), detailing five reasons for this setback, which include "the loss of all of the equipment and infrastructure that was put in place to begin full commercialisation of the Delbuoy in St. Croix when hurricane Hugo devastated the island and the premature death of Dr. Pless, the inventor of the technology". Although its future application is still an unknown, its pioneer character will remain untouched.

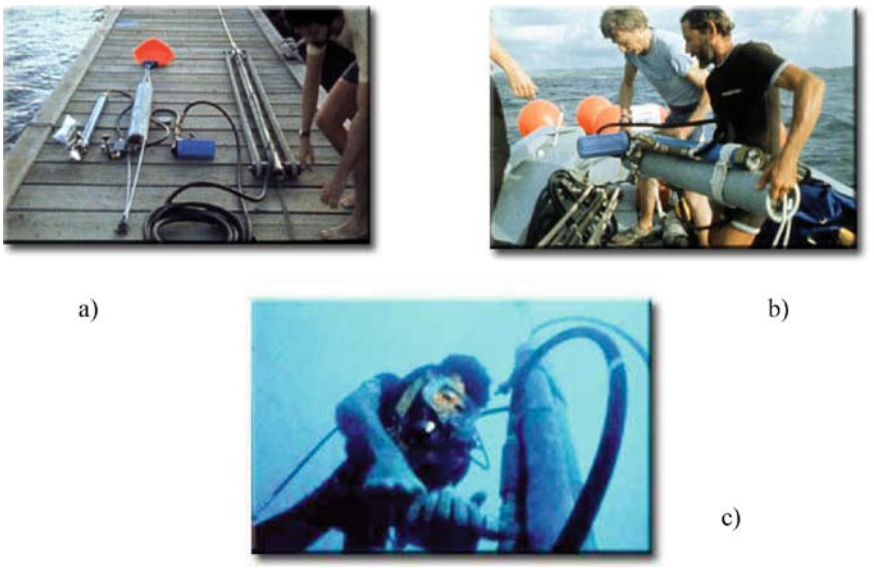

Fig. 6.61. a) Desalination unit preparation on dock; b) Lowering the Delbuoy; c) Desalination unit being checked (Hicks, 2004)

The Vizhinjam OWC plant

In Sharmila et al. (2004) details are given about the commissioning of a rated 10,000 *l/day* reverse osmosis desalination plant coupled with the Vizhinjam demonstration Oscillating Water Column (OWC) plant in Kerala, India. One distinctive characteristic is that electricity produced from the waves is used for the desalination module, not the actual action of the waves that drives the desalination process. Thus this is an indirect process, similar to the schemes that involve other renewable energy sources, with one main advantage when compared to ones that use these other resources, which is the distance to the seawater. But the option is clearly not as appealing as the complete approaches offered by the Delbuoy and the Edinburgh Duck (see pp. 270), that are stand alone desalination units, independent from the equipment needed for the conversion of wave to electrical energy. The concept is generically described in Fig. 6.63, where it can be seen the clear distinctive nature between the desalination and electricity production stages, with all the advantages and disadvantages involved (e.g.: additional losses are introduced in the energy conversion chain but the use of batteries allows a steady input to the reverse osmosis module). The system underwent a series of tests and numerical modelling, and operates in the benefit of the local community. The same technological solution could be extended to the existing OWC plants spread throughout the world, or indeed any other wave energy converter that produces electricity.

Fig. 6.62. Wave energy plant at Vizhinjam (Sharmila et al., 2004)

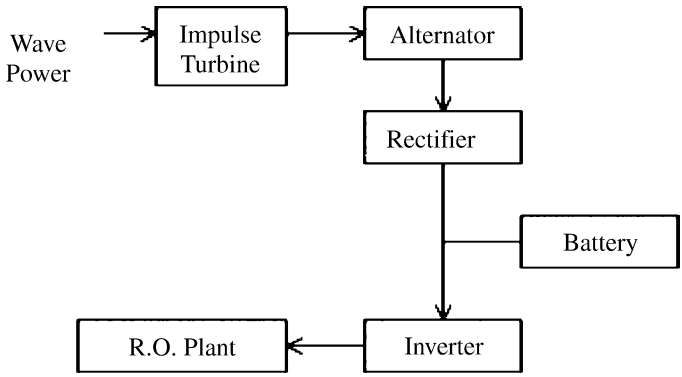

Fig. 6.63. Wave powered desalination scheme at Vizhinjam (Sharmila et al., 2004)

The Edinburgh Duck (Desalination Version)

Another concept based on the use of wave power for desalination was introduced by Prof. Stephen Salter in 1985, following the work on the wave energy converter known as the Edinburgh Duck (Salter, 1985). This paper was recently extended (Salter, 2005), and a detailed description of the device is presented in this section. The motivation for the development of such a system is similar to the one of the Delbuoy: the direct use of wave energy to a run a desalination process in order to avoid the losses of all the intermediate electrical steps that are otherwise necessary. Desalination emerged within the Wave Power Group of the University of Edinburgh as a way of overturning the 1980's UK Department of Energy demand of a single 2 *GW* wave energy plant, offering an alternative end product and directing the research to smaller units, an approach that is now proven to be more realistic.

Early research lead to a PhD thesis (Crerar, 1990) linked with mathematical and experimental modelling, which allowed measurements of pressures, temperatures and condensation/evaporation rates on a compressor system which simulated the inside of a desalination duck (Crerar and Pritchard, 1991).

The desalination duck uses the vapour-compression principle to extract the salt from sea water, a thermal method. This uses the partial evaporation of the feed falling downwards on a sheet of heat transfer surface due to the reduction of pressure induced by the action of a pump. Evaporation cools the surface while compression warms the vapour. The pressurised output is then fed to the other side of the cooled surface, which allows condensation to occur and recycle latent heat for further evaporation. Instead of the high-speed turbo-compressor used in most vapour-compression desalination systems, the pumping action is provided by the water motion in a partially filled (with water) duck body rather than with high speed compressors. The pressure across the vertical dividing wall of the duck will be proportional to the angular velocity and so gives the ideal linear damping. The inner water is not only an inertial referential but also a double-acting piston (see the 'Compression' and 'Suction' chambers in Fig. 6.64). This is the major conceptual difference between such a system and the common vapour-compression one. Similarly to the electricity production version, it is manly the pitching (also referred to as nodding) motion of the duck about an axis that will produce useful work. A new series of hydrodynamic modelling, both numerical and experimental, has been recently conducted at the University of Edinburgh, for both versions of the duck. One of the key results lead to the change of shape of the concept, loosing the front beak and moving the rotation axis away from the cylinder's own axis (Cruz and Salter, 2006).

Other relevant components of this particular device include the loop pumps and the heat exchanger. The first ones are responsible for both the pumping of all the working fluids and of the product ashore, being based on the principle that pressure is induced in a flow around a coiled pipe subjected to alternating angular accelerations in the same way as a column of fluid in a vertical tube induces pressure at the bottom. The use of several loops ensures the required capacity, as each 360 degree loop is expected to produce a pressure of 30 kPa.

The basic design motivation of this specific heat exchanger, developed by Maxwell Davidson also from the University of Edinburgh, is to ensure very large heat transfer areas at a cost similar to the one of the building material. A description of the heat exchanger is taken from Salter (2005): 'The Maxwell Davidson heat exchanger consists of sheets of the heat transfer material into which have been pressed corrugations that lie at 45 degrees to the sheet edge. The press tool is used twice to make two rectangles of corrugations separated by an area of plain sheet. Other holes can be punched out for pipe work and clamping rods. When a sheet is folded into a U shape the corrugations will contact one another and make the form of an X. A large number of U-folds are clamped together with short spacing tubes which can form feed sprayers and condensate collectors. The open ends are sealed by the inflation of an elastomeric bag to a pressure higher than the one chosen for the process. Sea water is fed to the gaps outside the U-folds. It then

moves as a falling film down the sheets and falls through the bottom from where it is collected for recirculation. Vapour is drawn off and pumped through a demister stack to the inner surfaces of the U-folds where it condenses and collects at the bottom and is drained. The falling film is ideal for good heat transfer and there is lots of demisting taking place in the heat-exchanger itself. This design allows the construction of heat exchangers with very large areas, many thousands of square metres, at a cost not much greater than that of the raw material.

The concept has been built in small scale but not as a stand-alone desalination unit (only the hydrodynamic behaviour has been fully characterised). A comprehensive mathematical model has been developed, predicting an output linear with regard to the significant wave height. A 12 m by 24 m module would produce between 1,000 and 2,000 m^3/day in a moderate wave climates (10 to 20 kW/m).

Other proposed wave-powered desalination technologies

Many other wave-powered desalination technologies have been proposed, with details on mode of operation for many very sketchy. Of the technologies described in sufficient detail to be analysed, they all propose the use of reverse osmosis for desalination. In this respect they are all essentially copies or modifications of the Delbuoy concept; however two ideas proposed are worthy of further discussion.

Waterhammer has been proposed as a method of providing the pressure required for reverse osmosis, utilising the hydro-ram (Maratos, 2003). The hydro-ram converts the energy of a large volume of fluid at low pressure into a small volume of fluid at high pressure. It is thus proposed that low head wave energy converters such as the Tapchan and WaveDragon could be used to supply large volumes of low pressure water. The conversion efficiency of the hydro-ram is claimed to be 90 %, though little data is provided to substantiate this important data. The pressure pulses that are inherent in a device that utilises waterhammer may also be problematic for RO membranes, though it is likely that an appropriately sized pressure accumulator would be able to eliminate excessive pressure fluctuations.

The Wavemill wave energy converter uses the same reverse osmosis desalination technology as Delbouy, but is supplemented by an energy recovery system that recycles the energy in the brine stream, which was simply discarded in the Delbuoy system. The energy recovery technology proposed is the Clark pump (Thomson et al., 2002), which converts the pressure energy in the brine stream directly into the feed stream. The extensive use of energy recovery technology in reverse osmosis desalination is a recent development, which has only become standard since the mid-1990's. However, because of the large reduction in specific energy consumption it is likely that any wave-powered desalination technology that utilises reverse osmosis will also use some form of energy recovery technology.

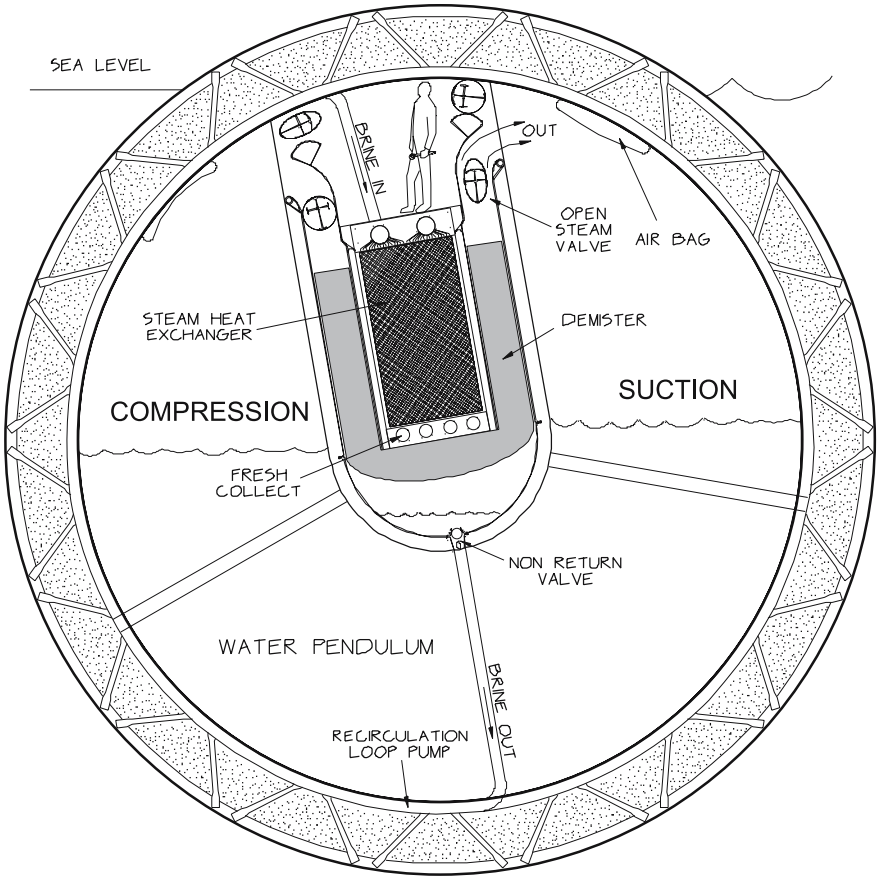

Fig. 6.64. A cross-section of the vapour-compression system. The duck hull is half full of water which acts like a double acting steam pump of enormous displacement but needing no accurate machined parts or sliding fits. All internal circulation and the pumping to shore performed using loop pumps (Cruz and Salter, 2006)

6.4.4 Challenges in Wave-Powered Desalination

The majority of the apparent challenges associated with wave-powered desalination are related to the variability of the power generated by a wave energy converter. Nevertheless, desalination plants have traditionally been designed to operate with a constant power supply; their ability to operate with a variable supply of power will differ, dependent on their basic operating principles and design.

One effect of a variable power supply is that at times the desalination plant will operating away from the optimal operating conditions that minimise the specific energy consumption of the desalination process. Ideally, the desalination plant would have a wide operating bandwidth, so that the specific energy consumption remains low for a wide range of input powers. Additionally, some form of energy storage, either inherent to the desalination process, or as a supplementary component, can help to maintain low specific energy consumption during short-term variations in the power supply. Configuring the desalination plant in modules that can be independently switched on can also help to match the power supply with the power demanded by the desalination plant.

In addition to maintaining low specific energy consumption, acceptable operating conditions for the desalination plant need to be sustained during the power variations to avoid damage to the desalination plant. For example, reverse osmosis membranes must operate between a maximum and minimum flow rate and below a maximum pressure. Manufacturers of reverse osmosis membranes also typically demand that their membranes experience a minimal fluctuation in pressure to avoid membrane fatigue. It is currently unclear whether this is a genuine problem or merely caution on the part of the manufacturers (Thomson and Infield, 2005). A particular operational scenario that must be considered is for periods of zero production, when the sea is calm, which though rare could last a number of days. Unless appropriate remedial measures can be taken, periods of zero production can result in irreversible fouling of reverse osmosis membranes and encrustation of heat exchangers.

If the only source of energy for the desalination plant is wave energy, then the variation in power means that at times the plant will be running at part-load, producing less water than its rated capacity. The economic effect of running at part-load is that the capital investment cost per unit of water produced is higher. This is no different from the economics when electricity is produced, except that the costs of desalination plants are typically much higher than electrical generator plants. A reverse osmosis plant, or vapour-compression plant typically costs about £1,000 per m^3/day of installed capacity. If the specific energy consumption of the desalination plant is 2–6 kWh/m^3, then this is equivalent to £4,000–12,000 per kilowatt of rated power. This is ten-times greater than the specific cost of an electrical generation plant, which is typically estimated to be £500–1,000 per kilowatt. If the costs of the desalination plant when coupled with wave energy are unchanged this implies that the wave energy converter used for desalination would have to be derated in comparison to its electricity-generating sister. Alternatively, the economics of wave-powered desalination can be made more attractive if the cost of a wave-powered desalination plant can be reduced with certain plant components

becoming redundant in a wave-powered desalinator and/or exploiting inherent characteristics of the wave energy converter that can provide necessary functions of the desalination plant.

Additional challenges for offshore (not shoreline) wave-powered desalinators include: the pre-treatment of the feed water, the maintenance of the desalination plant in a location that is difficult to access and the provision of a pipeline to carry the fresh water to shore, which is likely to be much more expensive than the equivalent electrical cable.

6.4.5 Prospects for Wave-Powered Desalination

In considering the prospects for wave-powered desalination only concepts that utilise the wave energy directly will be considered, i.e. wave energy converters that generate electricity to be used for desalination are not considered. Whilst wave-powered desalination via the generation of electricity is a valid concept it differs little from the generation of electricity for feeding to an electrical network grid and can best be considered with reference to the other sections in this chapter which deal explicitly with the generation of electricity. An attractive prospect for wave-powered desalinators that utilise the wave energy directly is that they are likely to have a higher wave-to-water conversion efficiency than concepts that involve the generation of electricity due to a smaller number of energy transforms. For similar reasons they are also likely have less components and therefore have the potential to be cheaper and more reliable.

Wave-powered desalinators can be configured in two basic ways: autonomous and hybrid. A hybrid configuration means that an additional source of power is available to run the desalination plant, whilst autonomous means that wave-power is the sole source of energy used. The appropriateness of each configuration will depend on the circumstances where the desalinator is installed, together with the characteristics of the desalinator itself. By coupling a wave energy converter with an additional power source many of the problems associated with the variable supply of energy can be avoided (assuming that the alternative source of energy is controllable). On the other hand, hybrid designs are likely to add complexity and cost so may not be universally suitable.

Due to the mechanical nature of wave energy, the only desalination technologies that appear to be suitable for exploitation are mechanical vapour-compression and reverse osmosis. The prospects for utilising these two processes are discussed in the final two subsections.

Utilisation of the vapour-compression cycle

Vapour-compression is a desalination technique that can have some advantages over the other options. Salter (2005) presents a review on the principles of vapour-compression: seawater close to boiling point is dropped down one side of a hot heat-transfer surface and the pressure is reduced so that some is converted to vapour by drawing the necessary latent heat from the heat transfer surface. In the

mechanical version of the technique (MVC; note that a pure thermal approach is also possible) a mechanical pump increases the pressure of the vapour by about $0.02\,MPa$, thereby increasing its temperature by a few degrees, and delivers it to the other side of the heat-transfer surface, which will of course have just been cooled by the loss of latent heat. The pure vapour condenses and releases its latent heat, which is needed for evaporation of more seawater. While the volumes of vapour are very large, the pressure drop is much smaller than for reverse osmosis. But more importantly the drop is from the product to the feed so that any leaks will lose small amounts of product rather than contaminating it. With an efficient demister to remove the small drops of water which are thrown from the boiling surface it is possible to produce an extremely pure output, better than 0.5 parts per million. As the output will have been taken to a high temperature for several minutes there is a further means for sterilisation. Pharmaceutically pure water has been produced from hospital sewage and the method has been used to dry the mash residues from whisky manufacture. The only intractable source of polluted output will be volatiles in sea water, which have boiling points close to the operating temperature.

The continuous recycling of the latent heat can make the process very efficient. The energy needed depends on the heat exchanger area and heat-transfer coefficients. The value is given by the product of the latent heat of steam ($2.256\,MJ/kg$ at $100°C$) times the temperature difference across the heat exchanger divided by the absolute temperature of operation. A part of the temperature difference is the result of the boiling point of salty water being above the condensing temperature of pure water. For 3.5 % *NaCl* sea water the elevation is $0.46°C$ but as soon as some has evaporated the strength of the remainder will rise, perhaps by a factor of two. The remainder of the temperature drop depends on the heat exchanger and, for economic reasons, is likely to be larger. With a perfect heat exchanger and 3.5 % *NaCl* feed operating at $373.3\,K$ the energy requirement would be only $2.78\,kJ/kg$ ($0.77\,kWh/m^3$). For a more realistic brine strength the requirement would perhaps double to $5.56\,kJ/kg$ ($1.55\,kWh/m^3$) for a very large heat transfer surface working at a very low rate. For practical throughputs the energy requirement would range from 9–35 kJ/kg (2.5–10 kWh/m^3).

All hot desalination methods are bedevilled by the problem that some of the many materials dissolved in seawater are close to their limit of solubility and that this solubility falls with rising temperature. They will therefore come out of solution and form a hard scale on any suitable substrate. This will grow in thickness and will rapidly reduce the heat transfer coefficients, halving them in a few days of operation. A series of heat transfer materials with steadily improving transfer coefficients and resistance to fouling have been developed by Maxwell Davidson at the University of Edinburgh. The present choice is a metal mesh which has been sprayed with a continuous layer of polyvynilidene fluoride, usually known as PVDF, filled with flakes of carbon to improve heat transfer. The PVDF layer has excellent high temperature properties and resists fouling in the same way as a non-stick Teflon-coated frying pan. It is also used for the fibres of some reverse osmosis modules.

This text refers clearly to the application of a mechanical vapour-compression technique to a wave energy converter. Such coupling is only possible with devices that have sufficient inner volume. Furthermore, such thermal energy storage can help to overcome the problem of the random nature of the energy resource. In the example of the duck, all the pumping can be associating with its nodding motion in response to the incoming waves, making it particularly suited for vapour-compression. The duck remains the most studied concept when it comes to directly link wave energy conversion and this desalination method.

Utilisation of reverse osmosis membranes

The dynamics of many wave energy converters is such that power is extracted by applying a large force, opposing the movement of a slowly moving body; this is ideally suited to hydraulics. By using sea-water as the working hydraulic fluid the feed water for the desalination plant it can be pressurised directly using wave energy, minimising the required equipment and maximising the potential system efficiency.

Reverse osmosis (RO) membranes for the desalination of sea-water have progressed dramatically in the last decade, with them becoming significantly more durable, which means that they can more easily be integrated into a wave-powered desalination plant that operates with a variable feed pressure and flow rate through the membrane. Although manufacturers continue to specify relatively tight constraints on the desirable operating conditions for the RO membranes, this does not always appear to be necessary. In particular, fatigue of the RO membranes is often quoted anecdotally as a reason why RO cannot be used with a variable energy source; however recently results from a number of projects have cast doubt on this restriction (Paulsen and Hensel, 2005; Thomson and Infield, 2005). Undoubtedly, operating RO membranes with a "correct" and constant pressure and flow rate will maximise their longevity; but as the cost of RO membranes has reduced and their durability increased this has become less of a concern. RO membranes continue to improve and if a market existed for membranes that must operate in variable conditions, i.e. wave-powered desalination, then there is no clear reason to except that suitable RO membranes would not be developed.

With the use of energy recovery systems, which recycle the energy in the pressurised brine flow exiting the RO membranes, it has been possible to reduce the specific energy consumption to less than $7\,kJ/kg$ ($2\,kWh/m^3$). As with the RO membranes the majority of the energy recovery technologies have operating constraints that may not be suitable for operation with a variable supply of energy, without an auxiliary energy supply, or where the water is pressurised directly without the use of a rotary-dynamic pump. Consequently, the energy recovery technology used needs to be considered with respect to the characteristics of the wave energy converter and current technology modified where appropriate to provide the characteristics required. Although current energy recovery systems may not be suitable for use in wave-powered desalination, there appears to be no fundamental reason why they cannot be adapted to achieve the low specific energy consumption that is currently achieved by other RO plants.

The efficient recycling of the energy in the brine flow from the RO membranes means that it becomes economic to have a low recovery ratio, which reduces or eliminates the need for chemical pre-treatment of the feed water. This clearly reduces problems for RO plants integrated in a wave energy converter that is not located on the shoreline; increasing the prospects for wave-powered desalination.

If the wave energy can be coupled to an additional, controllable, energy source in a hybrid solution then the desirable operating conditions for the RO membranes and energy recovery technology can more easily be obtained. If the additional energy source is an electrical network then it may be possible to configure the hybrid solution so that depending on the sea-state and/or electrical network conditions, the power can either be drawn from the electrical network or fed into it. This flexibility would enable the best economic use of the wave energy to be achieved, although this system requires additional equipment, which may make it less attractive than an autonomous system.

Finally, although improvements in sea-water hydraulics, the RO membranes and modifications to the energy recovery systems are required to exploit fully the potential for wave-powered desalination by reverse osmosis, no fundamental problems appear to exist. Moreover, that many wave energy converters are ideally suited to the utilisation of a hydraulic power-take-off, the reduction in equipment and potential improvements in efficiency mean that the prospects for wave-powered desalination by reverse osmosis are very good.

6.5 Discussion

In this chapter the main alternatives with regard to the power take-off systems that can be implemented in a wave energy converter have been discussed. As Chapter 7 will illustrate, such alternatives can be at the core of many different technological solutions.

In section 6.1 the use of air turbines was addressed. This is directly associated with the oscillating water column principle, and corresponds to the most studied alternative until recently. Nevertheless the amount of study should not be confused with the suitability of the technology to the resource; in the air turbine case this is mostly due to the experience of academics in the aerodynamics field. The Wells and Impulse turbines were presented in detail as the best and most commonly used examples.

In 6.2 the use of directly driven linear generators was discussed. The idea of direct drive is appealing since it enables simple systems with few intermediate conversion steps and reduced mechanical complexity. The requirements for the generator have additional challenges, mainly related to the nature of the energy resource. Connection to the grid is also an issue that needs to be addressed at an early design stage. Direct drive in wave energy conversion is similar in principal to direct drive in wind energy, where the moving part of the generator is directly coupled to the energy absorbing part.

Section 6.3 was dedicated to hydraulic power take-off systems. Such systems have been envisaged for several wave energy converters, namely the Edinburgh duck and the Pelamis. Hydraulics ideally suits all concepts based on the principle of converting energy by applying a large force opposing the movement of a slowly moving body, and so seem immediately appealing for wave energy conversion. A review on the pros and cons of hydraulics and on the major components such as cylinders, valves and pumps, was conducted. Examples from the Wave Power Project at the University of Edinburgh and several spin-off companies were also given. One of the latter, Artemis Intelligent Power Ltd, is now pursuing a technology patented with the name Digital Displacement™. Such active-valve hydraulic machines could improve considerably the efficiency of a hydraulic power take-off system when operating at partial load.

The chapter was concluded by considering an alternative to electricity production: desalination. Examples of concepts that directly use wave energy to run a desalination process, either thermal of physical, were addressed in detail. Vapour-compression and reverse osmosis were identified as the ideal technologies that can be applied in wave energy converters. Although at an earlier stage than the electricity production versions, wave-powered desalination can prove to be a vital solution to tackle the growing issue of water scarcity worldwide, and positively contribute to the energy mix in remote areas.

References

References (6.1)

Abbott IH, Von Doenhoff AE (1959) Theory of Wing Sections, 2nd edn. Dover Publications

Alcorn RG, Beattie WC, Douglas R (1998) Transient performance modelling of a Wells turbine. Third European Wave Energy Conference, Patras, Greece, pp 80–87

Boake CB, Whittaker TJT, Folley M, Ellen H (2002) Overview and initial operational experience of the LIMPET wave energy plant. 12th International Offshore and Polar Engineering Conference, Kyushu, Japan, vol 1, p 586–594

Count B (1980) Power from Sea Waves. Academic Press, New York (ISBN 0-12-193550-7)

Curran R, Denniss T, Boake C (2000) Multidisciplinary Design for Performance: Ocean Wave Energy Conversion. Proc ISOPE'2000, Seattle, USA, pp 434–441 (ISSN 1098-6189)

Curran R, Gato LC (1997) The energy conversion performance of several types of Wells turbine designs. Proc Inst Mech Eng A J Pow 211(A2):55–62 (ISSN 0957-6509)

Curran R, Whittaker TJT, Raghunathan S, Beattie WC (1998) Performance Prediction of the Counterrotating Wells Turbine for Wave Energy Converters. ASCE J Energ Eng 124:35–53

Curran R (2002) Ocean Energy from Wave to Wire. In: Majumdar SK, Miller EW, Panah AI (eds) Renewable Energy: Trends and Prospects. The Pennsylvania Academy of Science, pp 86–121

Dhanasekaran TS, Govardhan M (2005) Computational analysis of performance and flow investigation on wells turbine for wave energy conversion. Renew Energ 30(14)2129–2147

Eves ARW (1986) The biplane Wells turbine. Master of Science Thesis, The Department of Aeronautical Engineering, The Queen's University of Belfast, UK

Falcão AF, Whittaker TJT, Lewis AW (1994) Joule 2, Preliminary Action: European Pilot Plant Study. European Commission Report, JOUR-CT912-0133, Science Research and Development-Joint Research Center

Finnigan T, Auld D (2003) Model Testing of a Variable-Pitch Aerodynamic Turbine. Proc 13th Int Offshore Mechanics and Arctic Engineering Conf, ISOPE, Vol 1, pp 357–360

Finnigan T, Alcorn R (2003) Numerical Simulation of a Variable Pitch Turbine with Speed Control. Proc 5th European Wave Energy Conf, Cork, pp 213–220

Folley M, Curran R, Boake C, Whittaker TJT (2002) Performance investigations of the LIMPET counter-rotating Wells turbine. Second Marine Renewable Energy Conference, Newcastle, UK

Folley M, Curran R, Whittaker TJT (2006) Comparison of LIMPET contra-rotating wells turbine with theoretical and model test predictions. Ocean Eng 33:1056–1069

Gato LMC, Falcão AF de O (1989) Aerodynamics of the Wells Turbine: Control by Swinging Rotor-Blades. Int J Mech Sci 31:425–434

Gato LMC, Henriques JCC (1994) Optimisation of Symmetrical Blades for Wells Turbine. EU Report for JOULE2-CT93-0333: Air Turbine Development and Assessment for Wave Power Plants

Horlock JH (1966) Axial Flow Turbines: Fluid Mechanics and Thermodynamics. Butterworths

Inoue M, Kaneko K, Setoguchi T (1987) The Fundamental Characteristics and Future of Wells Turbine for Wave Power Generator. Sci Mach 39(2):275–280

Jacobs E, Sherman A (1937) Aerofoil Section Characteristics as Affected by Variations of the Reynolds Number. National Advisory Committee for Aeronautics, Report No. 586

Justino PAP Falcão AF (1998) Rotational Speed Control of an OWC Wave Power Plant. Proc of Int Conf on Offshore Mechanics and Artic Engineering (OMAE), Lisbon, Portugal

X Kim TW, Kaneko K, Setoguchi T, Inoue M (1988) Aerodynamic performance of an impulse turbine with self-pitch-controlled guide vanes for wave power generator. Proceedings of 1st KSME-JSME Thermal and Fluid Eng Conf, Vol. 2, pp133–137

Maeda H, Santhakumar S, Setoguchi T, Takao M, Kinoue Y, Kaneko K (1999) Performance of an impulse turbine with guide vanes for wave power conversion. Renew Energ 17:533–547

Mamun M, Kinoue Y, Setoguchi T, Kim TH, Kaneko K, Inoue M (2004) Hysteretic flow characteristics of biplane Wells turbine. Ocean Eng 31(11–12):1423–1435

Mei CC (1976) Power extraction from water waves. J Ship Res 20(2):63–66

Raghunathan S, Tan CP, Ombaka OO (1985) The Performance of the Wells Self Rectifying Air Turbine. Aeronaut J, pp 369–379

Raghunathan S (1995) A Methodology for Wells Turbine Design for Wave Energy Conversion. J Pow Energ IMechE 209:221–232

Raghunathan S, Beattie WC (1996) Aerodynamic Performance of Counter-rotating Wells Turbine for Wave Energy Conversion. J Pow Energ 210:431–447

Salter SH (1988) World Progress in Wave Energy. Int J Ambient Energ 10:3–24

Sarmento AJNA, Gato LMC, Falco AF (1990) Turbine-Controlled Wave Energy Absorption by Oscillating Water Column Devices. Ocean Eng

Setoguchi T, Kaneko K, Taniyama H, Maeda H, Inoue M (1996) Impulse turbines with self-pitch-controlled guide vanes for wave power conversion: guide vanes connected by links. Int J Offshore Polar 6:76–80

Setoguchi T, Takao M, Kaneko K (1998) Hysteresis on Wells turbine characteristics in reciprocating flow. Int J Rotating Mach 4(1):17–24

Setoguchi T, Santhakumar S, Maeda H, Takao M, Kaneko K (2001) A review of impulse turbines for wave energy conversion. Renew Energ 23:261–292

Stewart T (1993) The influence of harbour geometry on the performance of OWC wave power converters. Ph.D. Thesis, The Department of Civil Engineering, The Queen's University of Belfast, UK
Thakker A, O'Dowd M, Slater S (1994) Computational Fluid Dynamics Study of Air Flow in a Wells Turbine and Oscillating Water Column Device. EU Report for JOULE2-CT93-0333: Air Turbine Development and Assessment for Wave Power Plants
Thakker A, Dhanasekaran TS (2003) Computed effects of tip clearance on performance of impulse turbine for wave energy conversion Renew Energ 29:529–547
Thakker A, Dhanasekaran TS (2005) Experimental and computational analysis on guide vane losses of impulse turbine for wave energy conversion. Renew Energ 30:1359–1372
Thakker A, Hourigan F (2005) Computational fluid dynamics analysis of a 0.6 m, 0.6 hub-to-tip ratio impulse turbine with fixed guide vanes. Renew Energ 30:1387–1399
Watterson JK, Raghunathan S (1997) Computed effects of tip clearance on Wells turbine performance. Proceedings of the 35th Aerospace Sciences Meeting and Exhibit, Reno, NV, Paper No: AIAA-1997-994
Wells AA (1976) Fluid Driven Rotary Transducer. British Patent Spec 1 595 700
Whittaker TJT, Thompson A, Curran R, Stewart T (1996) Operation of the Islay shoreline wave power plant as a marine test bed for turbine generators, project phase 5. Energy Technology Support Unit Report, ETSU Report No. V/02/0017/00/REP, Harwell, UK
Whittaker TJT, Beattie WC, Raghunathan S, Thompson A, Stewart T, Curran R (1997a) The Islay Wave Power Project: an Engineering Perspective. Inst Civil Eng Water Maritime Energ, pp 189–201
Whittaker TJT, Thompson A, Curran R, Stewart TP (1997b) European Wave Energy Pilot Plant on Islay (UK). European Commission, Directorate General XII, Science, Research and Development – Joint Research Centre, JOU-CT94-0267
Whittaker TJT, Beattie WC, Raghunathan S, Thompson A, Stewart T, Curran R (1997) The Islay wave power project: an engineering perspective. Inst Civil Eng Water Maritime Energ 124:189–201

References (6.2)

Baker NJ (2003) Linear generators for direct drive marine renewable energy converters. Ph.D. thesis, School of Engineering, University of Durham
Baker NJ, Mueller MA (2004) Permanent magnet air-cored tubular linear generator for marine energy converters. In: IEE Power Electronics and Electrical Machines & Drives Conference, Edinburgh
Boldea I, Nasar SA (1999) Linear electric actuators and generators. IEEE Trans Energ Convers 14(3):712–717
Chen Z, Spooner E, Norris WT, Williamson AC (1998) Capacitor-assisted excitation of permanent-magnet generators. IEE Proc Electric Pow Applic 145(6):497–508
Danielsson O (2006) Wave Energy Conversion – Linear Synchronous Permanent Magnet Generator. Ph.D. thesis, Acta Universitatis Upsaliensis Uppsala
Danielsson O, Eriksson M, Leijon M (2006) Study of a longitudinal flux permanent magnet linear generator for wave energy converters. Int J Energ Res 30(14):1130–1145
Danielsson O, Leijon M, Sjöstedt E (2006) Detailed Study of the Magnetic Circuit in a Longitudinal Flux Permanent-Magnet Synchronous Linear Generator. IEEE Trans Magnetics 41(9):2490–2495
Falnes J, Budal K (1987) Wave power conversion by point absorbers. Norwegian Maritime Res 6(4):2–11

Harris MR, Pajooman GH, Abu Sharkh SM (1997) The problem of power factor in vrpm (transverse-flux) machines. In: Eighth International Conference on Electrical Machines and Drives, no 440, pp. 386–390

Harris MR, Pajooman GH, Abu Sharkh SM (1997) Comparison of alternative topologies for vrpm (transverse-flux) electrical machines. In: Proceedings of the 1997 IEE Colloquium on New Topologies for Permanent Magnet Machines, Jun 18 1997, IEE Colloquium (Digest), pp 2–1

Leijon M, Bernhoff H, Agren O, Isberg J, Sundberg J, Berg M, Karlsson K, Wolfbrandt A (2005) Multiphysics simulation of wave energy to electric energy conversion by permanent magnet linear generator. IEEE Trans Energ Convers 20(1):219–224

Leijon M, Danielsson O, Eriksson M, Thorburn K, Bernhoff H, Isberg J, Sundberg J, Ivanova I, Ågren O, Karlsson KE, Wolfbrandt A (2006) An electrical approach to wave energy conversion. Renew Energ 31(9):1309–1319

McLean GW (1988) Review of recent progress in linear motors. IEE Proc B Electric Pow Applic 135:380–416

Mueller MA (2002) Electrical generators for direct drive wave energy converters. IEE Proc Generation Transmission Distribution 149(4):446–456

Neuenschwander VL (1985) Wave activated generator. US Patent (540602), 1985-09-03

Nilsson K, Danielsson O, Leijon M (2006) Electromagnetic forces in the air gap of a permanent magnet linear generator at no load. J Appl Phys 99(3):1–5

Polinder H, Damen MEC, Gardner F (2004) Linear pm generator system for wave energy conversion in the aws. IEEE Trans Energ Convers 19(3):583–589

Polinder H, Mecrow BC, Jack AG, Dickinson PG, Mueller MA (2005) Conventional and tfpm linear generators for direct-drive wave energy conversion. IEEE Trans Energ Convers 20(2):260–267

Prado MG, Gardner F, Damen M, Polinder H (2006) Modelling and test results of the Archimedes wave swing. Proc I Mech E Part A, J Pow Energ 220(8)855–868 (14)

Thorburn K (2006) Electric Energy Conversion Systems: Wave Energy and Hydropower. Ph.D. thesis, Acta Universitatis Upsaliensis Uppsala

Xiang J, Brooking PRM, Mueller MA (2002) Control Requirements of Direct Drive Wave Energy Coverters. Proceedings of IEEE TENCON'02

Waters R, Stålberg M, Danielsson O, Svensson O, Gustafsson S, Strömstedt E, Eriksson M, Sundberg J, Leijon M (2007) Experimental results from sea trials of an offshore wave energy system. Appl Phys Lett 90:034105

Weh H, Hoffmann H, Landrath J (1988) New permanent magnet excited synchronous machine with high efficiency at low speeds. In: International Conference on Electrical Machines, pp 35–40

References (6.3)

Chapple P (2002) Principles of hydraulic system design, Coxmoor Pubishing Company, Oxford (with the British Fluid Power Association)

Douglas JF, Gasiorek JM, Swaffield JA, Jack LB (2005) Fluid Mechanics, 5th edn. Pearson Prentice Hall, Harlow, UK, (ISBN 0-13-129293-5)

Edinburgh-SCOPA-Laing (1979) Report to the Department of Energy, UK

Ehsan MD, Rampen WHS, Taylor JRM (1995) Simulation and dynamic response of computer controlled digital hydraulic pump/motor system used in wave energy power conversion. 2nd European Wave Power Conference, Lisbon, November 1995, pp 305–311

Hägglunds (2006) Installation and maintenance manual. EN320-20h 2006, Hägglunds Drives AB, URL: http://www.hagglunds.com/Upload/20060809110542A_en320.pdf, accessed 1st July 2007
Henderson R (2006) Design, simulation, and testing of a novel hydraulic power take-off system for the Pelamis wave energy converter. Renew Energ 31:271–283
Hunt T, Vaughan N (eds) (1996) Hydraulic Handbook, 9th edn. Elsevier Science (ISBN 1856172503)
Hydraulics & Pneumatics (Monthly), trade journal of fluid power equipment and systems, published monthly by DFA Media Ltd, Tonbridge, free subscriptions are available to UK residents. URL: http://www.hydraulicspneumatics.com/
Ivantysyn J, Ivantysynova M (2000) Hydrostatic pumps and motors: principles, design, performance, modelling, analysis, control and testing. Akademia Books International, New Delhi (ISBN 1-85522-16-2)
Majumdar SR (2001) Oil hydraulic systems – principles and maintenance. Tata McGraw-Hill Publishing Company Limited, New Delhi (ISBN 0-07-463748-7)
Nebel P (1992) Maximizing the efficiency of wave energy plant using complex conjugate control. Proc Inst Mech Eng I J Systems Control Eng 206(14):225–236
Payne GS, Stein UBP, Ehsan M, Caldwell NJ, Rampen WHS (2005) Potential of digital displacement hydraulics for wave energy conversion. Proc 6th European Wave and Tidal Energy Conference, Glasgow, UK, 29th August – 2nd September, pp 365–371 (ISBN 0-947649-425)
Rampen WHS, Almond JP, Taylor JRM, Ehsan MD, Salter SH (1995) Progress on the development of the wedding-cake digital hydraulic pump/motor. 2nd European Wave Power Conference, Lisbon, November 1995, pp 289–296
Salter SH (1974) Wave power. Nature 249(5459):720–724
Salter SH (1980) Recent progress on ducks. IEE Proc A 127(5)
Salter SH (1982) The use of gyros as a reference frame in wave energy converters. Proc. second international symposium on wave energy utilization, Trondheim, 22–24 June
Salter SH (1993) Changes to the 1981 reference design of spine based ducks. Report to the UK Department of Trade and Industry, June 1992, reprinted as Renewable Energy Clean Power 2000, IEE Conference, 17–19 November, pp 121–130, IEE, London
Salter SH, Clerk RC, Rea M (1988) Evolution of the Clerk tri-link hydraulic machine. Proc 8th International Symposium on Fluid Power, Birmingham, UK, 19–21st April, Elsevier, Barking, pp 611–632 (ISBN 1-85166-201-4)
Salter SH, Rampen W (1993) The wedding cake multi-eccentric radial piston hydraulic machine with direct computer control of displacement. BHR Group 10th International Conference on Fluid Power, Brugge, Belgium, 5–7th April, Mechanical Engineering Publications, London, pp 47–64 (ISBN 0-85298-869-9)
Salter SH, Taylor JRM, Caldwell NJ (2002) Power conversion mechanisms for wave energy. Proc Inst Mech Eng M 216:1–27
Yemm R, Henderson R, Taylor C (2000) The PWP Pelamis WEC: Current status and onward programme. Proc 4th European Wave Energy Conference, Alborg Denmark

References (6.4)

Abdul-Fattah AF (1986) Selection of solar desalination system for supply of water in remote zones. Desalination 60(2):165–189
Al Suleimani Z, Rajendran Nair V (2000) Desalination by solar-powered reverse osmosis in a remote area of the Sultanate of Oman. Appl Energy 65:(1–4)367–380

Andrews W, Laker D (2001) A twelve-year history of large scale application of work-exchanger energy recovery technology. Desalination 138:201–206
Barlow M, Clark T (2002) Blue Gold. New Press, New York, USA
Belessiotis V, Delyannis E (2000) The history of renewable energies for water desalination. Desalination 128(2):147–159
Bouguecha S, Hamrouni B, Dhahbi M (2005) Small scale desalination pilots powered by renewable energy sources: case studies. Desalination 183:151–165
Clément A, McCullen P, Falcão A, Fiorentino A, Gardner F, Hammarlund K, Lemonis G, Lewis A, Nielsen K, Petroncini S, Pontes M, Schild P, Sjostrom B-O, Sorensen H, Thorpe T (2002) Wave energy in Europe: current status and perspectives. Renew Sust Energ Rev 6(5):405–431
Crerar AJ, Low RE, Pritchard CL (1987) Wave powered desalination. Desalination 67.127–137
Crerar AJ (1990) Wave powered desalination. PhD Thesis, The University of Edinburgh
Crerar AJ, Pritchard CL (1991) Wavepowered desalination: Experimental and mathematical modelling. Desalination 81(1–3):391–398
Cruz JMBP, Sarmento AJNA (2004) Wave Energy: Introduction to the Technological, Economical and Environmental Issues (in Portuguese). Portuguese Ministry for the Environment (ISBN: 972-8577-11-7)
Cruz JMBP, Salter SH (2006) Numerical and Experimental Modelling of a Modified Version of the Edinburgh Duck Wave Energy Device. Proc IMechE Part M. J Eng Maritime Environ 220(3):129–147
Davies PA (2006) Wave-powered desalination: resource assessment and review of technology. Desalination 186(1):97–109
Dempster WF (1999) Biosphere 2 engineering design. Ecol Eng 13(1–4):31–42
El-Dessouky H, Ettouney H (2000) MSF development may reduce desalination costs. Water Wastewater Int, pp 20–21
Einav R, Harussi K, Perry D (2003) The footprint of the desalination processes on the environment. Desalination 152(1–3):141–154
Engelman R, Cincotta RP, Dye B, Gardner-Outlaw T, Wisnewski J (2000) People in the Balance: Population and Natural Resources at the Turn of the Millennium. Population Action International, Washington D.C., USA
García-Rodríguez L (2002) Seawater desalination driven by renewable energies: a review. Desalination 143(2).103–113
García-Rodríguez L (2003) Renewable energy applications in desalination: state of the art. Solar Energy 75(5).381–393
Geisler P, Krumm W, Peters T (1999) Optimisation of the energy demand of reverse osmosis with a pressure-exchange system. Desalination 125:167–172
Harris C (1999) Energy recovery for membrane distillation. Desalination 125:173–180
Hicks DC, Pleass CM (1985) Physical Mathematical Modelling of a Point Absorber Wave-Energy Conversion System with Non-Linear Damping. In: Evans DV, Falcão de O AF (eds) Hydrodynamics of Ocean Wave-Energy Utilization. Springer-Verlag, Berlin
Hicks DC, Mitcheson GR, Pleass CM, Salevan JF (1989) Delbouy: Ocean wave-powered seawater reverse osmosis desalination systems. Desalination 73:81–94
Hicks DC (2004) Communication to the Horizon Solution Site (available online at http://www.solutions-site.org/artman/publish/article_60.shtml)
Höpner T, Windelberg J (1996) Elements of environmental impact studies on coastal desalination plants. Desalination 108:11–18
Husseiny AA, Hamester HL (1981) Engineering design of a 6000 m^3/day seawater hybrid RO-ED helio-desalting plant. Desalination 39:171–172
Isaacs JD, Seymour RJ (1973) The ocean as a power resource. Int J Environ Stud 4(3):201–205

Koklas P, Papathanassiou S (2006) Component sizing for an autonomous wind-driven desalination plant. Renewable Energy 31(13):2122–2139
Pleass CM (1974) The use of Wave Powered Seawater Desalination Systems. Proc Int Symp Waves Energy. Canterbury
Maratos DF (2003) Technical feasibility of wavepower for seawater desalination using the hydro-ram (Hydram). Desalination 153.287–293
McCormick ME (1981) Ocean Wave Energy Conversion. John Wiley & Sons
Membrane Technology Newsdesk (2004) Desalination plant is wave-powered. Membrane Technol 2004(3):4
Miller JE (2003) Review of Water Resources and Desalination Technologies. Materials Chemistry Department, Sandia National Laboratories, Albuquerque, New Mexico
Paulsen K, Hensel F (2005) Introduction of a new Energy Recovery System—optimized for the combination with renewable energy. Desalination 184:211–215
Pontes MT (1998) Caracterização Energética das Ondas Marítimas e Estudo dos Problemas de Refracção no seu Aproveitamento. PhD Thesis (in Portuguese). Instituto Superior Técnico, Lisbon, Portugal
Pontes MT, Falcão AF (2001) Ocean Energies: Resources and Utilisation. Proc 18th World Energy Conf. Buenos Aires, Argentina (Paper 01-06-02)
Raluy RG, Serra L, Uche J, Valero A (2004) Life-cycle assessment of desalination technologies integrated with energy production systems. Desalination 167:445–458
Salter SH (1985) Wave Powered Desalination. Proc 4th Conf Energy Rural Island Communities. Pergamon Press, Inverness, UK
Salter SH (1989) World progress in wave energy – 1988. Int J Ambient Energy 10(1):3–24
Salter SH (2005) High Purity Desalination Using Wave-driven Vapour Compression. World Renew Energy Conf. Aberdeen, UK
Schiffler M (2004) Perspectives and challenges for desalination in the 21st century. Desalination 165:1–9
Sharmila N, Jalihal P, Swamy AK, Ravindran M (2004) Wave powered desalination system. Energy 9(11):1659–1672
Sommariva C, Hogg H, Callister K (2004) Environmental impact of seawater desalination: relations between improvement in efficiency and environmental impact. Desalination 167:439–444
Spiegler KS, El-Sayed YM (1994) A Desalination Primer. Balaban Desalination Publications, Santa Maria Imbaro, Italy
Stover R (2004) Development of a fourth generation energy recovery device. A CTO's notebook. Desalination 165:313–321
Subiela V, Carta J, González J (2004) The SDAWES project: lessons learnt from an innovative project. Desalination 168:39–47
Thomson M, Miranda M, Infield D (2002) A small-scale seawater reverse-osmosis system with excellent energy efficiency over a wide operating range. Desalination 153:229–236
Thomson M, Infield D (2005) Laboratory demonstration of a photovoltaic-powered seawater reverse-osmosis system without batteries. Desalination 183.105–111